Solid-Binding Peptides Enable Biomolecular Surface Assemblies and Mineralization

Carolyn Gayle Gresswell

A dissertation
submitted in partial fulfillment of the
requirements for the degree of

Doctor of Philosophy

University of Washington

2018

Reading Committee:

Mehmet Sarikaya

Candan Tamerler

Sami Dogan

Program Authorized to Offer Degree:

Materials Science and Engineering

University of Washington

Solid-Binding Peptides Enable Surface Assemblies and Mineralization

Abstract

Carolyn Gayle Gresswell

Chair of the Supervisory Committee:

Professor Mehmet Sarikaya

Materials Science and Engineering

The field of biomimicry spans many disciplines, with the common goal being to bring natural advances to modern technology. Understanding how organisms are capable of forming and modifying solids has been a fundamental question for decades. Organisms often utilize proteins in their interactions with inorganic materials. Despite many years of intense research, the key mechanism(s) of protein-mineral interactions and their pathways to mineralization still eludes us. Our lab's research delves into genetically designing and engineering peptides that have an affinity for solids with the purpose of using them as molecular building blocks in materials synthesis, assembly, and formation. As part of developing these tools for biotechnology, solid-binding peptides found via several methods were used in a variety of proof-of-principle applications. The research herein encompasses: 1. Self-assembly of peptides on solid substrates; 2. Selection of peptides for distinct polymorphs and their biomineralization; and 3. Peptide-ion interactions, via solution processing and peptide-controlled biomineralization. The research was undertaken using an array of molecular biology, genetic engineering, materials science and engineering techniques and approaches. Selected peptide structures and solid interactions were studied using computational biology, molecular dynamics and bioinformatics, while the solid formation was studied using solution and gel biomineralization. In research 1, sequences have been rationally designed, based on self-assembled peptide (SAP) nanostructures on atomically flat surfaces, from an Alzheimer's protein, Aβ, for assembly on a highly ordered pyrolytic graphite surface (HOPG) that mimic amyloid formation. Not only can this research advance technology, but it may also bring about a better understanding of protein fibrillation in neurodegenerative diseases. Research 2 was undertaken using the example of

calcium carbonate, which is known to be a major biomineral constituent in shells of numerous mollusks. In this research a cell surface library was used to select peptides that bound to two polymorphs of $CaCO_3$: calcite and aragonite. The genetically selected peptides were used to modify the polymorph and to understand possible functional domains of their biological counterparts. Finally in research 3, a biomineralizing soft-matter diffusion couple has been developed to control interface formation between two hard tissues mimicking the dentin-enamel junction (DEJ) in mammalian teeth containing hydroxyapatite (HAP). In all three cases, the peptides used are significantly shorter and simpler (7-18 amino acids) than their counterpart proteins in biology (100s of AAs long), but yet enabled material formation under controlled biological conditions of neutral pH in water at room temperature. A list of molecular biomimetic lessons learned from this study will have significant implications in future practical technologies.

TABLE OF CONTENTS

LIST OF FIGURES

LIST OF TABLES

ACKNOWLEDGEMENTS

I am grateful to all those that helped me with these projects and made them a success. I owe my deepest gratitude to Professor Mehmet Sarikaya for providing guidance and the mentorship that has altered the way I approach scientific problems. I would also like to thank Professor Candan Tamerler for her help and incites to the biological aspect of my projects.

It is my pleasure to thanks those that made this thesis possible, my examination committee: professors Sami Dogan, Candan Tamerler, Burak Berk Ustundag, Cole DeForest and Mehmet Sarikaya,. Thank you again for evaluating my work.

I am also grateful for assistance received from Dr. Marketa Hnilova, for teaching me cell surface display and giving me assistance and guidance. I would also like to thank Dr. Ersin Emre Oren, for undertaking the similarity analysis and Dr. Hanson Fong for teaching me the SEM and TEM. Finally, I would like to express my appreciation to my fellow grad students, Deniz Yucesoy, Chris So, Dmitriy Khatayevich, Tamon Page, Mustafa Gungormus, David Starkebaum Sanaz Sadt; I appreciated all their advice and guidance that they have given me over the years as both coworkers and as friends. I would also like to thank all of the undergrads that have worked with me over the years, Erin Hanada, Trish Evans, Spencer Johnson, Aashna Abrol, Grant Dunn, Shiori Baba, Milton Lau, Adriana Raybould, Andrea Dao, Madelyn Milligan and several more that might have only stayed to help with peptide synthesis then moved on, but they have taught me so much about teaching others and being able to manage other students' times as well as my own.

I am also thankful to my wonderful family who has been a constant source of encouragement and advice over the years.

I would also like to thank the funding I received from NSF-MRSEC, DMREF and GEMSEC. This research was supported by NSF-MRSEC and DMREF programs (DMR-0520567 and DMR-1629071) at GEMSEC, Genetically Engineered Materials Science and Engineering Center, University of Washington.

Chapter 1: **Why Peptides?**

Proteins are one of the main biological workers in the cell and allow it to maintain homeostasis, multiply, create inorganic structures and fascinate the field of biomimetics trying to understand and incorporate nature into technology. An individual protein can often exhibit many functions, such as the potassium channel where one segment allows it to cross the cell membrane; another recognizes the ion which then changes its conformation and another for binding with more potassium channel proteins to make the finished channel.[1] Each of these functions are very important to the cell, but not so to the scientist who often wish to do one of these functions, but not necessarily all of them. For this reason, peptides can be a very useful tool in helping understand and provide similar functionality as the full-length protein.

Peptides are defined as short amino acid chains that only differ from proteins in that they are smaller than an arbitrary cut off. For many the cut off is approximately 50 amino acids though it varies between groups, with many considering Aβ (1-42) a protein and insulin (1-51), a set of two peptides combined with a disulfide bridge. For this thesis, a peptide will be defined as any amide chain that can be synthesized easily using solid phase synthesis, roughly 32 amino acids. Amino acid chains of this length and shorter have many advantages over the larger sized proteins typically used. One of the main advantages is the ease of synthesis and modification since solid phase synthesis does not require as many steps as other methods. Another feature of having smaller sequences is how easy mutations are to make that can lead to understanding which amino acids are crucial to its purpose. Understanding how these peptides work both as a possible segment of the larger protein in the cell or having their own function can be crucial in allowing us to mimic how nature is able to design material morphologies at the nanoscale.

As a materials scientist and engineer the function that is often the most intriguing is how organisms recognize and organize the large plethora of inorganic substrates they incorporate into their structures. Over the years material scientists have needed to engineer ways to interact with inorganic materials to create biological and molecular functionalized devices, often without this understanding to help them out. Methods for adhering organic and inorganic materials without examining nature's techniques have several drawbacks when compared to peptides, which will be discussed with these procedures in the follow sections: thiol-based "click" chemistry and silanes.

1.1. Thiols-based "click" chemistry

Thiol-based "click" chemistry is when sulfur is used as the main linker between a ligand and either a surface, another sulfur group, amino acid, polymer or molecule.[2] Sulfur based chemistry has been a tool for organic synthesis since 1964 when it was first reported and has become a staple in materials development in recent years.[3-6] The weak sulfur-hydrogen bond allows for a the reaction to occur under fairly mild, solventless reaction conditions with a wide range of substrates.[4,6] Weak bonding such as this can often lead to a false sense of security when working with biological systems. For instance, when attaching molecules to gold nanoparticles making the surface chemically inert if these molecules could be removable under biological conditions which some studies have found, that could be dangerous depending on the molecule or the substrate it is coating.[3,7,8] Reversibility can be an advantage if used properly, but can also complicate matters when the sulfide bonds are removed from the surface and oxidize or form disulfide bonds with each other. Peptides can mitigate their removal by having multiple contact points to a surface rather than one weak bond as seen with results from several of our lab's papers.[9-11] Multiple points of interaction also allows peptides to recognize a surface rather than indiscriminately bind.

The versatility that "click" chemistry provides is considered to be a positive aspect of this method, but can limit its usefulness in certain situations. Thiol-based chemistry becomes extremely complex when trying to functionalize proteins or enzymes onto a surface that contain a cysteine or methionine within their sequence due to the difficulty in selecting which sulfur group attaches to the surface. Solid binding peptides are able to mitigate this since there is no separate "click" reaction that needs to take place, but rather the peptides preferentially bind displaying the protein or enzyme accordingly.[10-12] Just one example of this has been in displaying a maltose-binding protein on a gold surface using a gold binding peptide with just water as the solution and having it still be functional.[12]

Surface specificity is another aspect that thiol-based chemistry often lacks due to its versatile nature. Thiols do not have the ability to differentiate between different noble metals or polymers that it binds to. Genetically engineered peptides on the other hand have shown that they can selectively bind to one noble metal over another.[13] For instance a gold binding peptide (AuBP1) was shown to selectively bind to gold over an equally reactive noble metal, platinum, which

would not be possible with any of the thiol methods.[13] "Click" chemistry is a very useful method for certain processes, but does have its limitations which peptides can possibility mitigate giving scientists another tool in their molecular toolbox.

1.2. Silanes

Silane is another coupling agent used to attach organics to inorganic components. As dangerous as this pyrophoric gas is, many industries utilize it in both material science and biomedical applications. Some applications silane can be used for are coatings in composites and attaching bio-inert layers to titanium implants and even dental cements.[14-17] Being liable to ignite spontaneously when exposed to air is one of the major drawbacks for this method compared to the use of peptides for adhesion layers. Even though there have been some fatalities in the industries that use this attachment method many electrical companies do not see that there are other ways of being able to attach gold onto quartz successfully. [18,19] These companies are not noticing that peptides have shown time and time again that they are up to this task as an interface layer.[12,20-25] Our group has shown that using a bifunctional peptide with a quartz binding peptide on one side and a gold binding peptide on the other we can create patterned gold film arrays on the micron scale.[25] These patterns can be fine-tuned with stamping and other methods to create intricate 2D structures on a surface.

Unlike thiols, silanes are often very specific and prefer interacting with transition metals, with silicon and oxide layers being more advantageous to adhesion.[26,27] Peptides can be selected for these types of layers and rather than needing to be the adhesion layer they can be the inert or functional layer needed as the coating.[28,29] Titanium is one example where our group was able to functionalize the surface to be antimicrobial with the help of peptides selected for a specific titanium alloy and even to current implant devices.[28,30] As stated in the thiol section our peptides can be very specific as well, but if material needs an adhesion layer we merely need to select a new solid binding peptide for it using one of the many ways discussed in the next chapter.

Dental applications for silanes are mainly due to their adhesion promotion between resin composites and silica restorative materials.[17,31] Fillers made of these materials are then put into caries or as preventative on the enamel surface where adhesion is often very difficult. Inevitably due to the harsh conditions within the mouth for inorganic materials they often wear away and need to be replaced periodically.[31] [32] Our group has also done work on peptides binding to the

hydroxyapatite surface using peptides derived from the amelogenin protein as well as from selection processes.[33,34] These peptides are not only able to bind to the hydroxyapatite surface very well, but can help mineralize it as well.[33,34] In a later chapter further work is done on how these peptides are able to do this remarkable repair.

These surface modification methods have their place in many processes, but peptides offer many advantages in this field. Many of the benefits that the peptides have for specificity and versatility is conferred by the way they are found.

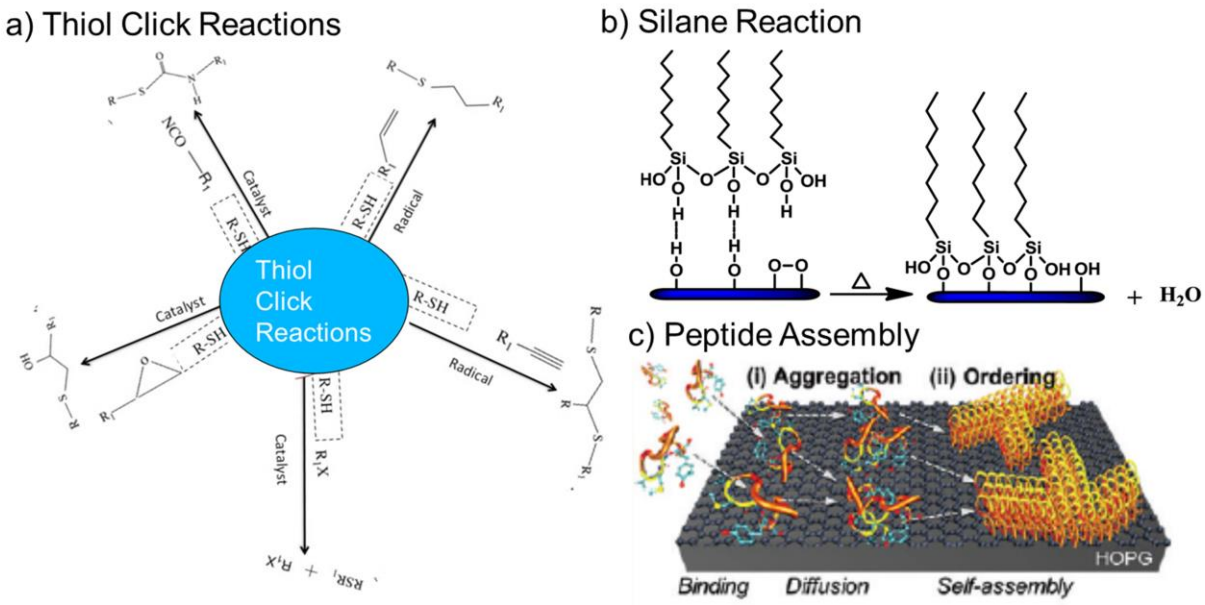

Figure 1.1: Schematic of Thiol Click Reactions, Silane Reactions and Peptide Assembly on a surface. [Adapted from Nair et. al. 2014, Wan-Ta et. al. 2015, and So et. al. 2014][4,9,18]

Chapter 2: **Finding Solid Binding Peptides**

Even though proteins are what are found to be interacting with surfaces when taking apart a cell, peptides often provide more answers due to how complex the system is when analyzed as a whole. Unlike with proteins, lysing a cell and sequencing what comes out is not helpful so other methods must be employed. Literature has given us many ways to find, create or functionalize fa peptides for specific tasks, which will be discussed in the following sections: combinatorial selection, computational, rational design and functionalization of peptides.

2.1. Combinatorial Selection of Peptides

Combinatorial peptide libraries have been used for decades to find peptides that are able to bind to biological particles and in more recent years solid surfaces. [35-37] There is very little difference between selecting a peptide for an organic molecule vs inorganic, though there are some experimental design characteristics to take into account. First is selecting the material crystallinity or alloy, since a single crystal may result in different binders than a poly crystal or from one alloy to another since peptides can be specific enough to recognize these intricacies. Along with this one must make sure the material is not hazardous to the cells or phage that is attempting to bind to the surface. The material also must not be reactive or changing its surface chemistry due to buffer or cell interactions.[38] Once the ideal material is chosen, the combinatorial library and processes can then be selected.

There are many similarities between all the combinatorial selection techniques found out there and what makes each special and why they are used. First off, all of these procedures involve fairly large randomly created libraries and some method of screening them for binding activity. The most common technique many of these processes use is the creation of a large pool of random DNA sequences with differing lengths, using PCR or other methods, which are then incorporated within the genome of a host organism. Each display technique has their own unique locations where the DNA sequences are spliced so that the peptide is displayed on a permissive site within the host's display mechanism. The length of the peptide sequence is also a determining factor in what display method is used since some sites are better equipped to handle larger peptides. For instance, longer peptides are more difficult to display on P8 which is the major coat protein in the M13 bacteriophage, but easier on other minor coat proteins such as P7 and P9, but have fewer copies found around the phage.[39,40] Several groups have gotten around this size limitation for certain permissive sites by creating their peptide library via solid phase

peptide synthesis using different methods to create random sequences.[41-43] Once the correct site and host organism is decided or method of random sequences generation, the library can then be screened against the ideal material to determine which peptides bind the best.

The screening procedure for the organic libraries within in the organism is analogous with evolutionary selection processes where we are providing the selective pressure of surface binding affinity as a way to increase an organism's survival and by proxy the peptide's percentage in the population. This is done by a technique called biopanning, where we incubate the full library of random peptide displaying microorganisms with the solid surfaces chosen with the considerations explained above. After incubation the surfaced is washed, removing all hosts that are not binding and then amplifying those that are still bound to be used in further biopanning rounds and/or sequenced. Depending on the display technique the amplification can either be quick in the case of bacterial surface display or long in yeast display. The complexity of the library also varies between display systems though most have above 10^8 peptides with each of these being displayed on a hundred or so clones so that there is a high likelihood of at least one clone reaching the surface for possible binding. If even one of these clones is able to bind, then it will be multiplied significantly during the amplification round allowing the peptide to survive on in subsequent biopanning. On the other hand, if the peptide doesn't bind to the surface than the host is more likely to be washed off and not contribute this sequence in future rounds.

The wash step is not sadly not a hundred percent in terms of some organisms are able to stay on the surface even after washing and so our group often does further binding characterization to test how well our peptides are binding to the surface. Some groups believe having multiple copies of the same sequence in later biopanning rounds to be a sign that these peptides are stronger binders, but this is not the case in the fact that the repeating sequence could be providing a growth advantage to the host or be selected by happenstance instead of a stronger binder.[44,45] The fact that some peptides are able to confer a slight growth advantage or disadvantage is why doing a very large number of panning rounds is not as beneficial as it might seem. Where as in the beginning of biopanning there is a large number of peptide hosts to choose from after only 3 or 4 rounds it often reduces considerably and enrichment occurs of preferential, easy to grow, peptides.[45] This is one advantage of the solid phase peptide synthesis technique in that the peptide cannot confer this growth advantage to the hosts though a related disadvantage is the need to sequence and synthesize after every step of biopanning since there is no amplification

that can be done naturally.[41-43] In the following sections there is breakdown of each of these selection processes with what sets them apart from the others in terms of why a group would use them and how each differ from each other.

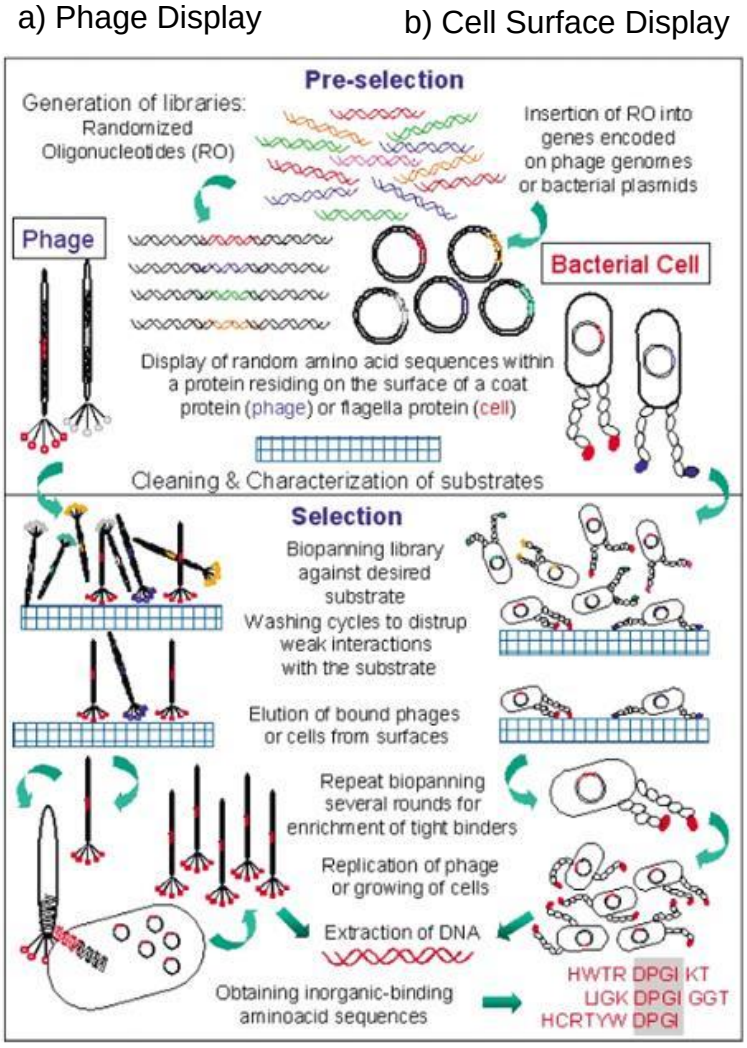

Figure 2.1: Schematic of cell surface and phage display techniques [Courtesy of Sarikaya et al 2004][46]

Three main combinatorial selection processes have been utilized in the literature for finding solid surface binding peptides: Cell Surface Display, Phage Display and Combinatorial Solid Phase Peptide Bioassays. Schematics of the two biological based ones are shown in Figure 2.1.[46] In each of the following sections further characterization of what each of these broader categories will be discussed. These processes have many similarities, which are discussed above and so these sections will be going into the differences in further depth.

2.1.1. *Cell Surface Display*

Cell surface display (Figure 2.1b) comprises of two main categories: bacterial cell surfaces (*Escherichia coli*) and yeast cell surfaces (*Saccharomyces cerevisiae*). These categories are very different, but still are considered a part of this broader section since they both display the peptide on their outer membrane or flagella and do not need a secondary organism for their amplification. The bacterial cell surface display system was first discovered by Roland et al, when they found a permissive site on the outer membrane protein OmpA of E. coli.[36,47] Since this study came out several other permissive sites have been found on this very versatile bacteria, though only one has been commercialized due to the ease of modification and the range of

peptides it can display. The FliTrx bacterial flagellar display (Thermo Fisher Scientific) was the second display library available commercially from what was then Invitrogen. This display library contains $1.77x10^8$ random dodeca-peptides cloned into the active site of the thioredoxin protein, which is displayed on the flagella of the cell.[38,48] These peptides are constrained in a cyclic loop via a disulfide bond and in multiple copies on one E. Coli.[38] One of the major advantages in this display is that there is no separate organism needed for amplification and that E. coli grows very quickly.[41]Along with this several groups have a method called fluorscence activated cell sorting (FACS) that allows for high throughput screening of bound cells.[41]

Yeast display on the other hand doesn't possess many of these advantages that the bacterial claims, but has its own. The advantages it shares with the bacterial selection is that there is no other organism needed in any part of the selection, but unlike the bacterial display yeast has a much longer growth curve. Along with this both can be fluorescently labeled and screened through FACS to reduce sorting time. Unlike in any bacterial display, the yeast display fuses the protein or peptide to the Aga2p protein, a mating mediator protein on the surface of the cell, and displayed above the cell surface.[49,50] One of the biggest advantages of the yeast display system is that these cells are eukaryotic and allow for post-translational modification, which is something no other systems provides.[50] Along with this they can display much larger sequences even protein length on their surface, which are not easily handled by the much smaller bacterial cells or phage.

Due to not needing the larger peptide and eukaryotic ability of the yeast cell for our surface functionalization our group mainly utilizes the bacterial cell surface or phage display when interrogating surfaces binding. The bacterial displays that we have done were on gold to provide a different set of possible sequences due to the difference in amino acid content between these two different displays.

2.1.2. ***Phage Display***

Phage display (Figure 2.1a) has become the most common combinatorial display system since the idea was first introduced in 1985. [35] The reason for this is due to the many advantages this system possesses and that it is commercially available as the Ph.D. M13 bacteriophage display (New England Biolabs).[38] One of the advantages that the M13 bacteriophage possesses is that there are multiple permissive sites throughout its coat protein and so it can offer different length peptide libraries or if they are constrained by a disulfide bridge or not.[38,41] The one commercially

available from Biolabs uses the minor coat protein P3 to fuse the peptide to since it can have longer sequences of up to 11 amino acids where as it would need to be shorter if the major coat proteins were used.[40,51] That being said these peptides must be short in order to not affect the phages function and so protein length peptides are not feasible. One of the major drawbacks that this display system suffers from is that it is a two-step process that requires amplification in a different bacterial host cell and this extra pressure can reduce the libraries diversity. That being said phage display does have a library that ranges from 10^8 to 10^{11} clones available which is on par and even higher than cell surface display. Phage are also very resilient compared to their cellular counterparts and so can bind to surfaces that might be more toxic to the cell since the bacteria doesn't need to interact with the material only the phages that are sonicated off. Along with this phage can survive in a -80°C freezer almost indefinitely and tolerate a wide range of pH and salt conditions allowing storage for later amplification or sequencing or different buffer conditions.

Phage display has been used by many to find solid binding peptides and has even been utilized for calcium carbonate, which we did cell surface display on to vary the amount of sequences found (Chapter 4). In comparison to our selection one set of researcher just used the phage with the peptide expressed on both calcite and aragonite to see how it would modify $CaCO_3$ growth.[44] They found that their peptides while on the phage would just inhibit the growth of $CaCO_3$ and create some irregularities, but not throughout the entire sample.[44] Another researcher then selected for just calcite and pick a few from the binders and synthesized them.[52] They had slightly better success in the fact that one of their binders stabilized vaterite in their solution, though they did not quantify how much vaterite was present, nor did they give any other selection results.[52] Aragonite has also been used as a substrate for selection and three binders have been selected from this and used in a vapor diffusion and kinetics experiment.[53] In the vapor diffusion experiment the peptides did slight etching to the calcite crystals, but in the kinetics they were shown to slow the transformation of vaterite slightly.[53] None of these peptides were classified as strong or weak binders so it is uncertain if binding strength has an effect on being able to control crystal structure.

Along with this our group has used phage display to select peptides for hydroxyapatite (Chapter 5), graphite, gold, quartz, titanium and are currently in the process of selecting for even more materials that has not yet been publish.[9,30,34,54,55]. Unlike in the previous examples of phage

display our lab does binding characterization and synthesizes several sequences from the selection to test their interactions with the material. The binding information is then inputted into a computational program to help find still more sequences or interrogate larger proteins for binding sites.

2.1.3. *Combinatorial Solid Phase Peptide Bioassays*

Combinatorial solid phase peptide bioassays are relatively recent in terms of selection systems and most are used for finding ligands or other biological binding peptides, with none currently being used for inorganic binding. One of the first of these bioassays created was the one-bead one-compound (OBOC) library by Lam et al in 1991.[41,56] The OBOC library has peptides synthesized on small resin beads displaying around 10^{13} copies and uses a "split mix" method.[41,56] Split mix synthesis separates the resin beads into different pools each containing an amino acid that is desired in the sequence they are then conjugated with that sequence and from there each group of resin is then split again and randomly coupled with the other amino acids and so on and so forth until you have every combination of those amino acids.[41] This easy of library generation and size of the library which is often in the 10^8 different peptides is one major advantage of this method. The OBOC library can also incorporate non-natural and chiral amino acids as well as secondary structures that would disrupt other natural combinatorial displays. Even with these advantages this library is not widely used due to how involved this technique is and the equipment needed to create larger sequences in comparison to the biological systems. Along with this there is no commercially available OBOC library out there at this time, making it difficult for new labs to pick up this method.

The other well-known combinatorial solid phase peptide bioassay makes use of positional scanning synthetic peptide combinatorial libraries (PS-SPCLs). These libraries are created by holding one of the amino acids constant while varying those added onto it and then "scanned" by changing that one amino acid and doing it again.[41,42,57] If one is interested in moieties being present they can hold one those set of amino acids constant while varying those around it or its location in the sequence. So even though this bioassay's library size is comparable to the OBOC and it can be modified with non-natural amino acids it suffers from a similar problem in that specialized equipment is needed and it is not commercially available. Along with this it is difficult to find an ideal peptide sequence since the binding motifs must first be found and then held the same and another library created to get the best binding possible.

Both of these bioassays provide ideas of what might be used in the future to discover more solid binding peptides, but at this time they are only used for ligand and finding organic binding peptides. They might be valuable when combined with computational methods since then only the amino acids that are believed to be valuable in binding will be tested instead of starting from all 26 available.

2.2. Computationally Derived Peptides

Computational creation of peptides can be broken down into two major categories: structure-free and structure based analysis.[58] Structure-free models like the name implies does not take structure into account and is focused completely on sequence interaction with the surface. On the other hand, structure based models focus mainly how what structure the sequence might convey to the peptide. A schematic depicting the two different categories is shown in figure 2.2.

Sequence focused methods primarily consider that similar protein sequences develop between species for similar functions, due to several constraints such as biochemistry and evolution. [59,60] Protein alignment has been used for decades in inferring possible evolutionary relationships between proteins and often utilize an optimization procedure to do so. Dynamic programming is one such procedure that allows for amino acid arrangement to be found maximizes the similarity score between two different proteins.[61,62] Scoring matrices are also used to determine a score for two aligned amino acids in two separate sequences where the higher score indicates a high similarity between the biochemistry or side groups of the amino acid. The most widely known scoring sequences are BLOSUM and PAM which were developed from natural occurring sequences.[61,63-65] They have been used widely to evaluate evolutionary relationships found in not just protein sequences but also nucleotides in nature. The major limitation with these techniques is that they often require a significant amount of experimental data already gathered to be reasonably accurate. They also are only good at determining how well a computational peptide might compare to those found already and not as good about creating new ones other than simply modifying already found ones to be better.

Computational models have been used to create new peptides with possible binding motifs incorporated based on the proteins found in nature. For instance, some groups have developed models for interacting with $CaCO_3$ based on charge interactions and possible binding motifs to create de novo designed peptides that interact with the $CaCO_3$ surface.[66,67] These peptides often inhibit growth formation in certain directions since they bind to that area and slow precipitation

creating irregular step edges or etching, but so far none have been able to control the crystal structure. [66,67]

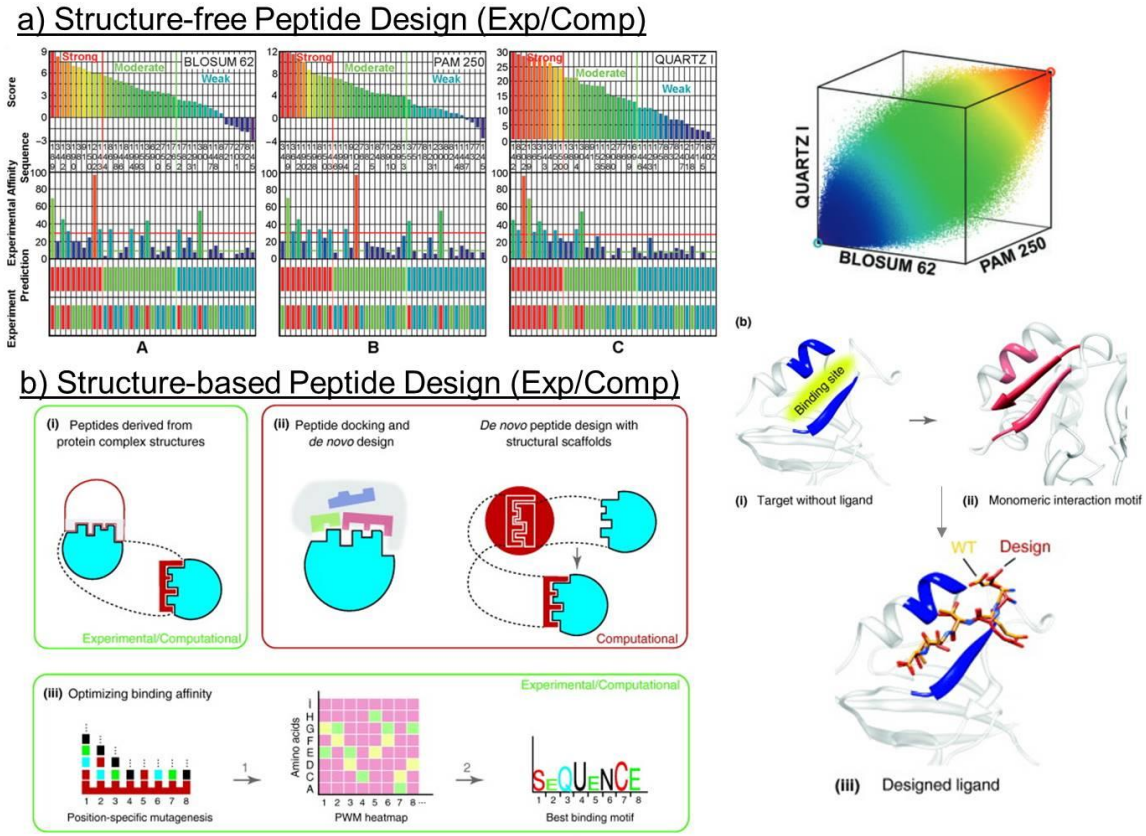

Figure 2.2: Schematic of the two computational categories for deriving peptides. [Adapted from Vanhee, P. *et al.* 2011 and E.E. Oren et al. 2007]

More recently structure-based peptide design has become popular to help find peptides that are able to interact with proteins as possible drug solutions. This method like the other computational method relies heavily on there being some experimental results already found and in this case for the structural conformation between the peptide and protein or ligand or surface that it is trying to predict binding to. Luckily, for many structural-based researchers there is a databased that contains around 505 peptide-mediated interactions identified that can be mined for designing new peptides.[58,68] Of these 505 many have exhibited unique packing structure which contains more hydrogen bonding making it tighter than the protein interfaces previously found.[58] This structure difference is mostly likely due to the fact that peptides can only be so hydrophobic in solution before they began aggregating and so in order to maintain this high level of bonding they must compensate with side-chain hydrogen bonds and main chain interactions.[58] This database has been utilized by many along with the protein database to find peptides that interact

with many cell surfaces, from ones that can apparently target cancer cells to antimicrobial ones.[69,70] As for structural peptide designed for a inorganic surface one group just recently published a paper concerning their attempt at creating a benchmark for peptide-biomineral interactions.[71] They used the RosettaSurface algorithm to attempt to predict the binding of multiple peptides on the surface of brushite.[71] They found that this algorithm was great at determine which mineral face and step-edge would bind certain peptides the strongest, but due to several key feature missing out of their program they were unable to determine which peptides would bind strongest out of a set when compared with the experimental results.[71] The future of computational design is creating these benchmarks experimentally that allow better characterization and prediction in the programs. Experiments such as the ones presented in this thesis help increase our understanding of these peptide interactions and so create more benchmarks that computational methods must live up to.

2.3. Rationally Derived Peptides

Due to the incredible amount of data provided by both the combinatorial and computational methods some groups choose to use a rational approach to determine possible new peptides. This approach is often difficult to distinguish from computational since it still sometimes use computer analysis to help determine possible binding motifs, but human understanding of the molecular basis of the protein's property is what separates it from pure computation.[72,73] Human understanding of not only the biochemical properties of amino acids, but also recognizing the similarities found structurally or through sequences between proteins and the peptides one is hoping to create. For some this rational designing is which part of a protein might be the functional group or motif and removing that to test it on its own or to do knock out mutations to see how the rest of the protein is affected.[73] For instance in finding possible peptides that interact with calcium carbonate several groups tried to rationally design shorter peptides off the full length protein through different rationalized methods.

The most common sequences are either the N or C terminus of the protein which encompasses approximately 30 amino acids off one of these ends since they are often assumed to be exposed to the environment. Five proteins called: AP7, AP24, AP8α, AP8β and Lustrin A, were separated from the pacific red abalone (*Haliotis rufescens*) while only Asprich originates from *Atrina rigida* .[74-77] AP7 was shown to form aragonite when mineralized on Kevlar, and

irregular step edges in mineralizing calcite in solution. A group then synthesized the N and C terminus and found that the N-terminus, AP7-N, also creates irregular step edges, but did not form aragonite on Kevlar and the C-terminus of this protein did not show any change from the control. From the japanese pearl oyster (*Picntada fucata*) six proteins were extracted from different areas and called: N16, ACCBP, Nacrein, CaLP, n19, PFMG1, Aspein and Prismalin14.[78-83] N16 has been shown to form aragonite in certain cases but it needs the help of beta chitin a structural matrix found within certain marine animals generally squid.[84,85] When the N-terminus of N16 was used it was also able to synthesize aragonite, with beta-chitin with similar morphology to the complete protein, indicating that this sequence is involved with polymorph switching.[85] AP24's terminus peptides did not show as strong of inhibiting affects as the full length, but were still able to etch the calcite slightly on the Kevlar threads.[86] PFMG1-N term was able form aragonite particles while the C-term is only able to create twinning calcite.[81] D4 is a peptide created from Lustrin A that exhibits calcium and mineralization interactions by changing the morphology of the overgrowth layer.[87] All of these were rationally designed one way or another from the full length peptide to have an effect on this mineral and many of them did, but not all indicating that human rationality is not full proof.

Others have also rationally designed peptides to have their own functionality and not just for binding. For instance a group rationally designed a peptide's assembly to be pH sensitive, which it was. Below a pH of 5.8 it would not assembly into larger fibrils, but above this pH it would due to the protonation state of the imidazole side chain.[88] These examples show the many different ways that researchers are able to design new peptides from either the larger proteins, combinatorically, computationally and rationally. We use several of these techniques in the studies that follow to find our own peptide that are able to interact with solid surfaces.

Chapter 3: **Rationally Designed Solid-Binding Amyloid Assembly Peptide**

Surface recognition is one the main traits that peptides selected using combinatorial display have if they are able to last more than one biopanning round. This binding is not always the found in other naturally occurring peptides or proteins especially against materials that are not found in nature or have similar biogenic properties. Using information gathered from these displays about what motifs are important for binding we can then look into how other peptides or protein in nature exhibit these sequences and so could be also interact with said material.

Assembly for any peptide onto a surface is even more unlikely given the fact that the peptide not only has to bind, but also interact with others to create wires or other ways to organize while still attaching to the material. Several proteins found in nature already possess a strong tendency to amass into highly ordered structures, which could be useful in biotechnology to provide scaffolding on devices or these devices could be used to help investigate the assembly process. Amyloids are the most well-known examples of unplanned molecular level fibrillation that occurs within the body and are found in many different diseases. These unintended assembly structures are created by misfolded proteins and peptides that form wires, which then agglomerate together into the larger amyloid. Instead of this structure forming within the body, it could be used technologically outside the body by forming an ideal framework to provide a conductive path along a semiconductor material. Along with this the material could be used as a mimic for biological surfaces and so provide more information on how this assembly occurs in nature.

For our studies, an amyloid peptide was rationally selected from the larger full-length amyloid-β (Aβ) protein involved in Alzheimer's disease to bind and assemble on graphite. The selection was done by comparing different regions in the full length Aβ known to have some influence on its assembly process for similarity to a known graphite binding peptide found in our group, GrBP5. Once the sequence was selected many conditions were then tried to see which would result in possible assembly and how that might compare to the selected solid binding peptide. We were as interested in determining which amino acids were instrumental in the binding and assembly functions for this amyloid peptide which was determined via mutations of different regions. These mutations were mainly knockouts, though in one of them we switched known weak binding amino acids with known strong binders to graphite to see how this might affect the surface assembly.

3.1. Background

3.1.1. *Defining Amyloid Formation*

The term amyloid was first coined for human plaques by a German physician and scientist Rudolph Virchow in 1854 to denote an abnormal growth in brain tissue that stained blue with iodine and purple with sulfuric acid. [89,90] Due to the current medical knowledge at the time he categorized this plaque as a cellulose deposit, which was often confused with starches though these have sense been shown to be very inaccurate.[89,90] In 1859 just 5 years after this term originated researchers Friedreich and Kekule demonstrated that this masses were not carbohydrate based as previously thought due to their high nitrogen content, but instead were formed from proteins.[89] Once electron microscopy was invented, further research done by Cohen and Calkins in 1959 showed that amyloids were formed of highly ordered fibrils of proteins which is where our current definition comes from.[90,91] After this study, the amount of research has exploded in this area with the number of publications increase more than 500 times in recent years to over 24000 in last four years alone giving us a much better definition of what an amyloid is though there is still debate within certain fields on exactly what classifies.[90] Amyloids in the broadest sense are currently defined as insoluble plaques caused by proteins in a cross- β sheet structure.[92,93] In histology, they further define that this plaques must be found in the body and show birefringence when stained with Congo Red to be considered an amyloid.[89] The proteins that make up these masses are found harmlessly throughout the body until at some point their assembly is triggered and the disease state begins. Even though many of the amyloid proteins probably serve other purposes before amassing they appear to lose whatever their original function was. So far there have been only a few studies on what might be triggering this aggregation and will be discussed in further detail in the follow section. There have been some

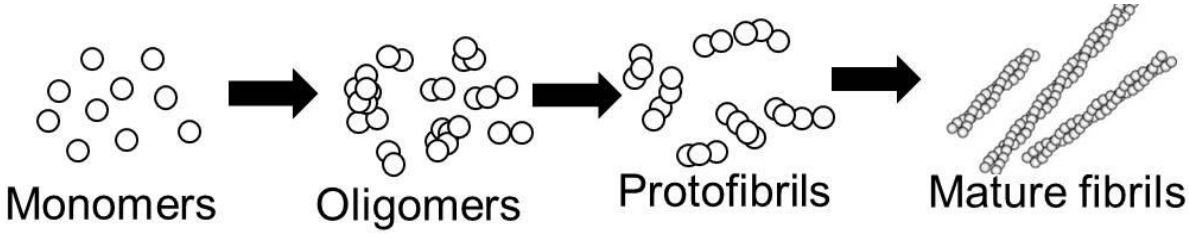

Figure 3.1: Schematic of protofibril formation

studies as to how this aggregation progresses even though there are very few ways to accurately determine when it first begins.

Peptide aggregates, called amyloid fibrils, are often preceded by smaller discrete intermediates termed protofibrils that could be influential in the toxicity of the disease (Figure 3.1). [93-97] Protofibrils are generally less than 400nm long and have diameters of 2-5nm making it very difficult to observe using classic light scattering techniques, which is how they are commonly found in clinics. [96,98,99] For this reason, protofibrils are generally only observed during in vitro studies where they can be monitored using AFM or other more accurate techniques.
As for observing the aggregated amyloid plaque, at this point there are very few ways that researchers and physicians use, with many of them being discovered post mortem. The most common practice used today for determining if a mass is an amyloid plaque is observing the birefringence upon staining with Congo Red.[93,100] This staining happens once the tissue is dead to determine the cause and whether it is a cancerous growth or other abnormalities vs an amyloid. This method is so instrumental in historically defining what an amyloid is that some fields still use it as the only way a mass can be considered this type of plaque. Recent studies have shown though that this stain is not as specific to only beta sheet forming proteins as previously thought.[101-103] How this stain works is fairly complex and some evidence supports electrostatic interaction while others appear to indicate it is more specific than that.[101] For the studies that indicate a specificity of binding they suggest that the Congo red forms rod-like stacking of the aromatic groups between the molecules which then interact with the β sheets, due to the regular spacing both possess.[104] A more recent study on the other hand shows Congo red binding to native proteins with a wide variety of secondary structures, indicating the dye might be intercalating between multiple protein layers which is typical in β-sheets, but not specific to them.[101] In order to insure that this staining technique is accurate many groups do other techniques to insure that there are fibrils and that they are displaying the β-sheet structure.
Another major characterization technique for determination of fibrils within the plaque is with transmission electron microscopy (TEM). The major consideration when doing TEM is making sure that the sample composition doesn't harm the EM grids and that salt is avoided since it can obscure the fibrils. Another thing with this technique is that many artifacts of the procedure can sometimes look like agglomeration, but with careful observation and focusing on different depths they can be separated out from true fibrils.[93] Even though this technique can observe

protofibril formation or segments of it, the small sample size limits the capability of observing this very often and can definitely not be done to observe any living tissues.

Finally, if staining and fibrils have found amyloids being formed then it is often beneficial to check to insure that they express a β-sheet structure under Fourier transform infrared (FTIR), X-ray diffraction or other methods of protein structural analysis. Fourier transform infrared spectroscopy is a technique that obtains an infrared spectrum of absorption or emission of the sample over a wide spectral range and can observe the formation of β-sheet conformation. This technique is very useful though can be difficult since one needs to start with sample that doesn't have the secondary structure to provide a control and then it can detect the change once fibrillation is occurring. There has been some modification of the standard technique in order to get consistency for the rate of fibrillation in a specific amyloid protein.[93] Along with this due to the high level of hydrogen bonding within many of the amyloids even before secondary structure formation that can affect the wavelength found on the FTIR, so that must also be taken into account when using this method. For the X-ray diffraction method the amount of amyloid that is necessary is often large enough that it is beneficial for this to come from the dissection of the infected tissue. The sample for X-ray diffraction also needs to be pure enough that this diffraction pattern can be read as well as it should be devoid of salts and other possible contaminants. Having dehydrated samples often makes this technique significantly easier since it often concentrates the fibril so a better pattern can be found.[93]

All of the techniques discussed previously are useful for either determining if a protein has amyloid forming potential or as a forensic analysis after death. The only technique that has shown any kind of diagnosis ability is magnetic resonance imaging (MRI) since one can observe the effect that the amyloid has on the tissue, with reduction in size for most organs.[105-109] Most MRI imaging is unable to detect the early stages of amylogenesis that involve protofibrils since they are merely observing the plaques effect on surrounding organs. One group did show some success with detecting early stage Alzheimer before symptoms developed by doing regular scans on those patients whose family history indicated a high risk of the disease, but unfortunately there was only so much the treatment could do to slow it down.[105] There are many diseases associated with this protein misfolding and unfortunately we only have so many techniques that can be employed to discover them and only one that has any chance of diagnosis.

3.1.2. *Amyloid Formation in Different Diseases*

Amyloid formation is one of the most biologically damaging examples of molecular self-assembly in nature and has been linked to Alzheimer's, Parkinson's, type II diabetes and at least 20 other diseases.[98] Alzheimer's diseases is the most common form of age-related neurodegenerative disorders and is possibly caused by highly insoluble aggregation of amyloid-β (Aβ) peptide in the brain. [96,110] This slow moving disease makes up 60-70% of dementia patients with early symptom's being short term memory loss and progresses to language problems, disorientation, and gradually the loss of bodily functions and death.[111] Aβ is also associated with another disease that is highly linked with sever forms of Alzheimer's, Cerebral Amyloid Angiopathy (CAA). Even though this disease is rarely found on its own it is associated with amyloid depositions in the walls of small brain arteries and reduces blood flow to the brain with respect to how large the plaque is.[112] Another well-known amyloid related disease is Parkinson's which also effects the brain, but has a slightly different progression than that of Alzheimer's. Unlike Alzheimer's, Parkinson's disease mainly affects the motor system, though there are occurrences of thinking and behavioral problems as well.[113,114] The protein involved in this disease is alpha-synuclein and can often be confused with Lewy body dementia which involves the same protein, but has different early symptoms.[115] Type II diabetes mellitus might not be caused by the amyloid, IAPP (Amylin), and its disruption of a particular organ, but instead it could be through this plaques ability to form permeant toxic oligomers.[116] These are probably some of the most well-known disease and with the others being less common with the amyloids being found in many different locations around the body and are often confused with other diseases such as cancer or normal arthritis when first found.[100,109,117] One of the possible triggers behind Alzheimer's disease could

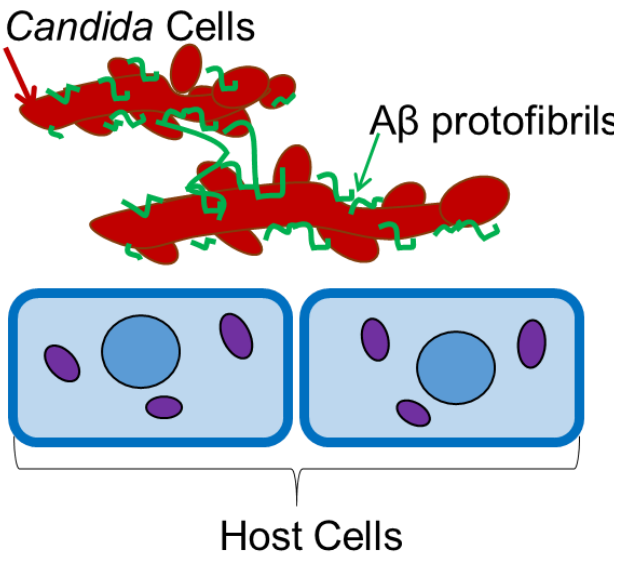

Figure 3.2: Schematic of how Aβ might inhibit Candida cells from binding to the host cell and agglomerating them together. [Adapted from Balin et al]

be a pathogen infection since Aβ is able to bind to bacteria cells in culture to prevent them from binding to the host cell and then agglomerate them to prevent further spread (Figure 3.2).[118-120] The results from Kumar et al. shows distinct antimicrobial properties as well as shows increase life expectancy for mice that had Aβ vs the knock out mice when their brain was infected with bacteria.[120] Aβ has also been found to bind to the herpes simplex virus and appears to be acting as a defensive mechanism against its continued spread.[121,122] Along with pathological triggers, brain trauma also increases the risk of Alzhiemer's, perhaps due to lipid bilayer damage.[123] These triggers all indicate that Aβ most likely preferentially binds to a surface to start misfolding, and not just spontaneously in the solution giving us a way to possible sense this diseases development.

3.1.3. *Aβ in Literature*

Using a full length Aβ 1-40 or 1-42 increases the complexity of interactions and makes analyzing specific domains very difficult. NMR studies have shown that the regions 12-24 and 30-40 in the Aβ protein adopts similar β-strand conformation to the full length peptide.[124] Researchers have also shown that the hydrophobic core (Aβ 16-20: LVFFA) is essential for fibril formation and will form β-sheets in solution though its interactions with surfaces is unknown.[125-130] Any sequence less than 11 amino acids does not form fibrils with the same morphology as the full length Aβ.[127] Due to the difficulty of dissolving the full length Aβ peptide, DMSO is often used while the smaller fragment Aβ12-24 is highly water soluble which adds less non-natural elements to the experiment.[126,131] Mutations to investigate potential mechanisms of binding and assembly can be done easily with the smaller peptides.

Surface interaction mechanisms are important for understanding Aβ fibril formation since there are many surface characteristics found inside the body all of which can influence aggregation leading to possible toxicity in the body.[132] For example, Aβ tends to be localized around lipid bilayers and has been shown to undergo a conformation change from random to β-sheet in their presence.[131-133] Hydrophobic graphite has been used as a model substrate for the interior of the lipid bilayer and allows more sensitive characterization since it is an atomically flat single layer material.[131] Graphite also has many unique properties such as high conductivity, and optical transparency, which make it attractive for a variety of nanomaterial applications.[134] Being able to control and understand these surface interactions can open new avenues to forming unique

nanostructures via self-assembly as well as sensors that allow early detection of these fibrillation processes before they become a problem in the body.[21,135,136]

Previous experiments use high concentrations above 10μM of the full-length peptide, which from our group's previous experience often began fibrillating in the solution rather than on the surface. With these high concentrations it is likely that other researchers are observing solution fibrillation due to homogeneous nucleation and fibril deposition onto the substrate rather than the peptide-surface interactions and heterogeneous nucleation, and therefore the initial stages of the formation are not observed. [95,97,99,131,132,137-139]

3.1.4. *Graphite Mineral*

Graphite has many unique properties that make it ideal for biotechnology and device creation due to its structure and elemental make up. Hexagonal carbon structures make up each layer of graphite which when layered together by Van der Waals is called graphite (Figure 3.3).[140] Many of this material's properties such as its high electrical, thermal and acoustic conduction are very anisotropic and travel along the layers. Another property that is often utilized for mechanical applications is graphite's amazing ability to lubricate joints and other moving parts. Another than its lubricating properties graphite's mechanical properties can vary considerably depending on how the layers are stacked on one another, though in all arrangements it is very brittle. Even though mechanically it might not seem useful it can still be used in composites to lead strength to the carbon fiber-reinforced plastics and heat resistant composites. The properties that are instrumental in this study though is the fact that graphite is atomically flat and due to the carbon-carbon chain and hydrophobicity it can be considered a decent mimic for the inner surface of the lipid bilayer. Being atomically flat allows for easier characterization of assembly on the surface with the atomic force microscope. Highly oriented pyrolytic graphite (HOPG) is used widely in research since it is organized so that the degree between planes is minimized sometimes even being less than 1° of spread between them.

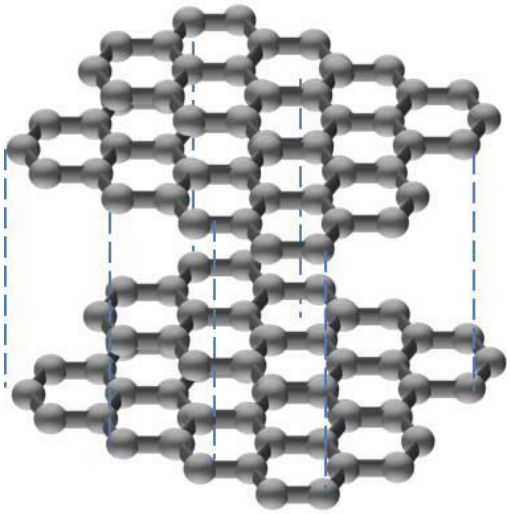

Figure 3.3: Graphite structure schematic where the gray spheres are carbon and the dotted lines are secondary structure [Adapted from Delhaes et al][133]

3.1.5. *Solid Binding Peptide on Graphite*

Due to the many advantageous properties that graphite possesses many groups are interested in trying to harness this material for many device and other applications. Our group has done a significant amount of work on selecting peptides that are able to interact with the surface of graphite. We have done selection on graphite for strong binding peptides using phage display.[9] Due to the quenching ability of graphite we were unable to perform normal fluorescent microscopy techniques to characterize the peptides found, but instead used absorbance scanning to determine the level of binding onto graphite particles. Once characterized, several of the strong binders were synthesized and binding was tested on the surface of graphite. One of the peptides, GrBP5, showed remarkable ability to recognize and assemble onto the surface of the mineral as seen in Figure 3.4.[9] Several mutations were chosen rationally that would help determine which motifs within GrBP5 were responsible for binding and assembly. From these mutations it was found that the two tyrosines near the C terminus were heavily involved with binding and that the N-terminus region was amphiphilic which was involved in the assembly process.[9] From this discovery others in our lab have proceeded to functionalize this peptide even more by adding hydrophilic groups on the N-terminus that would be displayed at assembly and biotin to then attach other peptides onto the surface.[11,29] GrBP5's motifs have been instrumental in helping rationally decide which possible segment of the larger amyloid proteins could possibly be involved with assembly.

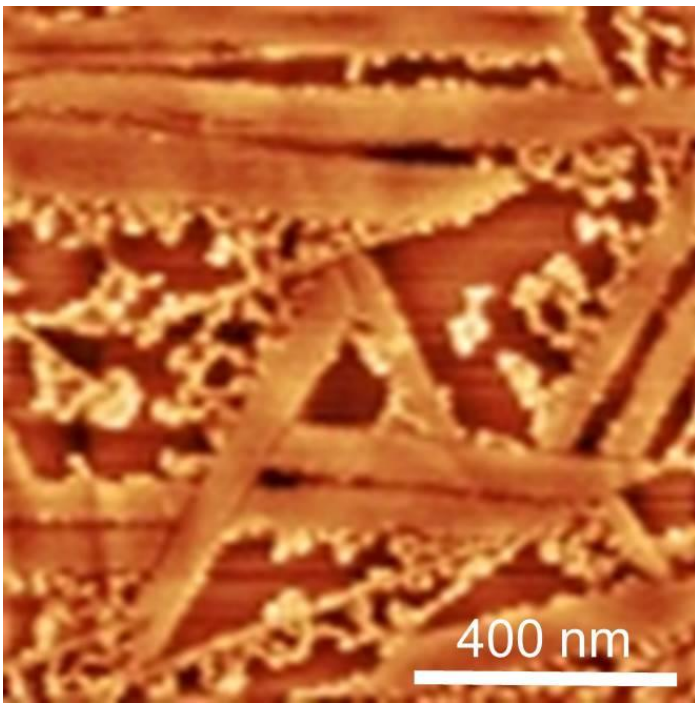

Figure 3.4: AFM image of GrBP5 in water on graphite at 1μM at 1hr incubation. [Courtesy of Tamon Page]

3.2. Methods

3.2.1. *Sample Preparation for Microscopy*

Ex situ imaging was done on freshly cleaved HOPG surfaces mounted on a nickel specimen puck (Ted Pella Inc., Redding, CA) and incubated with 30uL of aqueous peptide solution for 1hr to 3hrs in a 100RH sealed chamber at room temperature. As shown in figure 3.5 the liquid was wicked off with a KimWipe and dried under a gentle stream of N_2 gas. For the rest of the images the sample was places on a piece of copper submerged in liquid nitrogen and it would freeze in less than 10sec. The samples were then quickly moved to a modified scintillation vial that contained a glass column elevating the sample to minimize contact to any warm elements. These vials were then immediately places in a standard freeze-drier with a liquid N_2 condensing plate to sublime the frozen incubation solutions. The samples were left for 3hrs to dry with a rate of ~10μL/h. We performed wide-ranging concentration and time measurements using the Aβ peptide and mutants and found similarities in coverage, height and density trends taking at least 3 images per sample.

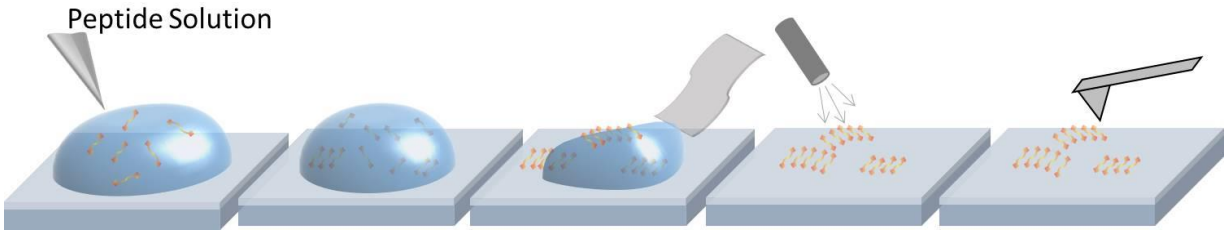

Figure 3.5: Sample preparation for microscopy of peptide solution.

3.2.2. *Atomic Force Microscopy*

AFM was done on a Digital Instruments (Veeco, Santa Barbara, CA) Multimode Nanoscope IIIa scanning probe microscope equipped with high frequency NanoSensors PPP-NCHR (NanoandMore, USA, Lady's Island, SC, USA) noncontact probes, with a 42N/m spring constant at a 2-3 amplitude set point.

3.2.3. *AFM Image Processing*

Topographic features that originate from the HOPG surface were removed by image subtraction to allow large area coverage analysis of peptides. The image filters and simple image operations

were applied by the software Gwyddion (Czech Metrology Institute, Czech Republic) to the raw AFM data. Images were corrected for tilt by a first order plane subtraction, while fast scan lines were corrected by aligning their median z-offset. If large wavy features were present an erosion filter was applied to get a secondary image with only the topography of the bare surface present. Subtracting this secondary image from the original AFM image yielded a background subtracted image that was used for surface coverage analysis.

3.2.4. *Molecular Structure Modeling*

HyperChem 7.5 modeling system was used to determine the possible binding motifs of Aβ on a graphite surface. First the lowest energy was found in a vacuum with no surface added and then the lowest energy state was put into a system that contained water and then a multi-layered graphite surface (5 layers). The lowest energy state was also rotated when created to help with finding its lowest energy state on the surface. Once the energy state was finished visualization of the lowest energy structure was done on VMD (Visual Molecular Dynamic) an open source visualization program provided by the University of Illinois.[141]

3.2.5. *Contact Angle*

The samples were incubated in the same conditions as AFM in order to get similar assembly results. Static contact angles were measured using an FTA1000B Goniometer (First Ten Angstroms, Inc., Portsmouth, VA) with an automatic camera system by placing 1µl of the same solution as was used to produce the sample in two to three different locations on each surface. The measurement was made immediately. The liquid surface tension was determined by pendant drop shape method, and was found not to vary significantly for different solutions. In all, at least two measurements were taken on two different samples for each data point. The samples were then dried with nitrogen and the coverage was measured by AFM.

3.3. Results and Discussion

3.3.1. *Aβ Fragment Wild Type Characterization*

We analyzed the interaction of the Aβ 12-24 fragment (VHHQKLVFFAEDV, Figure 3.6a) with a graphite surface over several time points. The atomic force microscope (AFM) image of the HOPG substrate incubated in 1μM of Aβ 12-24 for 3hrs shows unique organized self-assembly (Figure 3.6b). The highest point on the image is at ~1.8nm indicating that the peptide is likely not fully stretched at this point and that a monolayer is forming on the surface since the longest dimension of the fully stretched peptide is ~5nm. This effect has been observed in an elastin-like amyloid forming peptide that formed several layers on the AFM at ~50°C with the layers having a height of 0.65nm.[142] Though this is a possibility it would require that the surface of the first layer be atomically flat since in the 1μM case the area surrounding the wires had a change of less than 0.5nm in height, which is consistent with flat graphite. The discrete maxima on the fast Fourier transform, FFT, (Figure 3.6c) shows six-fold symmetry that is off by 7 and 4 degrees which can be due to scanning artifacts in the AFM or might be due to the peptides organizing slightly off from the carbon patterning. From this symmetry is it is clear that this fragment is also able to recognize the hexagonal graphite lattice and preferentially grow along the specific crystallographic directions similar to the full length protein on graphite.[131]

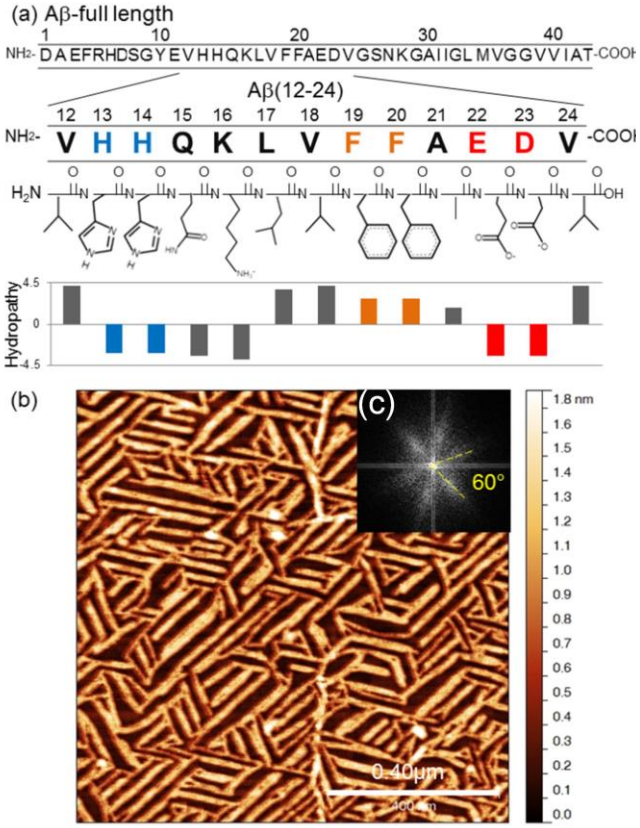

Figure 3.6: Chemical properties of Aβ12-24 sequence and its ordered self-assembly nanostructure on graphite. (a) Aβ12-24 sequence with hydropathy (defined by Hopp-Woods) being negative for hydrophobic regions and positive for hydrophilic regions. (b) AFM image of Aβ12-24 on graphite showing ordering and displaying unique symmetry in (c) the FFT of the AFM image.

Further investigation on the formation of organized assembly was done by varying concentrations and times while calculating coverage (Figure 3.7). These samples were produced

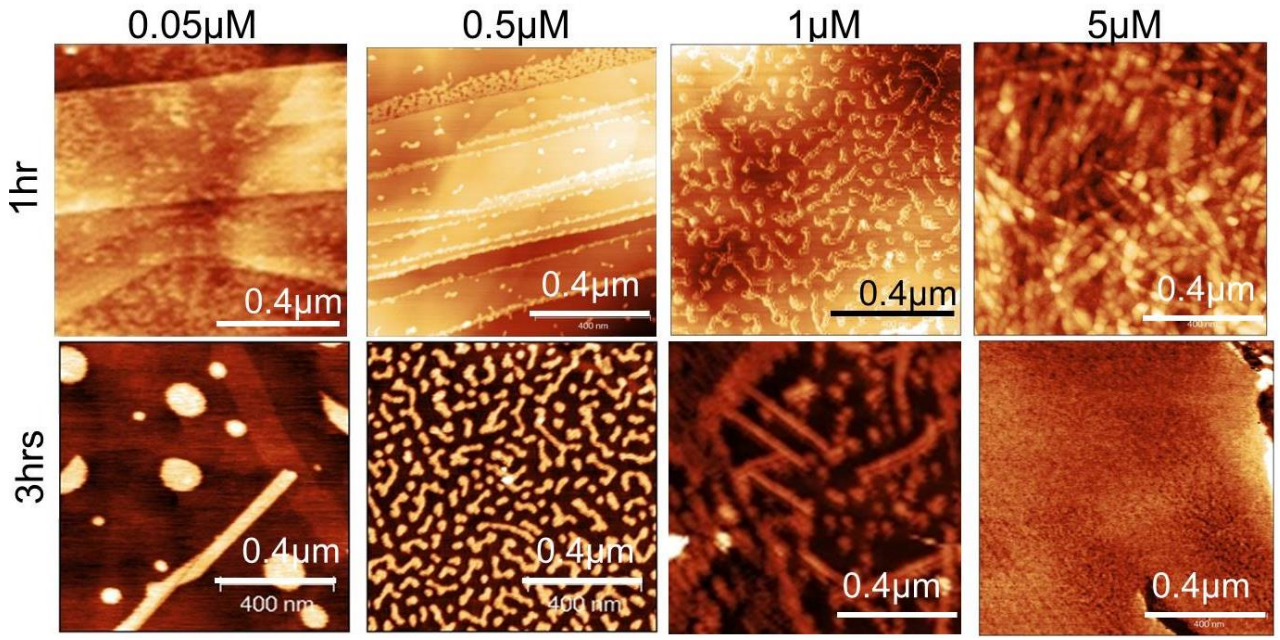

Figure 3.7: Time-lapsed images of Aβ12-24 at different concentrations

using a freeze drying approach discussed in the methods section to reduce the amount of drying affects that are sometimes seen at lower concentrations using the wicking method, but organization can still be seen at around 1μM concentration. For the lower concentrations below 1μM for both the 1hr and 3hrs unorganized agglomerations are seen with a higher frequency near cleavage planes (Figure 3.7). At 1μM peptide concentration after 1hr small wires appear though small and disorganized while after 3hrs organized self-assembly is apparent in many areas with some amorphous agglomerations surrounding it (Figure 3.7). From the coverage analysis it appears that coverage changes slightly from 1hr to 3hrs which can be expected since the peptides would have more time to interact with the surface and grow after 3hrs than just 1hr (Figure 3.8).

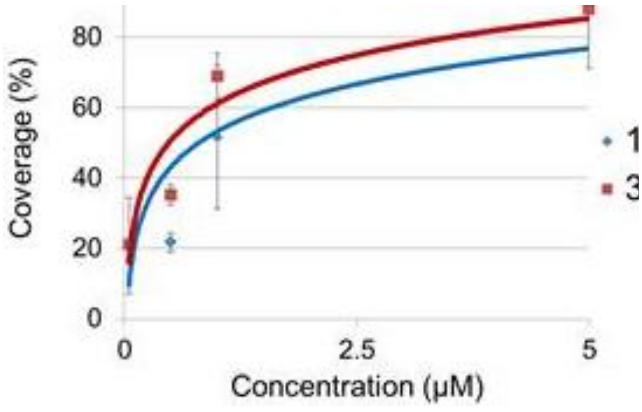

Figure 3.8: Plot of peptide coverage showing differences between the 3hrs and 1hr incubation times.

3.3.2. *Finding Domains using Computational Method*

In order to demonstrate that this film of Aβ 12-24 can be further interrogated by rational mutations of the peptide we identified two unique regions that we classified as the binding domain and the assembly domain. These domains were chosen based on the minimum energy conformations that Aβ (12-24) forms on the surface as determined by molecular dynamics (Figure 3.9).

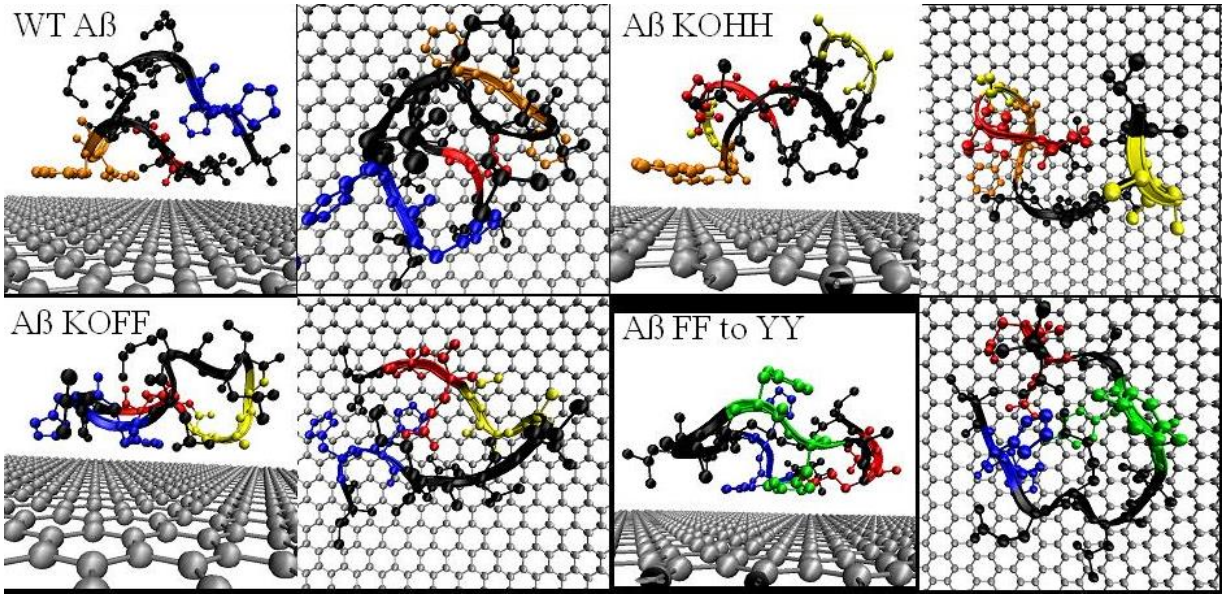

Figure 3.9: Minimum energy conformation of Aβ (12-24) and mutations. Images created in HyperChem7. The orange regions are the phenylanalines, the blue is histadine, yellow is alanine and green is tyrosine.

In this model the wild type Aβ appears to be binding with the phenylanalines exclusively and displaying the histadine for possible assembly. In order to test this we did a knock out of the phenylanalines and the histadine to see how this might affect the conformation via the comutational model. In the knock out mutation, KOFF, the binding region switches to be histadine which was expected since they can function similar to aromatic groups under certain siutations. The histadine knockout did not seem to affect the binding motif which is good, but due to computational limitations assembly affect is unknown via this method. In the tyrosine substitution both the histadine and the tyrosine bound to the surface, which would probably create a better binder to the surface, but not so much to other peptides so the assembly may or may not occur.

3.3.3. ***Mutation Characterization***

The binding domain is shown to be comprised of the two phenylalanines present in the peptide, while the histidines appear to have a large role in assembly. To experimentally confirm this hypothesis, we did two sets of alanine knockout mutation: KOFF targeted the phenylalanines in the hydrophobic core while KOHH removed the histidines believed to be the assembly domain (Table 3.1). Knockout of HH did show small wires being formed even at 0.5μM, but they appeared to be in random orientations and never reached the level of ordering as see in the

wildtype peptide (Figure 3.10). From the structural analysis (Figure 3.9) it appears that the histidines began binding to the surface once the phenylalanines are removed. This is consistent with other literature indicating that histidine binds to carbon surfaces, though it is much weaker than other aromatic groups.[143,144] Knockout of FF at the lower concentrations acted very similar to the wild type peptide in that small wires could be seen, but mostly small agglomerations were apparent after 3hrs (Figure 3.10). Even at the higher concentrations no organized self-assembly was seen unlike with the wild type peptide (Figure 3.10). For mutant 1 KOFF, the coverage actually seems to increase compared to the wild type, reaching 80% at 2µM concentration (Figure 3.10). This increase in binding could be due the switching of the binding domain to the histdines which may have a stronger interaction with the surface for this peptide. At the same conditions as the wild type peptide this mutant is unable to form organized wires, but instead forms agglomerates. On the other hand, KOHH has a decrease in binding compared to the wildtype since at 2µM it reaches 50% coverage unlike the wildtype which reaches it at 1µM (Figure 3.10). These results indicate that these amino acids contribute significantly to, but are not solely responsible for binding. One possibility is that for this mutant the phenylalanine is switched over to the role of binding and so only slight amphiphilic bonding remains to form wires and so they are unable to organize on the surface as well as the wild type. In order to further investigate these domains a knock in mutant was created where a known strong binding amino acid, tyrosine (Y), was substituted for the phenylalanines (F), and called Aβ FFtoYY (Table 3.1). The knock in mutant showed an increased coverage, but did not show organization until it reach a certain concentration where it created a multilayer and began organizing. These results conclude that Aβ 12-24 is able to recognize the HOPG surface using its binding domain of phenylalanines to assistant with complex organized assembly (Figure 3.10).

Table 3.1: Mutations made in 12-24 Aβ. Positively Charged AA (K,R) – blue, Negatively Charged AA (E,D) – red, Hydrophobic AA (A,I,L,M,P,V,G) – black, Polar AA (N,Q,S,T,C) - bright green, Aromatic AA (F,W,Y) - orange, Histidine (H) - light blue, pI and charge computed using ProtParam Tool at expassy.org

Peptide	Sequence	MW	pI
WT Aβ (12-24)	VHHQKLVFFAEDV	1568.80	5.99
Aβ KOHH	VAAQKLVFFAEDV	1436.67	4.37
Aβ KOFF	VHHQKLVAAAEDV	1416.60	5.99
Aβ FF to YY	VHHQKLVYYAEDV	1600.79	5.99

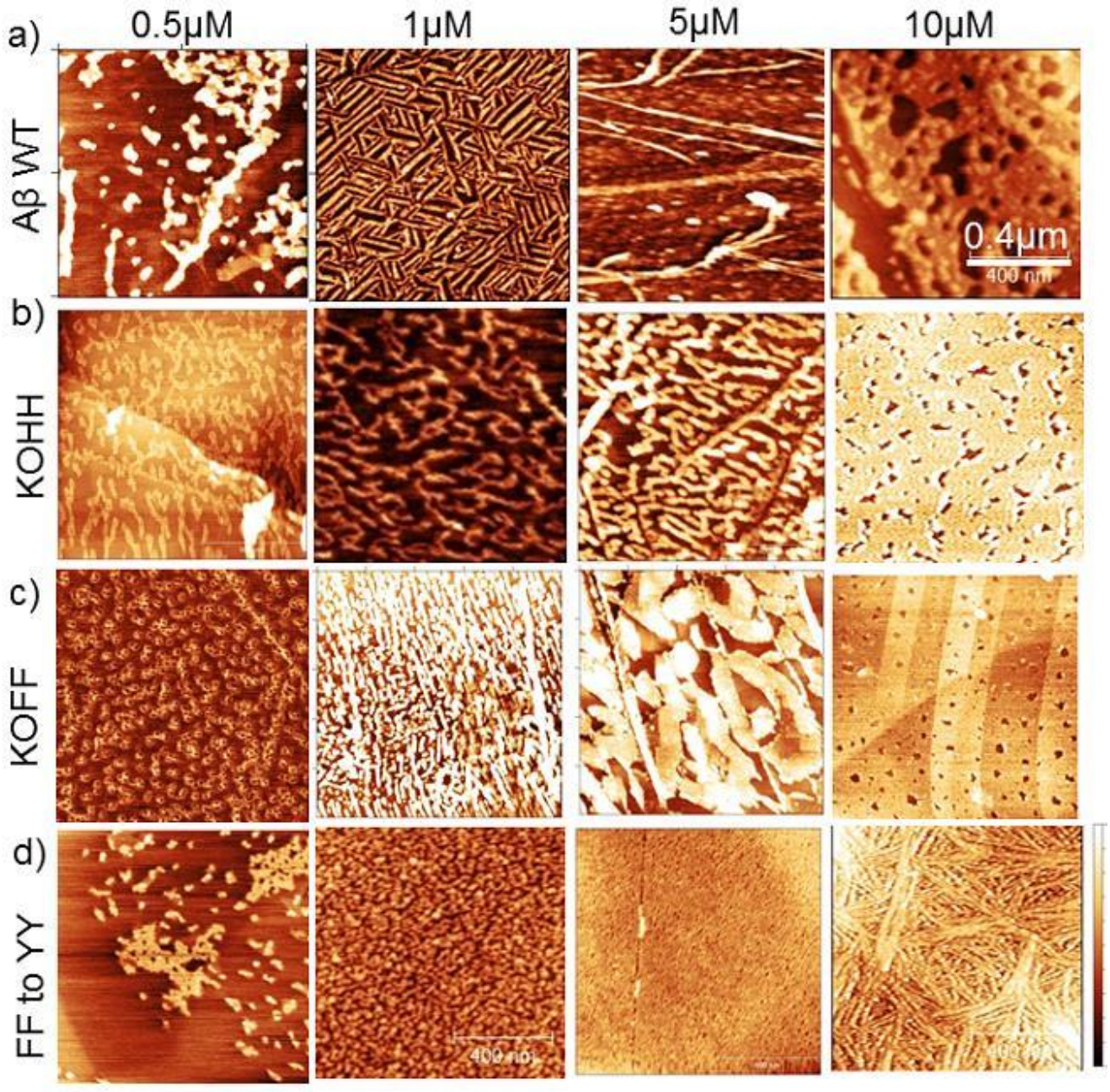

Figure 3.10: AFM images of Aβ WT peptide and mutates under the same conditions, 1μM and 3hr incubation time.

3.3.4. *Contact Angle*

Contact angle measurements were done on each of the mutants to see how they affect the surface hydrophobicity and to help with determining possible display groups (Figure 3.11). Bare graphite has a surface a contact angle of 79.5°.[11] The wild type and the tyrosine knock in both were very similar to the bare graphite surface, having an average contact angle of 75.6° +/- 6° and 80.7° +/- 3.6° though the wild type being slightly more hydrophilic than the FF to YY mutant. Both knock outs KOHH and KOFF dropped the hydrophobicity with average contact angles of 75.9° and 64.2°. This drop makes sense due to the fact that they are missing an aromatic or aromatic-like group which contributes significantly to a peptide's hydrophobic profile. The KOHH had low enough coverage of around 28% that the standard deviated was very high of 8.5°, due to if the drop was placed on an area was bare or not.

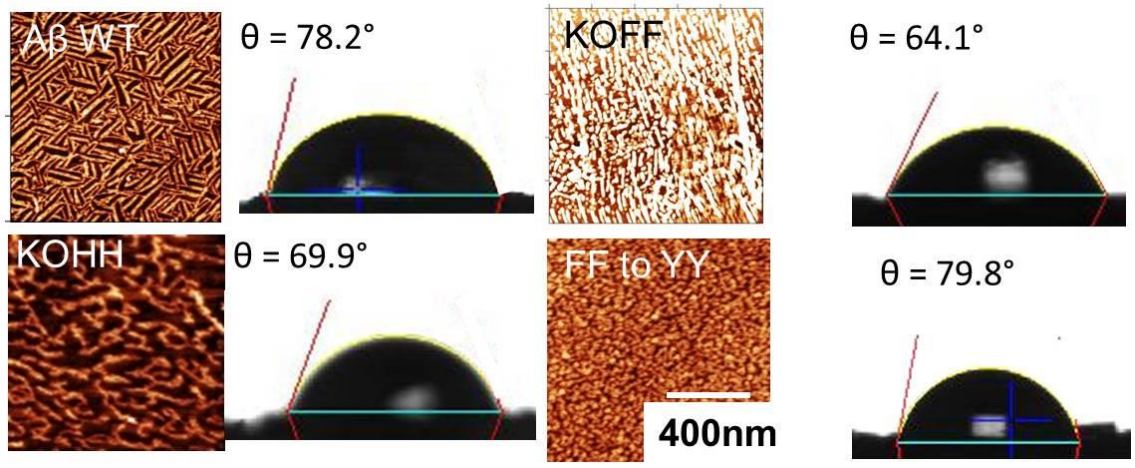

Figure 3.11: Contact Angle measurements on the surface modified with Aβ and mutates

3.3.5. *Inhibiting Fibril Formation*

The fact that the Aβ KOFF mutant does not bind well to the surface, but is still able to form fibrils, indicates that this mutant could also be able to form complexes with the wild type peptide and reduce surface binding. To test whether Aβ KOFF could be used as an inhibitor, 1μM of the wild-type Aβ peptide was incubated with different concentrations of the mutant for 3 hours to see if assembly would be able to proceed (Figure 3.12). Figure 3.12 (b), shows that small concentrations of KOFF is able to inhibit formation, but at a certain concentration, 0.5 μM, the overall coverage increases significantly to the same level as the 1 μM wild-type alone, but does not assemble on the surface. When the concentration of the mutant is increased further the

coverage decreases on the surface. These results are consistent with the idea that the mutant is binding to the wild-type and inhibiting assembly, though binding is only affected at very low and high concentrations.

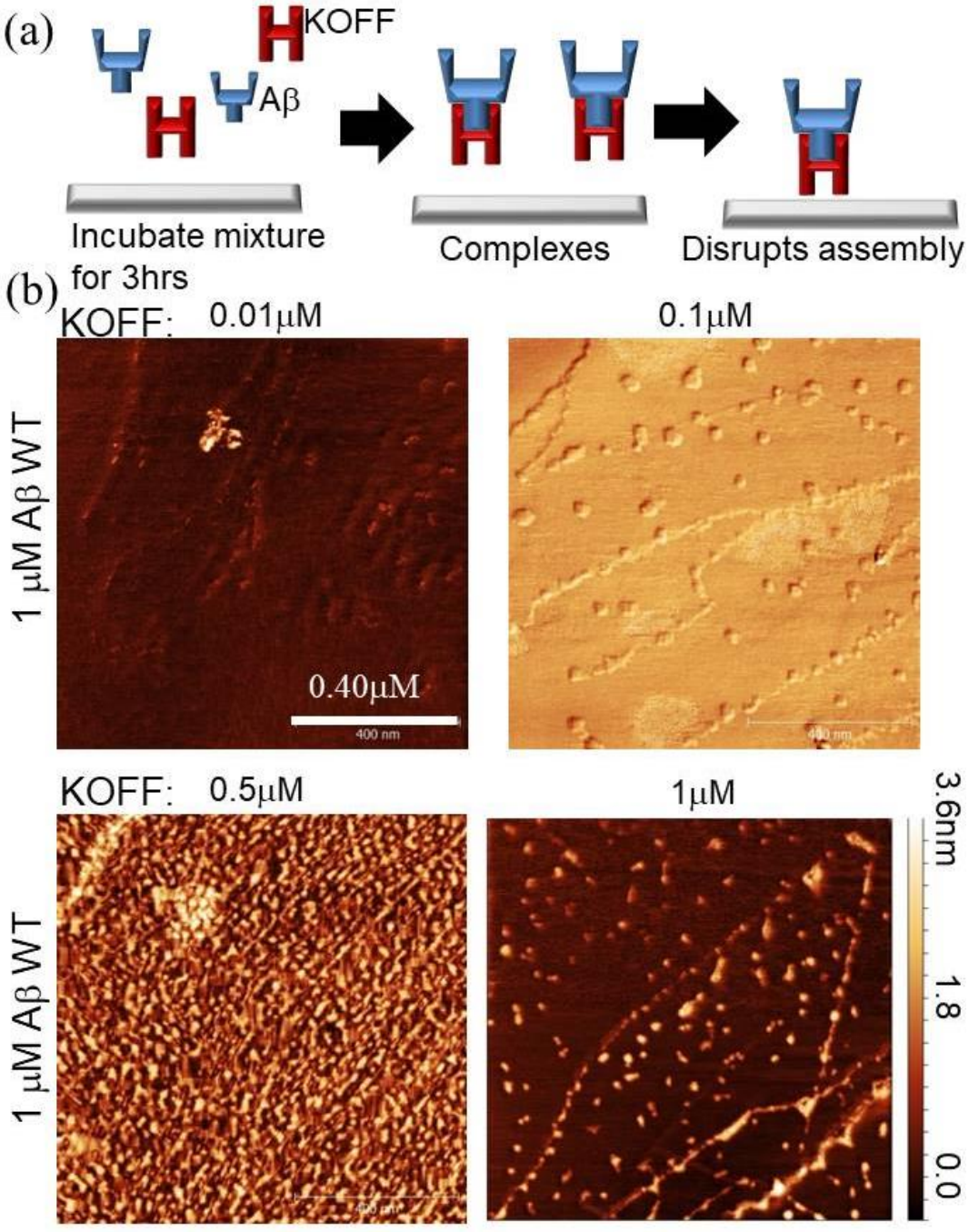

Figure 3.12: Effect of KOFF on Aβ mineralization a) Schematic of KOFFs hypnotized effect on Aβ assembly b) AFM of Aβs assembly being disrupted by addition of KOFFs at different concentrations. All images were taken at conditions that allow Aβ to assemble normally without KOFFs addition.

3.4. Conclusion

The detailed investigation discussed in the previous sections indicates that there are domains associated with the organized formation of the Aβ 12-24 fragment on HOPG. Domains within this peptide were identified that influenced its binding to the surface as well as fibril assembly. When the binding domain, which involved two histidines was knocked out binding was reduced and fibril formation was still seen though the six fold organization found on the surface was non-existent. Knockout of the two phenylalanines in the assembly domain increased the amount of binding to the surface resulting in a higher overall coverage at lower concentrations most likely due to removing the steric hindrances affecting the histidines. The knock-in mutation did provide some amount of assembly at higher concentration, perhaps this is when the histadine is not being needed to bind on the surface as indicated by the molecular dynamic computations. Identification of these different binding and assembly domains for this Aβ 12-24 fragment can give insight into the importance of this fragment in the full length protein used for medicine and help toward the development of new nanotechnology. Mutant inhibition work can also give many insights that might help with understanding possible treatments for this misfolded assembly process.

Chapter 4: **Control of crystal polymorph by peptides**

For millions of years, nature has created complex mineral systems that have unique mechanical properties due to their delicate organization of inorganic materials that have been molded into intricate architectures. The most well-known and abundant of these biominerals is calcium carbonate ($CaCO_3$).[145] Calcium carbonate is found in diverse geography and geology all over the world. Technologically, its one form or another has been used in almost every industry from paper (as filler particles) to pharmaceuticals for hundreds of years. Even with many researchers working on it for the last 100 years the current technology is nowhere close to the level of control that nature exhibits over this material's formation, crystallography and morphology with just proteins.[146,147] In spite of these extensive studies, however, the exact mechanism(s) of calcium carbonate (for that matter any kind of) biomineralization are still not well understood. Calcium carbonate is also a great model system for understanding polymorph determination in biology, which can then be utilized for different practical applications in everyday technology. Mainly because of the complexity of the naturally occurring proteins and their multi-faceted effects on a variety of biofabrication, the in depth study of biomineralization has been next to impossible so far.[148] Therefore, this chapter will focus on the effect of combinatorial selected short polypeptides on biominealization in a molecular biomimetics platform. Specifically, using a cell-surface display library, two sets (containing more than 50 sequences each) of dodecapeptides were selected using two forms of $CaCO_3$, aragonite and calcite, as substrates. These peptides were then characterized in terms of their binding characteristics to the respective forms of carbonates and then mineralization assays were generated using several of the peptides from each set to find out if they are able to exhibit specificity in binding and a control over polymorph formation through well-established biomineralization assays.

4.1. Background

4.1.1. *Calcium Carbonate Mineral*

To understand calcium carbonates' versatility in biology and industry, one must first recognize the different crystal structures that it possesses. Calcium carbonate exists in three anhydrous crystalline forms: calcite (Rhombohedra), aragonite (Orthorhombic) and vaterite (Hexagonal) and two hydrated forms: calcium carbonate hexahydrate and calcium carbonate monohydrate.[145,149,150] There is also an amorphous form which highly unstable at standard

conditions.[145] The anhydrous structures are the most commonly found with some being more prevalent than others.

Calcite is the most abundant polymorph since it is thermodynamically stable under ambient conditions of room temperature and atmospheric pressure, and has a Gibbs free energy of -1129.176 kJ/mol.[151] This low ΔG originates from the fact that calcite has a face-centered rhombohedral unit cell that allows for the distance between the calcium atom and the oxygen atoms to be shorter than any other crystal structures of $CaCO_3$, as seen in figure 4.1 (a).[145,149] Even though the distances between these atoms are very small, the overall density of the calcite mineral is actually quite low compared to, for example, the aragonite phase. The density of calcite is 2.71 g/cc while that of aragonite is 2.93 g/cc; this difference is due to the unique packing of the aragonite structure that allows the CO_3^{-2} ion groups to be closer to Ca^{+2} ions than those in calcite.[149] The aragonite phase (orthorhombic) has a slightly more positive gibbs free energy of -1128.355 kJ/mol compared to calcite. [151] Even though aragonite is metastable, if stored in dry conditions it will remain unaltered for tens of millions of years at temperatures below 400°C.[149] If water is present, however, aragonite will convert to calcite in a matter of months due to its solubility.[149] The difference in solubility is one of the reasons why aragonite is not as common in geological beds and is rarely found outside of organically controlled systems. As seen in figure 4.1 (b) the calcium ion is very close to the limiting value for transition making aragonite's orthorhomobic structure fairly easy to shift into the thermodynamically stable rhombohedral structure, though depending on approach the activation energy ranges from 159 to 452 kJ/mol.[145,149,150]

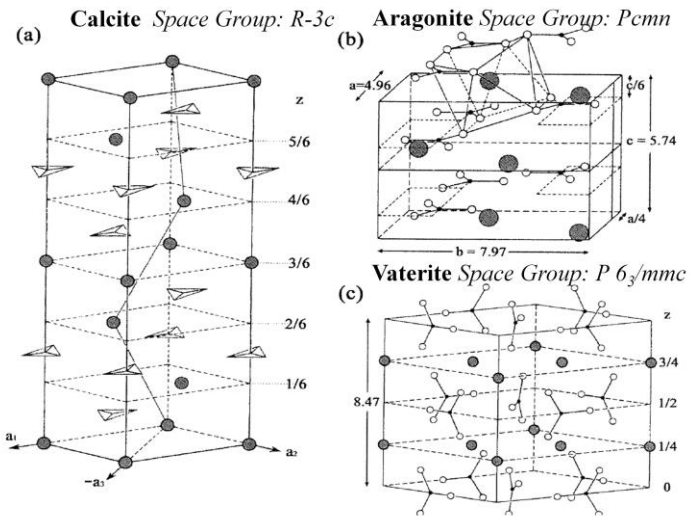

Figure 4.1: Unit cells of the three anhydrous CaCO3 polymorphs: a) calcite b) aragonite c) vaterite1 Grey circles are calcium, white circles or line endpoints are oxygen and black dots are carbon.

The kinetically favored polymorph of calcium carbonate is vaterite, which has a hexagonal unit cell with the CO_3 groups parallel to the c-axis (fig 4.1 (c)).[145] This metastable form has a density of 2.65 and requires a loosely packed structure which coincides with its low stability.[149] Vaterite is rarely found in nature since it is not thermodynamically favored and will often transform quickly into one of the other anhydrous polymorphs. If inhibitors to the calcite and aragonite polymorph are present however, vaterite can stabilized, which is why it can be found in laboratory experiments.

4.1.2. *Calcium Carbonate in Nature*

Throughout nature organisms have created structures out of inorganic minerals, with up to 60 biominerals being recognized, but none have achieved the prevalence of $CaCO_3$ within biological systems.[145] This extensiveness has led to a wide variety of functions and unique architectures. Different arrangements of $CaCO_3$ have been

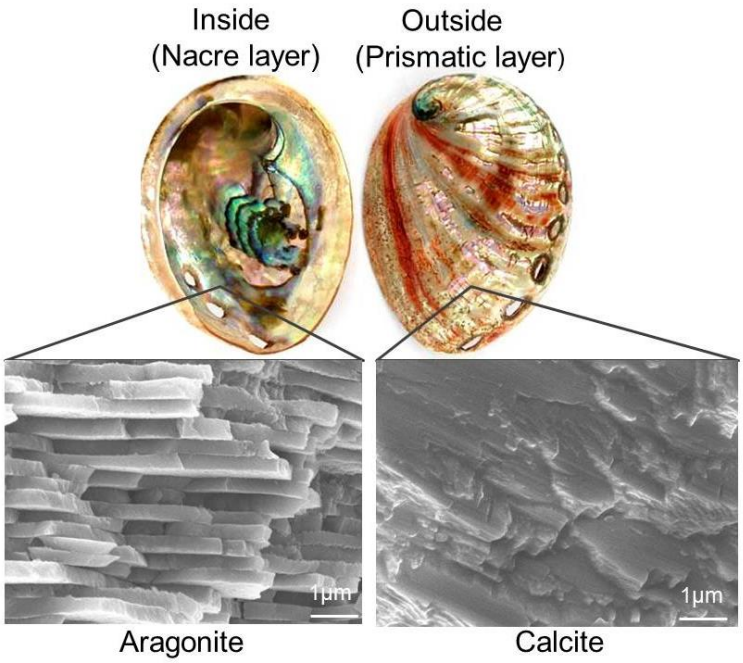

Figure 4.2: Abalone shell image with a SEM image of the nacre and prismatic layer at 15,000X magnification

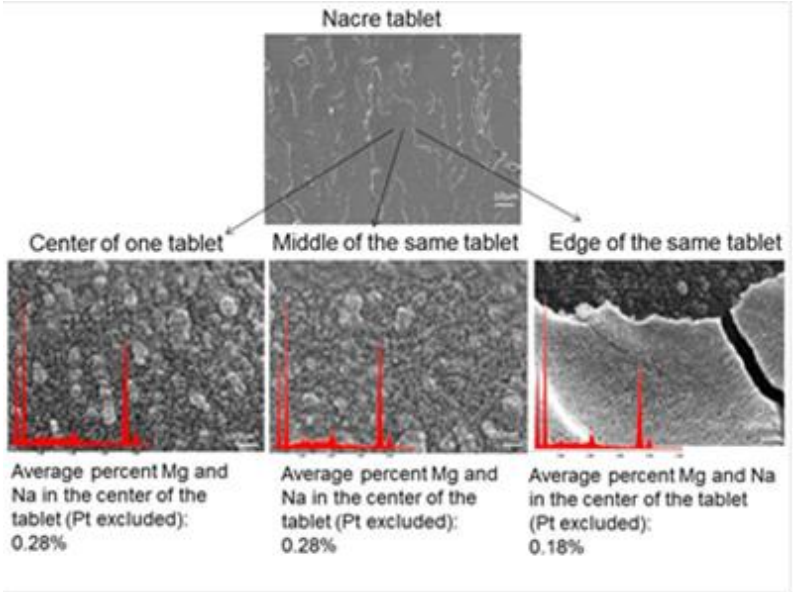

Figure 4.3: SEM and EDS showing the average magnesium percentage for different areas of a nacre tablet within an abalone shell.

known to increase its strength from 30MPa in its geological form to between 100-300MPa in shells.[152] Mollusks that live in colder environments, fresh water or have high levels of predation tend to form the toughest shells that have two different polymorph layers. The top prismatic layer (calcite) and the inside, nacre layer, (aragonite) helps protect the mollusk within by exemplifying the different physical properties of these crystal structures as seen in figure 4.2. In environments lacking high Mg concentration calcite is necessary on the outside of the shell to slow the dissolution of the ions back into the environment. Even though it does not have a well-defined microstructure the prismatic layer also has a higher compressive strength than the inside and acts like armor protecting the creature from piercing damage.[153] The nacre layer on the other hand is arranged in a brick and mortar configuration where aragonite tablets are stacked with an organic layer in between. This formation prevents uncontrolled crack growth if the stress is normal to the shell while if it is shear stress the tablets are able to slide over each other with the help of the organic matrix.[153] Also this inside layer has a very high bend and tensile strength that further deters predators.[153] Along with this being in two different crystal structure layers produces residual stresses that help absorb energy from the impact further lengthening the time before failure.[154]

Another unique finding of these shells is the lack of Mg that is incorporated within these layers even though the surrounding fluids contain a significant amount of this ion. Mollusk's extrapallial fluid where they build the shells has a similar ratio of magnesium to calcium as the surrounding ocean which can vary from 3:1 to 5.2:1 depending on the location.[155],[156,157] In one of Gower's papers she shows that with a 3:1 and 5:1 ratio of Mg to Ca and same amount of polymer added there is 20% to 30% of Mg incorporating into the films.[158] From the EDS on three different locations on several nacre tablets of an abalone shell there is an average of less than one percent on any particular area as seen in figure 4.3. These results are consistent with those in the literature which is around 60ppm of Mg in aragonite shell layers.[159] The level of control of all these aspects is done by the organism's use of proteins to organize this amazing biomineral.

4.1.3. *Calcium Carbonate in Industry*

Calcium carbonate is found in almost every major industry due to its versatile nature. In ancient societies shells were used as prestige goods that were fashioned into jewelry or other ornaments.[160] Today shells and pearls are still prevalent in the jewelry industry for their unique appearance. In pharmaceuticals $CaCO_3$ is found in calcium supplements as well as is often the

binder in many chewable pills.[161,162] The paper and paint industry use $CaCO_3$ as a filler or pigment due to its high brightness and apparent light scattering coefficient.[163] In the paper industry the size of the filler particles are very important since it determines how stiff and glossy the page is.[163] In the construction industry $CaCO_3$ is found almost everywhere since it is a major component of marble and limestone which is used in cement. Nature long ago realized $CaCO_3$'s building potential and has been using proteins to model with it for millions of years.

4.2. Experimental Approaches

4.2.1. *Selection and Characterization of Peptides (CalBPs and AraBPs) Using Cell Surface Display*

Calcite and aragonite binding peptides were selected from the FliTrx random peptide display library (Invitrogen, USA). This library contains FLITRX bacteria that have randomized dodecapeptides inserted into their flagellin protein allowing the bacteria to stick to a specific substrate. The two different polymorphs of calcium carbonate were both from Agate Design in Seattle and considered very pure. Cleavage of calcite was done with a razor, while a saw was used to cut the aragonite into approximately 0.5 cm square samples for the panning experiment. Several of these substrates were then cleaned using standard washing procedures

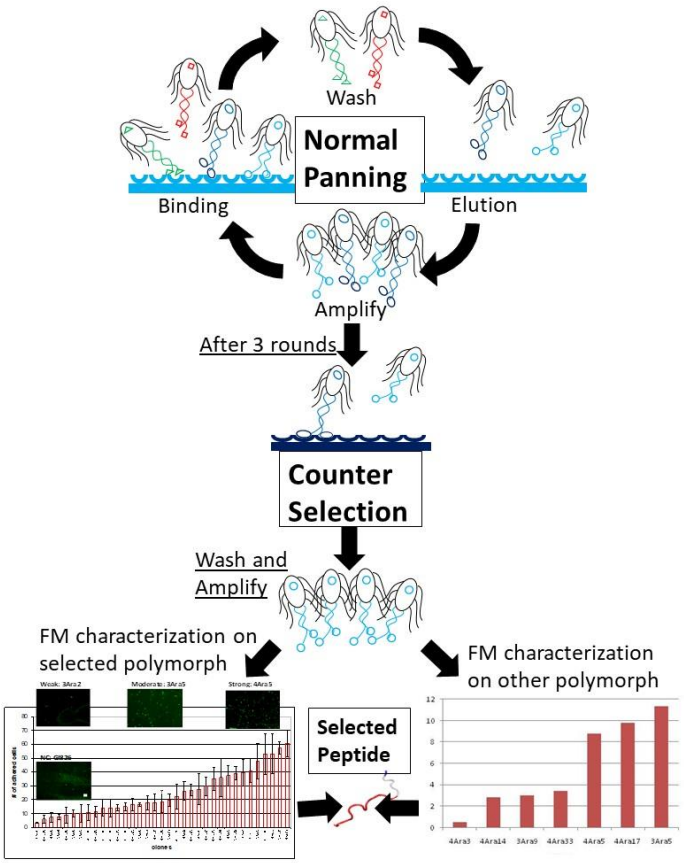

Figure 4.4: Schematic of cell surface display with counter selection.

where methonal/acetone (50:50), then isoproponal and then deionized water were added to the sample and sonicated after each addition.[54] Three rounds of panning were performed according to the method developed by Invitrogen on both materials. Afterwards a "counter selection" was done to insure the chosen peptides were specific to a particular polymorph of calcium carbonate. A schematic of the normal and counter selection rounds is shown in Figure 4.4. For the counter selection the amplified cells from the previous round were incubated with a different polymorph of $CaCO_3$ for 1 hr. Then the substrate was removed and the cells that did not bind were amplified in IMC overnight. Sequencing was done by the University of Washington Microbiology department. Molecular weight, pI and charge were calculated using the ProtParam Tool at expassy.org.

FM was used for the characterization experiments of all 86 clones. For the FM characterization, the aragonite was polished to create a more uniform surface while the calcite was freshly cleaved. Binding affinity for the clones was determined by comparing the number of adhering cells in at least three different fields on the substrate. By comparing the number of cells found on each substrate the clones were sorted into three groups: strong, medium and weak binders.

4.2.2. *Synthesis and Purification of Calcite and Aragonite Binding Peptides (CalBPs and AraBPs)*

Calcite and aragonite binding peptides were synthesized using a Fmoc solid-phase peptide synthesizer (CS336X, CSBio Inc., Menlo Park, CA) and purified using C-18 reversed-phase high- performance liquid chromatography (RP-HPLC) to a purity > 95% (Bio-Peptide Co.). During purification, several fractions were collected from the scaled semipreparative separation (Waters Deltaprep 600, semiprep mode). The collected high-peak solutions were later identified by MALDI-TOF mass spectrometry. The purified aqueous peptide was lyophilized overnight in a Vertis Benchtop K cryodessicator (SP Industries, Inc., Warminster, PA).

4.2.3. *Amino Acid Composition Calculations*

An expected and observed frequency of occurrence was found for each amino acid based on calculations done by Hnilova et al.[54] To get the expected frequency randomized dodecapeptide were synthesized as (XNN)12, where N was any nucleotide and X was a nucleotide that had a biased ratio of G:A:C:T of 7:7:7:3. The observed frequency was generated by sequencing all 86 clones that bound to substrates and counting the number of each amino acid using protparam.

These were then compared to create the relative abundance for a particular amino acid in the set of binders as seen in figure 4.6.

4.2.4. *Similarity Analysis and Protein Derived Peptides*

Protein derived peptides were selected using a knowledge based design approach developed by E. Emre Oren[54,60]. The binding characteristics of a set of calcite and aragonite binders (CalBP and AraBP) were compared with sequences of naturally occurring proteins to create new peptides with enhanced binding affinities. A similarity analysis was used to make these comparisons that utilized the Needleman-Wunsch dynamic programming algorithm, giving an optimal scoring alignment with a given scoring matrix.[60] This matrix was used to find the overall similarity score by summing all of the similarity values of the aligned residue pairs and subtracting a gap penalty of every insertion or deletion introduced into the alignment.[60] The similarity matrix was then applied to sequences found in nature to determine areas that may function as binding sites.

4.2.5. *Characterization of Synthesized Peptides using FM*

Synthesized peptides were functionalized with biotin while still on the resin and purified using RP-HPLC. Calcite and aragonite substrates were first crushed into a fine powder using a mortar and pestle and 10mg of each were weighed out into microcentrifuge tubes and cleaned using the method described in section 2.1. The clean substrates were then incubated with 100μl of 1mg/ml pure peptide stock solution for 2hrs. After this time the substrates were washed with 1X PBS solution twice. Then 50μl of 1:200 diluted fluorescent quantum-dot nanocrystals (QD) were added and allowed to incubate for 15mins. The substrates were then washed 3 times with PBS solution and dissolved in 30μl of this buffer. Only 10μl of this mixture was then plated onto a glass slide and mounted on a Nikon Eclipse TE-2000U Florescence Microscope (Nikon, Japan). This microscope is coupled with a Hamamatsu ORCA-ER cooled charged coupled device (CCD) camera for taking images and a QD605 (exciter 320-460, dichroic 475, emitter 605/40nm Chroma Technology Co, Rockingham, USA) filter set was used for QD detection. The images were recorded through Metamorph Software (Universal Imageing, USA) and the threshold and intensity were normalized to the control which did not contain any peptide.

4.2.6. *Mineralization approach to create calcite without peptides*

Calcite was consistently created using a slight modification of the approach developed by Coelfen et al.[164] This method uses vapor diffusion from ammonium carbonate to slowly add carbonate to a $CaCl_2$ system as shown in Fig 4.5. Instead of using glass beakers for holding the mineralization solution, 10ml petri dishes were used that contained a cleaned glass cover slide on the bottom so XRD sampling would be consistent. The ammonium carbonate (Sigma) and $CaCl_2$ 97% pure (Riedel-deHaen) were used without further purification. The aqueous solution of $CaCl_2$ (20mM) was freshly prepared before every experiment and 10ml was transferred into the petri dishes. The dishes were covered with Parafilm and several holes were punched into the film to allow for slower diffusion. This was then put into a desiccator with 20mg of the ammonium carbonate in a large petri dish covered with Parafilm punched with several holes. After 24 hours incubating at room temperature (~22° C) in a dark closet the precipitate was removed from the desiccator and rinsed with distilled water and allowed to dry at room temperature.

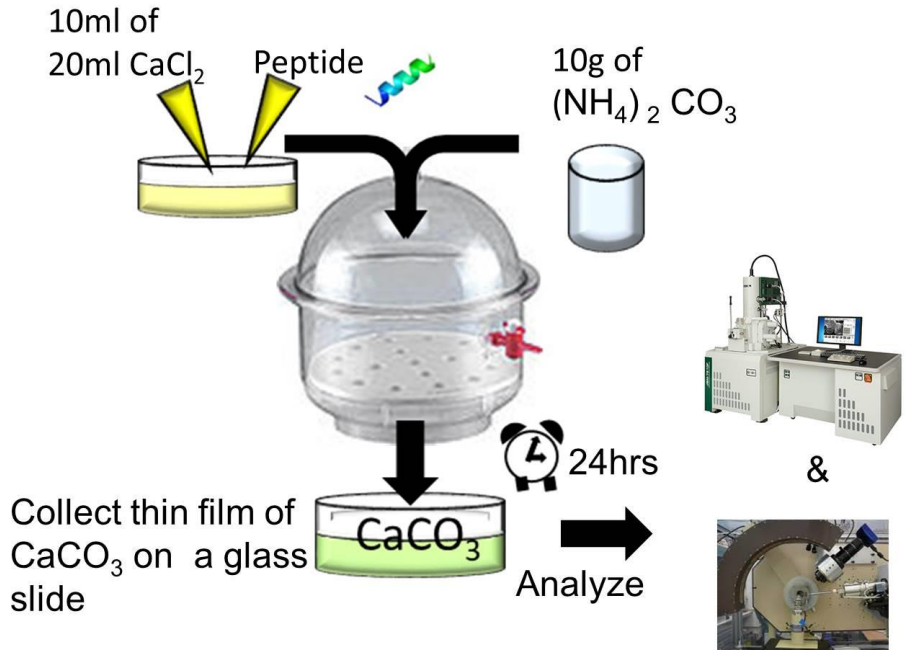

Figure 4.5: Schematic of biomineralization approach for forming calcite consistently.

4.2.7. *Mineralization approaches with peptides*

Peptides were added to the mineralization approach to observe formation differences. Amount of peptide was varied to find an optimum level that stabilized the most uncommon polymorph. Two concentrations (0.05mM and 0.1mM) showed creation of a different polymorph in calcite

forming mineralization experiments as well as in aragonite formation experiments. The peptide was added to the petri dish at the same time as the $CaCl_2$ and mixed by pipetting to create an even concentration of peptide.

4.2.8. *Scanning Electron Microscope (SEM)*

A JSM 7000F (JEOL) SEM was used at 10kV in secondary electron imaging mode to view particles and discover morphology changes. The $CaCO_3$ samples were first pipetted from the bottom of the petri dish and placed on carbon tape attached to a SEM sample holder. The precipitates were allowed to settle for 10mins and then extra liquid was absorbed using a kimwipe. This was then lypholized for at least an hour before viewing under the microscope.

4.2.9. *X-ray Diffraction (XRD)*

Polymorph identification and quantification were performed using X-ray Diffractometer D8 Focus (Bruker) at a constant current of 40mA and voltage of 40 kV. Scans were done in a continuous scan mode at step size 0.02, with time/step = 1 seconds, and a locked coupled angle 2θ between 10 and 95 or 135 degrees. The following slit sizes were used: divergence and antiscatter were set to 0.6 mm, detector was set to 6 mm and monochromator was set to 2 mm. The calcium carbonate samples were allowed to dry over night at room temperature. Slide containing the sample were attached to a polymer holder that allowed x-ray diffraction to occur consistently throughout the entire area. The scans were collected and then analyzed using Jade 7 analytical software, powder diffraction files (PDF) and excel. The percentage of the different polymorphs was calculated using equations from Konotoyannis et al.

4.3. Results and Discussion

4.3.1. *Sequence Selection*

The sequences in Tables 4.1 and 4.2 were selected using cell surface display and found using a BDSF's 3730XL sequencer. Strong aragonite binders (AraBP) had an average pI of 8.8 with a standard deviation of 2.9, which was lower than the overall average of 9 +/- 2.5. The strong calcite binders (CalBP) have an average pI around 9.3+/- 2.5 which is higher than the overall 8.5 +/- 3. A general trend for the calcite binders was that the stronger they interacted with the mineral the higher the average pI, while aragonite binders were the opposite. The charge varied considerably from the different binders. For aragonite a charge of zero had the highest prevalence with positive two charges a close second. The charges on the calcite binders varied considerably for the strong binders though most of the strong binders were positively charged.

Table 4.1: Sequence, molecular weight, pI and charge of aragonite binding peptides

	Clone	Sequence	MW	pI	Charge	Average Cell Count
Strong	4Ara17	GDAACLSLHDMR	1288.4	5.21	-1	61
	3Ara11	VARDPRVRSERG	1397.5	11.52	2	57
	4Ara5	KFAVNWDVGNLI	1375.5	5.84	0	53
	3Ara13	GVEKIVPVSNWA	1298.5	6	0	53
	3Ara9	GGPQCTLMQLLF	1307.5	5.52	0	48
	3Ara5	ARGRAERREQGL	1398.5	11.52	2	41
	3Ara1	QHNLLPLGAVIM	1305.6	6.74	0	40
	3Ara12	QHVREILKGVIR	1447.7	10.84	2	39
	4Ara3	KGEYGLRKPIGW	1403.6	9.7	2	37
	4Ara14	LRRAVHREWTLS	1523.7	11.7	2	36
	4Ara33	QVRRNNLMRHRD	1594.8	12	3	35
Medium	4Ara21	TRGRPCNSDDRD	1391.4	5.84	0	30
	4Ara9	ASRRLAGAELRQ	1327.5	11.7	2	28
	4Ara23	MNVHKRRTRWAQ	1582.8	12.02	4	27
	4Ara2	WGGKVWGDSRGA	1275.3	8.75	1	26
	4Ara22	SSVRLAKRTAVK	1315.5	12.05	4	22
	3Ara17	VTTAHGSDPKAQ	1211.3	6.71	0	20
	4Ara18	RRGSDIKIGDAV	1286.4	8.75	1	19
	4Ara11	TVTPNIQDCKPS	1302.4	5.5	0	18
	3Ara7	AGYRGKSEVIRQ	1363.5	9.99	2	18
	3Ara8	LRREEAGRVIGV	1354.5	9.51	1	17
	4Ara29	HRRRSRTGSPAW	1466.6	12.48	4	16
Weak	3Ara16a	VGVMGVRKVATQ	1244.5	11	2	15
	3Ara10	WASGCRRVRIIA	1387.6	11.7	3	14
	4Ara30	GHGFWGRTRGRH	1423.3	12.3	3	14
	4Ara39	GGRLRLRPRHRW	1559.8	12.6	5	14
	4Ara20	SAEGVTLMRRLV	1331.6	9.31	1	11
	4Ara19	HGFRNSKALTTR	1387.5	12.01	3	11
	3Ara3	QRKIPTHKLQWE	1563.8	9.99	2	10
	3Ara6	GGREAASSAILQ	1159.2	6	0	10
	4Ara16	KWFTHDVGVGGR	1358.5	8.75	1	9
	3Ara4	QVHLGWPVPSIL	1345.6	6.74	0	8
	4Ara8	SLFYSRVVHEHA	1444.6	6.66	0	7
	4Ara36	GGLVVDFSPRPY	1306.4	5.84	0	6
	3Ara2	CSRGGKDGLQCK	1251.4	8.9	2	3

Table 4.2: Sequence, molecular weight, pI and charge of calcite binding peptides

	Clone	Sequence	MW	pI	Charge	Average Cell Count
Strong	1Cal6	VDKRIGEGGPGR	1240.3	8.72	1	31
	1Cal13	SGTCLLHDSEKA	1260.3	5.3	-1	31
	1Cal15	PLSSRQCRPVNS	1343.5	10.39	2	29
	1Cal17	LSLPHFRSRRIQ	1509.7	12.3	3	28
	4Cal 31	GVSRQSAILHLC	1283.5	8.26	1	23
	2Cal15	STSGRKGFVIPP	1245.4	11	2	21
Medium	2Cal12	RRWDWVLKPVNG	1525.7	10.84	2	16
	2Cal20	GIGGCMGDRVAI	1148.3	5.83	0	16
	4Cal 30	RLRVREWMPLTT	1557.8	11.7	2	16
	1Cal7	RGCEVGSRSIAN	1248.3	8.25	1	16
	2Cal9	QYYQRKRNSHID	1607.7	9.7	2	15
	4Cal 7	GTTCRYLMKGGR	1342.6	10.05	3	13
	3Cal28	KVGGAGGRLLLG	1097.3	11	2	13
	3Cal9	LIGGVAVSANAR	1127.3	9.75	1	11
	3Cal7	RVWLSGGAKGAG	1158.3	11	2	11
	4Cal 23	LAWWMNLQATPG	1387.6	5.52	0	11
	3Cal2	GRKVGLRSVSNT	1273.4	12.01	3	11
	2Cal13	IKGVLVQNAADE	1256.4	4.75	-1	10
	4Cal 13	MVRSWRGSVGLL	1360.6	12	2	10
	3Cal29	RTWLWSHDVVTG	1456.6	6.74	0	10
Weak	3Cal20	VGRSSSRLGRAG	1202.3	12.3	3	9
	2Cal5	TFKGEATFPARG	1281.4	8.41	1	9
	2Cal6	EIFANGGLCMRR	1366.6	8.35	1	8
	3Cal23	VRRRPSRLEGFE	1501.7	11.52	2	8
	4Cal 1	AAPERGPTPIAQ	1207.3	6.05	0	8
	2Cal8	EPAKSASPIVAM	1200.4	6.1	0	8
	1Cal18	RLTWMLVKVVLF	1504.9	11	2	7
	4Cal 28	SGRGRARGPTLI	1240.4	12.3	3	7
	3Cal14	GGWLEDTLIVDL	1330.5	3.49	-3	7
	3Cal19	AGGCAKQESERD	1250.3	4.87	-1	7
	3Cal25	QLAKRKPHKAKG	1361.6	11.33	5	7
	3Cal16	RGLRWTGLIPGV	1324.5	12	2	7
	3Cal24	ELANEFECNIRR	1493.6	4.79	-1	7
	4Cal 11	GKRSASMAQKSS	1237.4	11.17	3	7
	4Cal 17	TGLKPHRIGDEG	1279.4	6.42	0	7
	4Cal 9	AGKKPPRMSGKS	1243.4	11.26	4	7
	1Cal3	GWFSLGTDGTQS	1255.3	3.8	-1	6
	4Cal 15	FTVHIEIPGGSA	1227.3	5.24	-1	6
	4Cal 21	KGAAEADDAGFV	1150.2	4.03	-2	6
	2Cal14	SLRNIKMGSEGM	1322.5	8.46	1	5
	3Cal21	AVRWRGVLRGGA	1297.5	12.3	3	5
	1Cal11	LLIKPKMATLVK	1354.8	10.3	3	4
	2Cal11	EAEYVGLHVLEA	1329.4	4.24	-3	4
	1Cal10	RHRKLKVGVNIR	1475.8	12.31	5	4
	1Cal14	PGRIGIPYRRSP	1368.6	11.71	3	4
	2Cal3	KGSMWRCANLLV	1377.6	9.51	2	3
	4Cal 22	RLAYPGDEEKVL	1389.5	4.68	-1	3
	1Cal20	DTAFVADISVGS	1181.2	3.56	-2	2
	4Cal 12	ACENKRMDIGSE	1352.5	4.94	-1	2
	1Cal1	VAIIPGAFLEKG	1214.4	5.97	0	2
	2Cal19	WKSETIWGQRRM	1577.8	10.84	2	2
	3Cal30	TGVVSGDGKGGT	1034	5.5	0	1

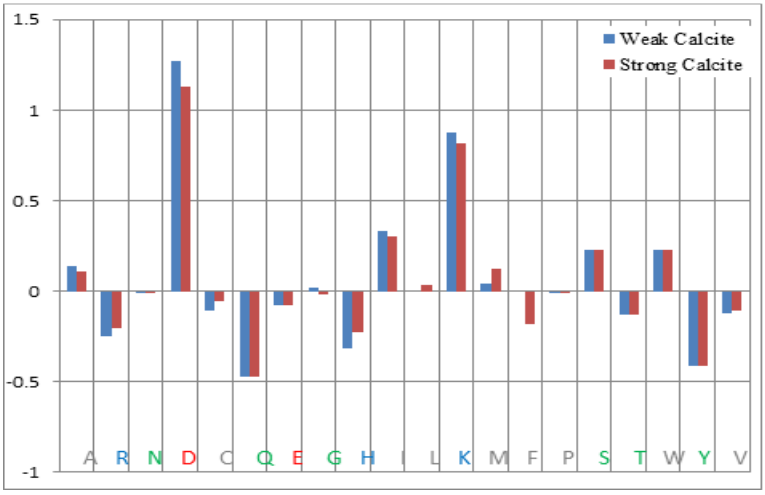

(a)

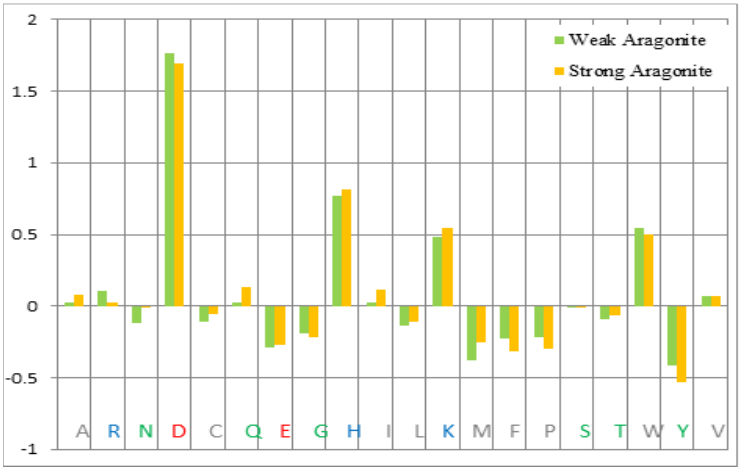

(b)

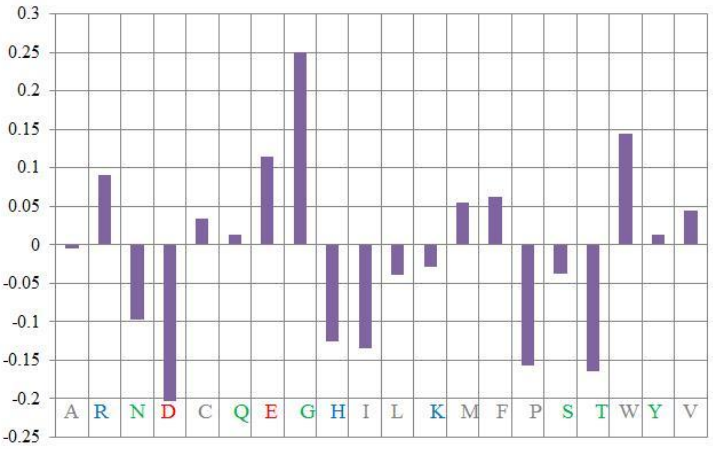

(c)

Figure 4.6: Relative abundance of amino acids in strong and weak groups of a) calcite and b) aragonite binding peptides and c) cell surface display's observed vs. expected percent differences. The columns are colored as blue = weak calcite, red = strong calcite, green = weak aragonite and yellow = strong aragonite binders. The numbers on the side are percentage away from the observed for the first two graphs and away from the expected for the last graph. The amino acids are colored by hydrophobicity and charge. Grey-Hydrophobic, Green-Polar, Red-Negatively Charged and Blue-Positively Charged

4.3.2. *Peptide Selection*

Peptides were synthesized using Solid Phase Fmoc synthesis described in the experimental section based on their characterization results while still on the cells. Not all the strong binders that showed specificity to a polymorph could be synthesized due to time constraints. For this reason a handful were selected based on the strength of their binding as well as their charge and pI values. Table 4.3 lists the selected peptides along with their properties that were synthesized for this study.

Amino acid composition among the strong and weak binders of the two different polymorphs was compared to the FliTrx unpanned library to find the relative abundances.

Calculations are found in the materials and methods section. Figure 4.6 shows that Asp, Lys, and Trp were all overexpressed in all sequences compared to the native library. Also, Arg, Asn, Gln, Gly, His, Leu, Met, Pro, Ser, and Val have significant differences in distribution between AraBP and CalBP. The differences between the strong and weak calcite binders were in the Gly, Leu, and Phe amino acids. For the aragonite binders only the Asn amino acid distribution was contradictory.

Table 4.3: Properties of aragonite and calcite binding peptides that were used in this study
Positively Charged AA (K,R) – blue, Negatively Charged AA (E,D) – red, Hydrophobic AA (A,I,L,M,P,V,G) – grey, Polar AA (N,Q,S,T,C) - bright green, Aromatic AA (F,W,Y) - orange, Histidine (H) - light blue, pI and charge computed using ProtParam Tool at expassy.org

Name	Sequence	MW	pI	Total Charge	Polymorph it binds to	Average cell count	Std Dev
3Ara11	VARDDRVRSERG	1415.5	11.52	1	Aragonite	57	5
4Ara17	GDAACLSLHDMR	1288.4	5.21	-1	Aragonite	61	10
4Ara33	QVRRNNLMRHRD	1594.8	12	3	Aragonite	35	8
1Cal13	SGTCLLHDSEKA	1260.3	5.30	-1	Calcite	31	14.03
1Cal17	LSLPHFRSRRIQ	1509.7	12.30	3	Calcite	28	2.87

The first two aragonite binding peptides were selected based on their extremely high binding affinity while on the cell along with the fact that they had exactly opposite charges. 4Ara33 was picked because it has a high amount of positively charged amino acids which is reported to have an effect on $CaCO_3$ formation.[74,87] 1Cal13 was chosen for its high binding affinity to calcite along with its large amount of polar amino acids and negatively charged amino acids which were unusual in the selection. Even though 4Ara17 has a negative charge as well, it also has a large amount of hydrophobic amino acids that may interfere with the charge being displayed in the

solution. 1Cal17 was chosen since it has the highest pI of all of the strong binding sequences and contains an aromatic amino acid along with its high binding affinity to calcite.

The distribution of amino acids for the selected peptides shows some overall trends as well as distinct tendencies for each of the polymorphs. Aspartic acid, a negatively charged molecule, had the highest relative abundance in both the aragonite and calcite binders. In the literature aspartic acid chains have been shown to interact with $CaCO_3$ and create unusual helical or layered morphologies in the calcite so having a high abundance in our selection would be expected.[165] Tryptophan, an aromatic molecule, was also found in many of the sequences both strong and weak, which may be due to van der waals forces being involved with binding to the surface. Distribution for the aragonite binders were found to be very similar between the weak and strong binders with only the amino acid asparigine (Asn) being different. Asn is a polar uncharged amino acid that contains an amide group one carbon from the backbone, while in Glutamine (Gln) this group is two carbons away from the backbone. Both sets of aragonite binders have a slight increase in Gln abundance, while there are fewer Asn in the weak binders and the expected abundance for the strong binders. One possible explanation is that the nitrogen group is not seen by the inorganic surface in Asn since it is smaller than the other nitrogen containing amino acids which were all selected for. Aragonite peptides also have a higher number of positively charged side groups than the library suggesting that the surface of the aragonite is negatively charged. Calcite binders on the other hand selected for only Lys that is positively charged while Arg and His were found less often than predicted. Aragonite appears to have a slightly higher charge density than calcite since its relative abundances for charged amino acids are much higher, which is consistent with it being denser. The following sections go into more detail on the peptides characterizations and their effect on $CaCO_3$ mineralization.

4.3.3. *Characterization results*

Characterization of the genetically engineered peptides (GEPIS) was done while they were still on the cells and after the strong binders were synthesized in order to find the binding capabilities to the different polymorphs. These methods were used rather than SPR and QCM for characterization because $CaCO_3$ can dissolve in flowing water and create a difference in mass possibly altering binding results.

4.3.4. *Characterization of cells with peptide on flagella*

Peptides' binding strength towards a selected substrate was characterized using FM while still on the flagella of the E.Coli. Figure 4.7 (a) shows the results of this characterization for CalBPs on calcite while Fig 8 (b) shows AraBPs on aragonite. The labeling of the peptides has been changed from those present on the graphs in order to simplify and prevent confusion. Arbitrary cuts off were used to determine which peptides were considered strong, medium and weak binders. The cut off for the calcite binding peptide was anything below 10 adhering cells was considered a weak binder while anything above 20 cells was considered a strong binder and everything in between a medium binder. For the aragonite binding cells a count below 20 cells was a weak binder between that and 40 cells a medium binder and above 40 cells a strong binder. The cutoffs were higher for the aragonite binders because of the larger sampling size due to lower magnification.

In the calcite selection a dramatic jump was seen from the medium to strong binders compared to aragonite which increased steadily from low to high affinity. Also the error bars are much larger for the CalBPs compared to AraBPs. Both of these observations may be due to the larger sampling size for calcite and the fact that it was cleaved instead of polished so its surface may be rougher. Differences in magnification were because two different people were counting the cells; Marketa Hnilova did the aragonite binders characterization while I analyzed the calcite binders. Polished aragonite was used because the saw used for cutting left a very uneven surface unsuitable for getting accurate FM results.

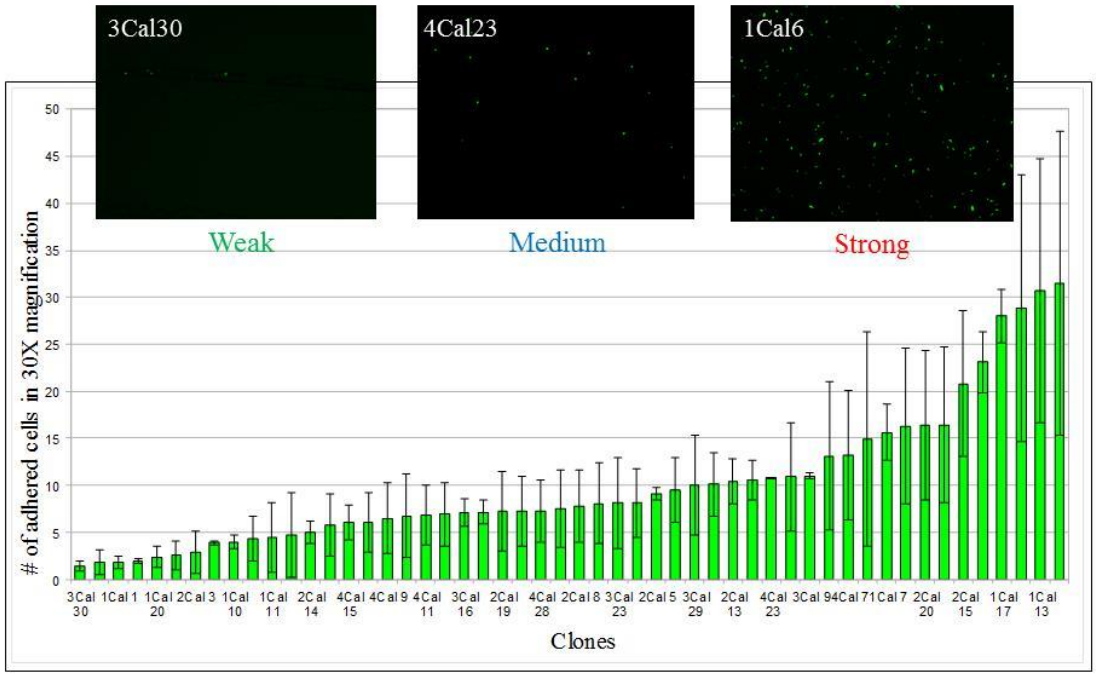

(a)

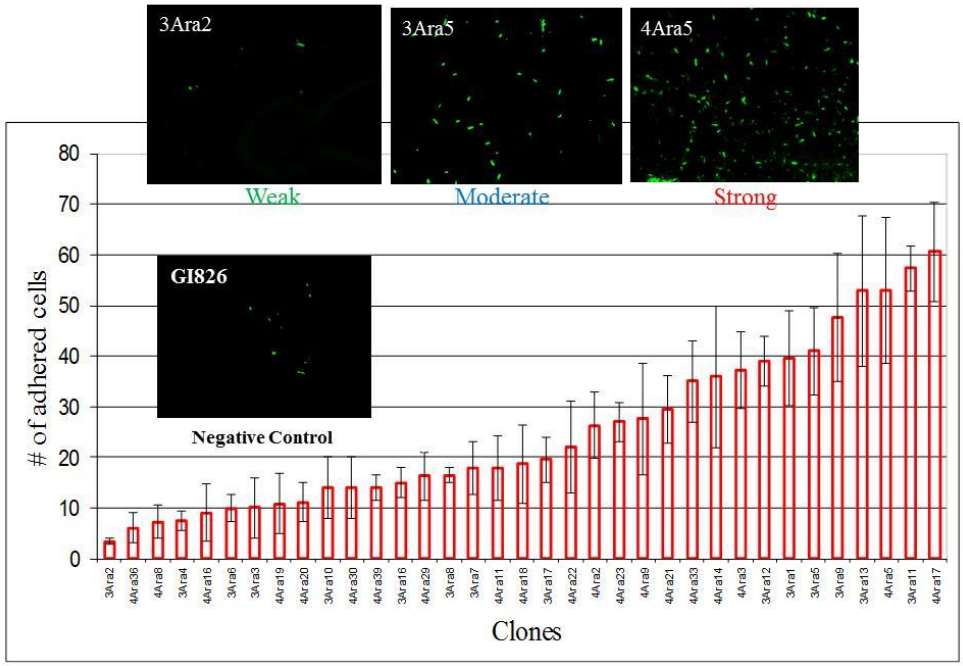

(b)

Figure 4.7: Characterization of sequences while still incorporated in the flagella of the E. coli: (a) Cell counts of calcite binding peptides on a calcite substrate, magnification 30X. (b) Cell count of aragonite binding peptides on aragonite substrate, magnification 20X (Courtesy of Marketa Hnilova).

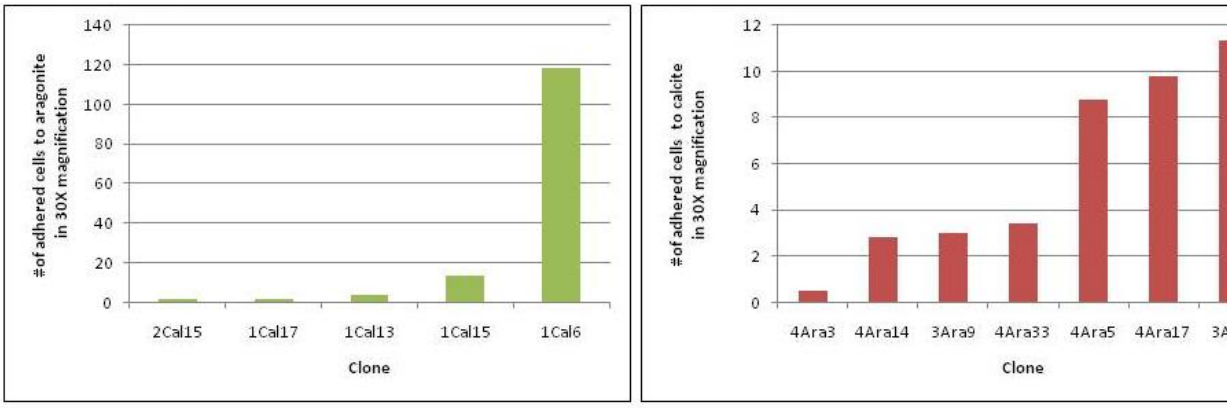

(a) (b)

Figure 4.8: Specificity of sequences to their specific polymorph while still incorporated in the flagella of the E. coli. (a) Cell count of calcite binding peptides on aragonite substrate. (b) Cell count of aragonite binding peptides on calcite substrate. Magnification 30X.

For the strong binding peptides further characterization was done to determine if the binding was specific to a polymorph or if the peptide bound indiscriminately to any crystal structure of $CaCO_3$. Figure 4.8 (a) shows the strong binders for aragonite on calcite and Fig 4.8 (b) shows calcite CalBP are specific to calcite while only 4 out of the 7 strong AraBP don't bind to calcite. This shows that even when doing a counter selection, it is difficult to insure that peptides are specific to only one polymorph of an element.

4.3.5. *Similarity Analysis and Protein Derived Peptides*

A similarity analysis was done on all of the characterized peptides to determine if the strong binders were more alike than the weak binders. Below in Fig 4.9 are the analyses of both sets of peptides which show the predicative power of the calcite binding analysis being 64% while for the aragonite binders it is 82%. The predictive power is an estimation of the chance of forecasting if a sequence is going to be a strong or weak binder for that specific substrate. The Needleman-Wunsch dynamic programming algorithm gives the optimal scoring alignment given a scoring matrix. The scoring matrix created by Oren iterative perturbs the known scoring matrices BLOSUM 62 and PAM 250 using a greedy procedure.[60] Both the total similarity scores (TSS) of the strong binders (TSSs-s) and the cross-TSS between strong and weak sequences(TSSw-s) were calculated after every perturbation.[60] Only perturbations that increased the difference between the TSSs-s and the TSSs-w were accepted to create the scoring matrix. The TSS were normalized according to equation 1 shown below:

$$[1] \qquad TSS_{A-B}([A]_{NA} - [B]_{NB}) = \frac{1}{NA \cdot (NB - \delta_{AB})} \sum_{i=1}^{NA} \sum_{j=1}^{NB} PSS_{ij}(1 - \delta_{ij}\delta_{AB})$$

Where, δ is the Kronecker delta function ($\delta_{ij} = 1$ *if* $i = j \wedge \delta_{ij} = 0$ otherwise 0). *NA* and *NB* are the number of sequences in sets *A* and *B*, and PSS_{ij} is the pairwise similarity scores (PSS) value between the i^{th} sequence of set *A* and j^{th} sequence of set *B*.[60] Once the scoring matrix was generated the overall similarity score for a pairwise alignment could be calculated by adding all the similarity values of the residue pairs together minus a gap penalty for insertion or deletions introduced for each sequence. The formula $g(k) = -\text{gop}-(k-1)\text{gep}$ was used to penalize gaps where k is the length and gop and gep are the gap openings and extension penalties.[60]

Using this analysis on a natural protein a peptide was designed and synthesized to see if it would be the aragonite binding domain on that protein. The natural proteins that were considered to have a domain that bind to aragonite were: AP7, AP24, Nacrein, N16, and Lustrin A. Using the similarity analysis developed for aragonite the different areas in the protein sequence were compared with the strong binders found using CSD to see how close they match. This involved calculating the TSS between each of the amino acids and the corresponding area of the protein. Amino acids were given a score based on their similarity to the strong binders as seen in figure 4.9. Areas that had a very high similarity to the strong binders were recorded as well as those that had a very low similarity. The red line in figure 4.10 indicates which amino acids sequences were similar enough to the strong binders to be considered as potential aragonite binding areas. Cut offs for the strong and weak binders were arbitrary though corresponded with values that were well above or below the average. The red box in figure 4.9 indicates the sequence that was chosen as a high similarity sections while the blue box indicates the section that has a very low similarity to the strong binders. The structure of the protein was also estimated using HyperChem to see if the sequences would be easily accessed or if they were folded inside the protein. The AP7 protein was the only one that had a sequence with a very high similarity that could also be easily accessed for binding. Table 4.4 has the high similarity and low similarity sequences found in AP7.

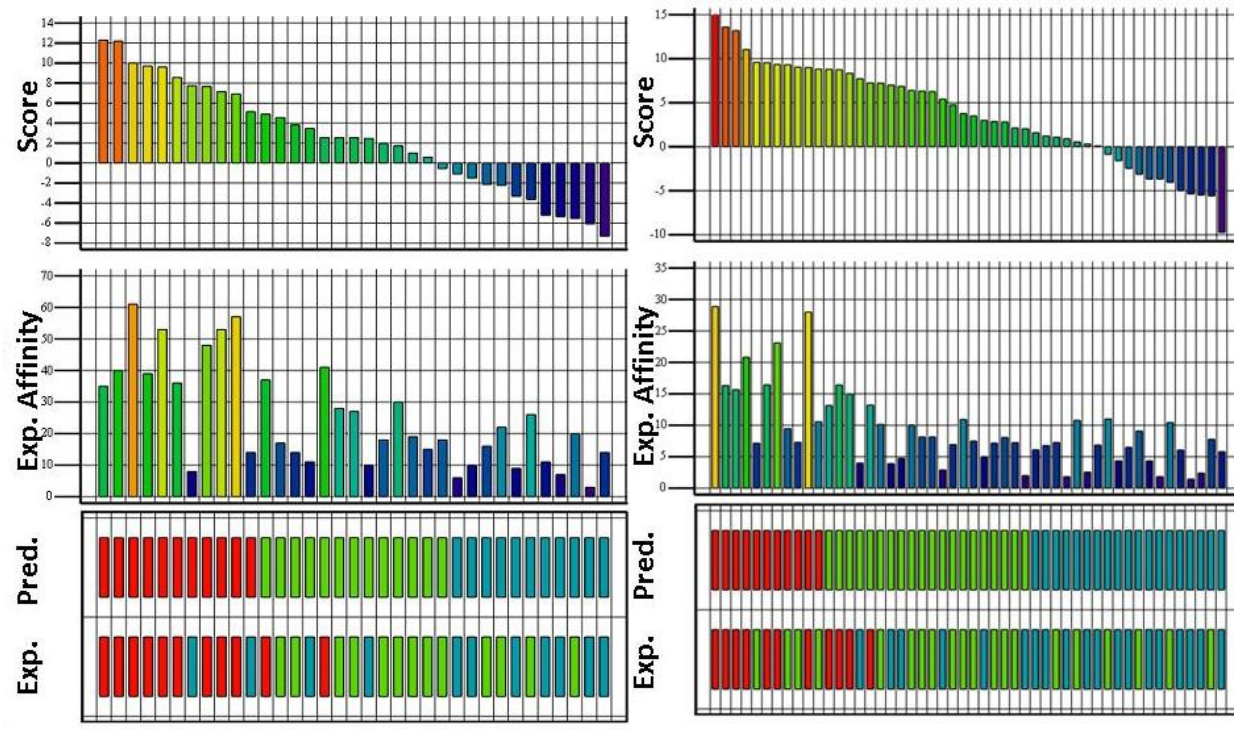

(a) (b)

Figure 4.9: Similarity analysis of selected peptides (a) Calcite (b) Aragonite

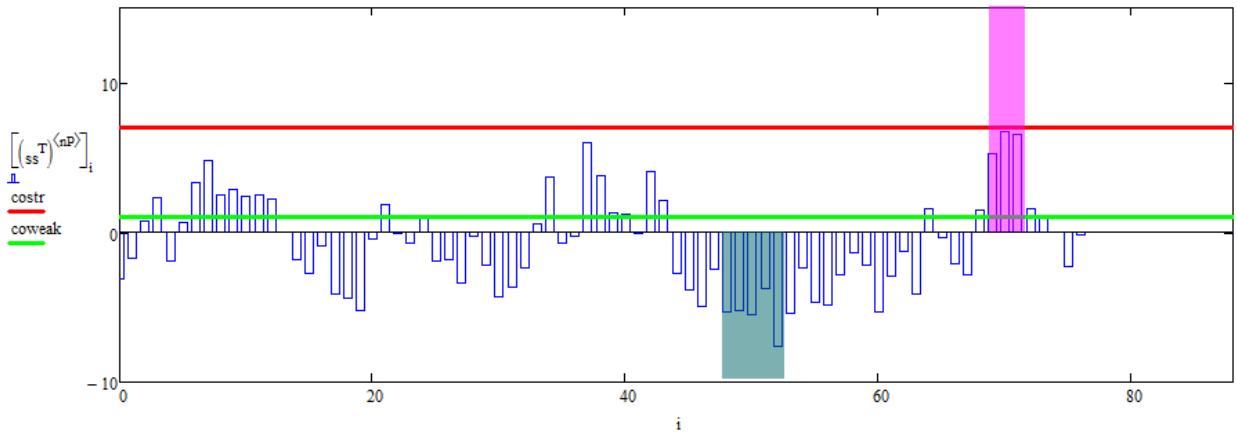

AP7:MTYMCSILICLVLILCARGAEADDNGNYGNGMASVRTQGNTYDDLASL**ISYLTRHSFRRPFHECA**LCY
S**ITDPGERQRCIDMY**CSYTN

Figure 4.10: Graphical comparison of AP7 with strong aragonite binders using similarity analysis. The x-axis shows the TSS score while the y-axis is the amino acid number counting from the N-terminus. The amino acids highlighted in

The similarity analysis of calcite indicated that perhaps the line between strong and medium binders may have been set too high, since many of the medium binders were predicted to be strong based on their sequence. The aragonite binders have a few weak binders that were forecasted to be strong perhaps because of their structure or effect on the cells. All the proteins that were used to find an aragonite domain were associated with the nacre of mollusk shells and two have been shown to form aragonite in vitro. The AP7 domains were promising mainly because the protein by itself can form aragonite without any additives using the desiccator method. The protein derived peptides had a considerable amount of charged amino acids, with the high similarity one being mostly negative amino acids while the low similarity had positive ones. Even though aromatics did not have a high relative abundance in our selection both de novo designed peptides contained a few of them, which may be due to the AP7 sequence.

Table 4.4: Properties of Protein Derived peptides that were used in this study
Positively Charged AA (K,R) – blue, Negatively Charged AA (E,D) – red, Hydrophobic AA (A,I,L,M,P,V,G) – grey, Polar AA (N,Q,S,T,C) - bright green, Aromatic AA (F,W,Y) - orange, Histidine (H) - light blue, pI and charge computed using ProtParam Tool at expassy.org

Peptide Name	Sequence	pI	Charge	Similarity to aragonite binders
AP7-PDP1	ITDPGERQRCIDMY	4.56	-1	High Similarity
AP7-PDP2	ISYLTRHSFRRPFHE	9.50	2	Low Similarity

Characterization of synthesized peptides

Further characterization was done on the CalBPs, AraBPs and the protein designed peptides after being synthesized. These experiments were performed in order to find the binding strength of the actual peptide without interference from the cell which may have affected the binding since they are much larger than the peptide. A schematic of the approach is shown in Figure 4.11. Also this experiment allows for better quantification of the binding for the actual peptides using the threshold calculator on the Metamorph software. The images in Figure 4.12 were normalized with respect to the control, which was incubated with Qdots but was not incubated with peptide. The normalization is necessary because Qdots can sometimes bind to a substrate even if no biotinylated peptides are present. From the images is it very hard to tell the different protein designed peptides apart since they both bind well to aragonite and slightly less to calcite which is

why threshold calculations were used. Along with this 4Ara17 was not able to be biotinylated effectively and so was not able to be characterized in this fashion.

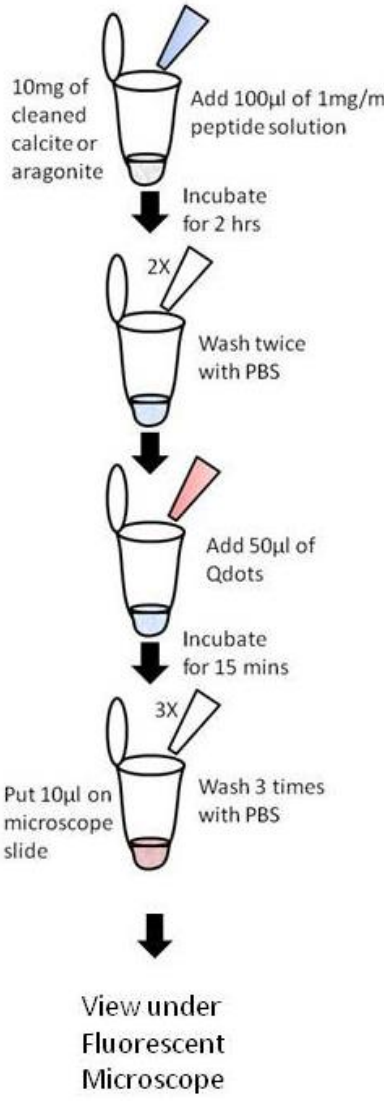

Figure 4.11: Schematic of FM characterization of peptides

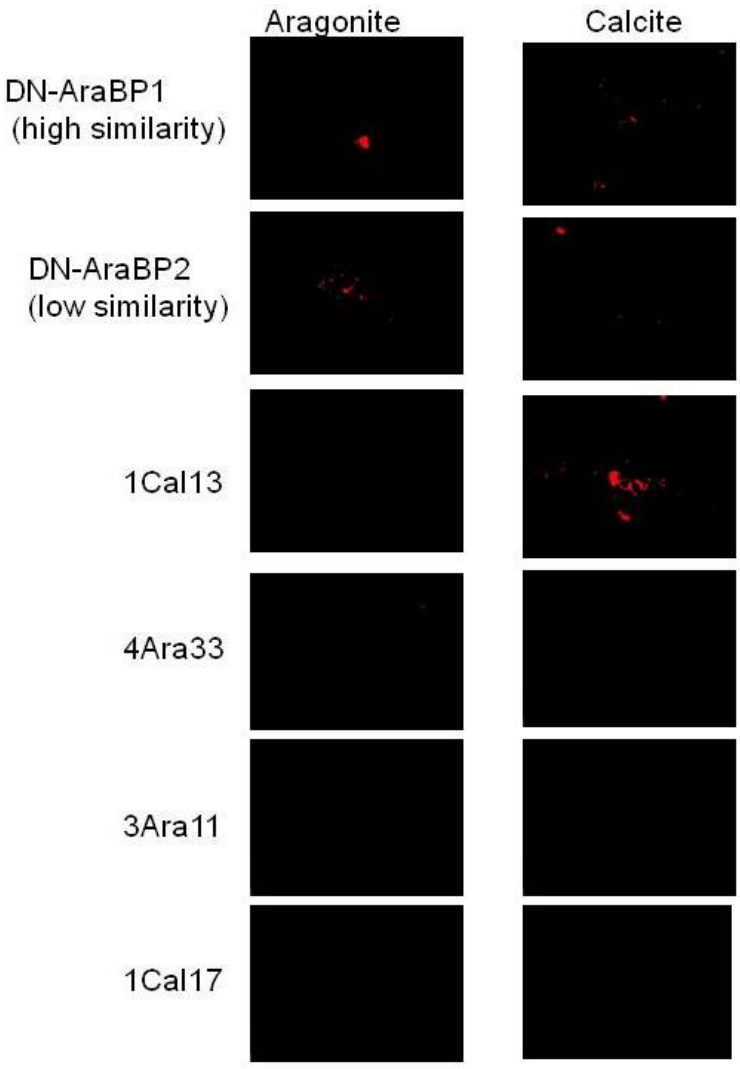

Figure 4.12: FM images of biotinylated peptide on aragonite and calcite (Images normalized with respect to control).

The threshold calculations were adjusted with respect to how much substrate was shown in the sample field. For instance 100% coverage would be maximum coverage of all the crystals shown in the bright-field image rather than complete coverage of the whole image. Figure 4.13 shows

the threshold measurements of the four peptides tested. From the graph it is clear that even though AraBP2 is the low similarity binder it in fact binds better to aragonite than its high similarity counterpart. Also both protein derived peptides show binding to calcite though much less than 1Cal13 which shows threshold coverage of about triple theirs. Along with this it appears that two of the peptides do not have any binding to $CaCO_3$ after being removed from the cells. This may be due to the peptide interacting with the biotin and reducing its binding ability to the Qdots. Also the peptide may be interacting with itself and not the substrate which would not happen when it is attached to the cell.

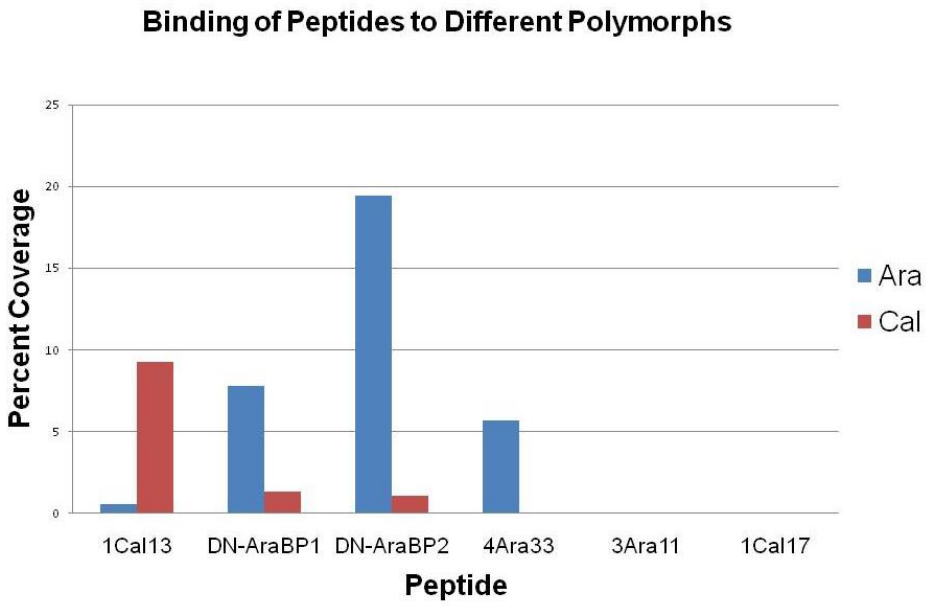

Figure 4.13: Percent coverage calculations for the peptides. (Threshold measurements were done using Metamorph software).

Binding affinities changed drastically for some of the peptides once they were synthesized, which can be seen in Fig 4.13. For instance, 3Ara11 and 1Cal17 did not show any binding to either polymorph even though they were very strong binders when expressed on the cell. One explanation for this lack of binding in the peptides is that they need to be cyclic in order to interact correctly. On the cell these peptides are displayed as a loop on the flagella and perhaps this rigid structure is needed to be able to interact with the surface correctly. Another reason for the difference between the characterizations could be that the cells are interacting with the surface by other means than the flagella, though this is unlikely since the cells would then all be

close to the same binding affinity. Biotin, a hydrophilic molecule that attaches to streptavidin-Qdots, may also be interfering with the structure of the peptide and not allowing it to bind. Another possibility is that the biotin is folded into the peptide and not able to see the streptavidin-Qdots.

4.3.6. *Optimization of Procedures*

Optimization of Calcite formation

Calcite formation was optimized to only produce this polymorph insure that they have all have similar morphologies. Three different approaches were found in the literature that would make calcite consistently. For some of the approaches the researcher mixed $CaCl_2$ with Na_2CO_3 or $NaHCO_3$ at different concentrations and another used NH_4CO_3 in a dessicator with the $CaCl_2$. After trying all of the methods listed above only the NH_4CO_3 consistently produced only calcite, while the others would sometimes produce a mixture of calcite and vaterite. Along with this the dessicator approach allowed the peptide the longest time to interact with the solution before crystals formed. This approach is also a slightly better mimic of nature in the fact that there is slow addition of carbon dioxide rather than it being instantaneous, which is probably why many researchers prefer this method.

Further optimization was done on the dessicator method since many researchers have slight modifications that can often change the results of peptide addition considerably. The two main optimizations for the control were in altering the amount of solution and taking samples from the bottom, middle and top of the solution for SEM and XRD. Unfortunately, when reducing the amount of solution below 10ml there was not enough crystals in the solution to be able to get an accurate XRD reading. TEM was also tried for polymorph identification in the smaller solutions, but the crystals were too big to be able to get a diffraction pattern from them. The crystals would also often break the TEM grid which is why this method is not used for characterization. For this reason, a 10ml solution was used in all the peptide mineralization experiments. As for taking SEM and XRD samples from different locations in the petri dish the bottom of the solution had highest concentration of crystals and so would give a better signal in the XRD compared to the middle and top of the petri dish. Also for the SEM images there was very little difference

between layers in terms of morphology unless it was at the top of the solution at which point there was very little $CaCO_3$ crystals and a lot of salts.

Optimization of Aragonite formation

Several optimization steps were needed in order to create aragonite consistently without raising the temperature above a level that would be harmful to the peptide. The procedures were modified in order to create the same level of aragonite every time if a mixture developed. Percentages of the different polymorphs were determined by the equations developed by Kontoyannis et al, where X is the molar fractions of the polymorph aragonite (A), calcite (C), and vaterite (V). [166] The intensities for the peak are represented as I with the peak number and the polymorph symbol.

[2] $$X_A = \frac{1.395 \times I_A^{700}}{I_C^{711} + 1.395 \times I_A^{700} + 9.30 \times I_V^{750}}$$

[3] $$X_C = \frac{X_A \times I_C^{711}}{1.395 \times I_A^{700}}$$

[4] $$X_V = 1.0 - X_A - X_C$$

Several different procedures found in the literature have been used to create aragonite that do not raise the temperature and would not take several weeks to complete. Figure 4.14 shows the composition of $CaCO_3$ at different temperatures and that you need to go above 100°C in order to get only aragonite formation.[167] An approach developed by Ahn et al was tried that has 0.2 moles of $Ca(OH)_2$ and 0.8 moles of $MgCl_2$ mixed with 10mls water at pH 8.7 and put in a dessicator with $(NH_4)_2CO_3$ overnight to form aragonite.[168] Aragonite was not developed for this approach but instead a mixture of ammonium magnesium chloride hydrate, magnesium chloride hydrate, $Mg(OH)_2$ and calcite was formed instead.

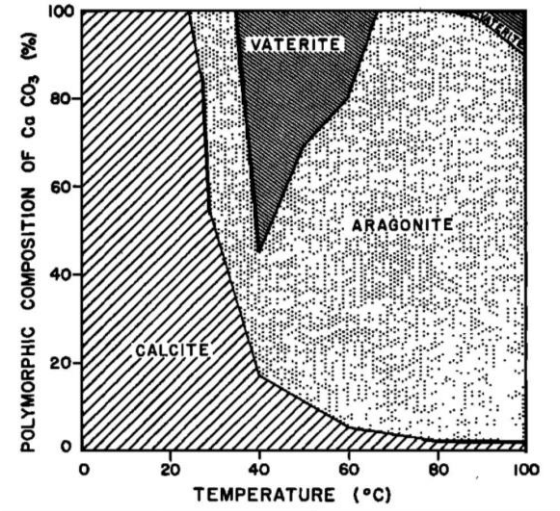

Figure 4.14: Composition diagram of $CaCO_3$ using the Ca(HCO3)-CO2-H2O approach without MgCl [Courtesy of .Kitano et al][167]

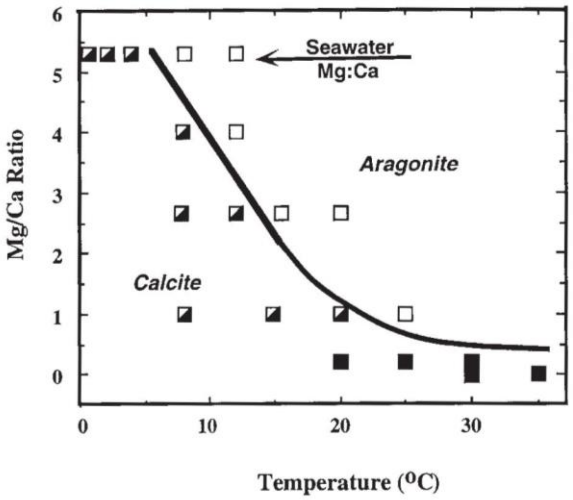

Figure 4.15: CaCO3 polymorph formed at different ratios of Mg:Ca and temperatures. White squares are aragonite, black is calcite and mix is situations where calcite initially precipitates and then aragonite grows on top of it. [Courtesy of Morse et al] 156

After the Ahn approach failed to produce aragonite, an Mg addition approach was used based on the ratio between the ions. Figure 4.15 shows which polymorph should develop based on the ratio of Mg to Ca using a slow addition of carbon dioxide.[156] This figure was used to determine the level of Mg to add to the two different approaches to form aragonite. The first approach was the optimized calcite procedure with a dessicator filled with NH_4CO_3 and then adding Mg to the $CaCl_2$ solution. The second approach was adding Mg to a $CaCl_2$ solution and then adding $NaHCO_3$ to this solution. Both of these approaches yielded aragonite as well as many other materials, but the NH_4CO_3 was more consistent in getting the percentage of aragonite to be around 25% of the mixture and so was used for the peptide addition studies.

4.3.7. *Mineralization with Peptides*

Calcite Formation with Peptides

All the selected peptides and two protein derived peptides were used in gas diffusion experiments in order to compare results with other literature studies. The starting pH values were not changed and range from around pH of 4-7 and the ending pH is around 8-9. All the peptides were tested at a concentration of 0.1mM. Those that showed interesting results were tested at two other concentrations of 0.05mM and 5mM. The higher concentration could not be tested on the

XRD since not enough crystals were developed indicating that at high enough concentrations the peptides are inhibiting the formation of crystals. The mineral is then analyzed using SEM for the morphology and XRD to accurately quantify the polymorphs and their concentrations.

SEM analysis

As shown in figure 4.16 many of the peptides show what appears to be considerable vaterite development in all cases compared to the control which shows only calcite development for the gas diffusion experiments. From Fig 4.17 (a) and (b) it appears that both 4Ara17 and 1Cal17 do not affect the morphology of the calcite crystals except a slight amount of etching at the 0.1mM concentration. The peptide 3Ara11 on the other hand was very unusual in the fact that it would sometimes create what appeared to be vaterite but it was not consistent in doing so even at the same conditions as seen from Fig 4.16 (c) and (d) which shows the vaterite when it was developed and the calcite which did not have any morphology change. When 3Ara11 did form vaterite it would sometimes have a very unusual morphology where the vaterite hexagonal platelets appeared to go from stacking normally to randomly stacking in different directions as seen in (c). Adding 0.1mM of 4Ara33 appears to form a mixture of regular spherical vaterite and calcite which appears to have many calcite crystals fused together as seen from Fig 4.16 (e) and (f). At lower concentrations of peptide the calcite is similar to that of the control and the vaterite looks the same as the slightly higher concentration. The highest concentration of 5mM the vaterite is covered by a layer of organic, though still seems to maintain its spherical shape though it is hard to tell due to the organic covering. For the 1Cal13 peptide there is no difference from the control at the low concentration of 0.05mM, but at 0.1mM, flower like vaterite begins forming along with very highly etched calcite as seen in Fig 4.16 (g) and (h). The protein derived peptides both produced what appeared to be a mixture of vaterite and calcite at 0.1mM, though the morphologies of the vaterite differ depending on which peptide was added. As seen in Fig 4.16 (i), AP7-PDP1, the high similarity protein derived peptide, produced vaterite that appears to be many small vaterite spheres arranged in a ring fashion and stacked on top of each other. The low similarity protein, AP7-PDP2, on the other hand has these vaterite spheres attached to one point localized in the center which is seen in Fig 4.16 (j). Control solutions that had no peptide added were run during each set of experiments and showed similar results to Fig 4.16 (k). The morphology developed by AP7-PDP2 appears to be unique to this peptide in the fact that no other researchers have yet shown this morphology using peptide, protein or polymer. On the

other hand the morphology of the vaterite developed by the 4Ara33 is pretty standard in terms of how it could be developed, but the calcite morphology is also unique to this peptide. The 1Cal13 creates vaterite similar to one of Coelfen's polymers, PEG(45)-b-PGL(27), that was found to also rely heavily on the surface tension of the solution.[169] How these different morphologies could have been developed is explained further in the discussion section. XRD was used to confirm that many of these morphologies are indeed vaterite.

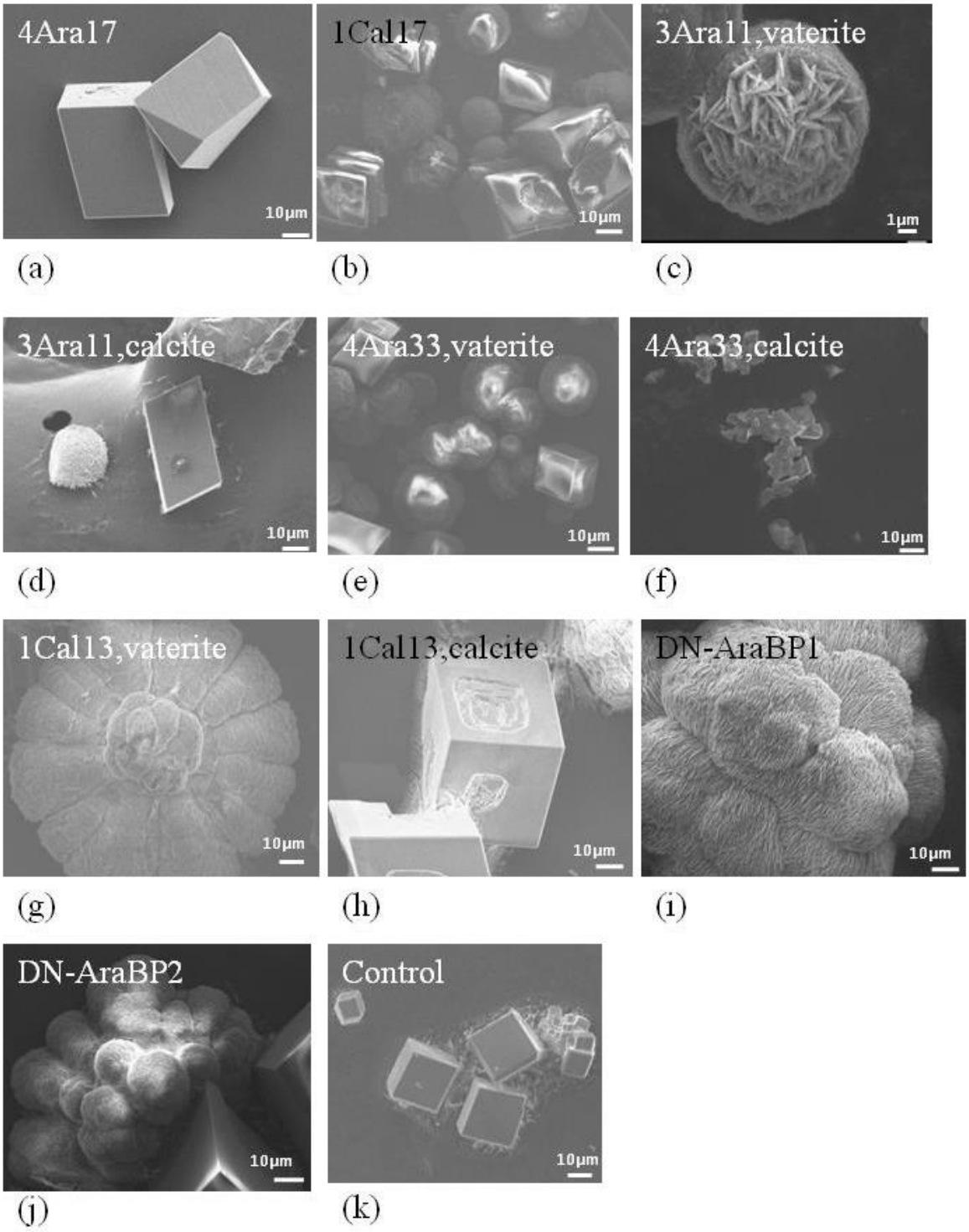

Figure 4.16: Representative SEM images of $CaCO_3$ developed using the gas diffusion method and with 0.1mM peptides added to the solution. (a) 4Ara17 (b) 1Cal17 (c) 3Ara11, vaterite's morphology (d) 3Ara11, calcite's morphology (e) 4Ara33 vaterite morphology (f) 4Ara33 calcite morphology (g) 1Cal13 vaterite morphology (h) 1Cal13 calcite morphology (i) DN-AraBP1 (j) DN-AraBP2 (k) Control without peptide. All images at 1,000X magnification.

XRD analysis

The XRD was done on at least three different runs for those peptides that produced polymorphs other than calcite to insure reproducibility of the quantification. Figure 4.17 shows XRDs of each peptide with the different polymorph peaks marked with C for calcite or V for vaterite. There is also a quartz peak marked as a Q on some of the images that is present when the crystals don't cover the entire glass slide. The quartz peaks can also be seen in the control Fig 4.17 (e) as well as when small amounts of the pure geological calcite is scanned.

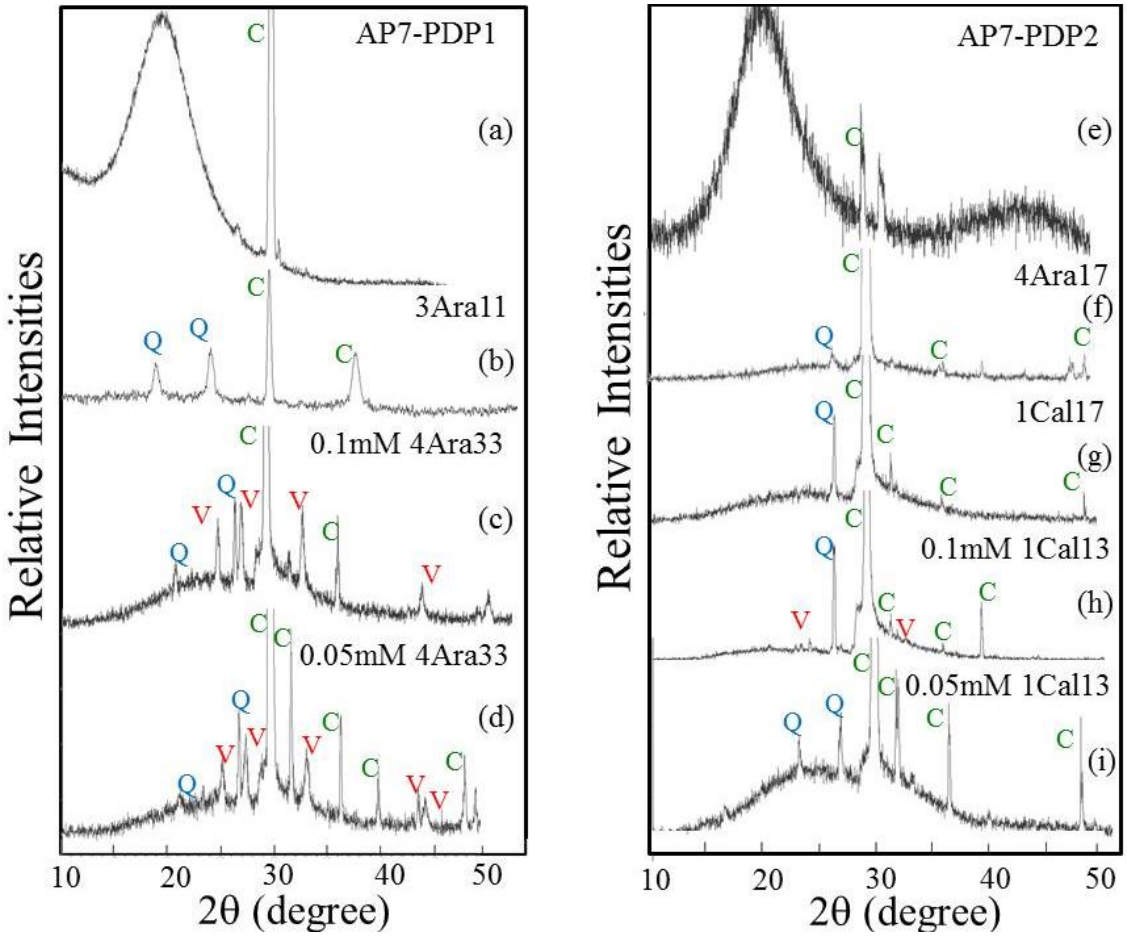

Figure 4.17: The X-Ray diffraction patterns of crystals created with the incorporation of peptides. (a) 0.1mM DN-AraBP1 (b) 0.1mM 3Ara11 (c) 0.1mM 4Ara33 (d) 0.05mM 4Ara33 (e) No peptide added (f) 0.1mM DN-AraBP2 (g) 0.1mM 4Ara17 (h) 0.1mM 1Cal17 (i) 0.1mM 1Cal13 (j) 0.05mM 1Cal13

For the protein derived peptides there was not enough crystal to produce a clear diffraction pattern reproducibly and would normally show amorphous crystal. On one occasion a single calcite peak was detected for AP7-PDP1 and AP7-PDP2 as seen in Fig 4.17 (a) and (f) though this was unable to be reproduced and even in these situations a large amorphous curve was seen.

The formation of amorphous crystal in these solutions is unlikely since there is clearly calcite and vaterite crystal morphology in the SEM images of the protein derived peptides as seen in Fig 4.16. As was clear from the SEM images 4Ara17 and 1Cal17 do not appear to affect the polymorph of $CaCO_3$ since they produce calcite peaks as seen in Fig 4.17 (g) and (h). Fig 4.17 (b) shows that 0.1mM of 3Ara11 forms calcite with large quartz peaks since amount of crystal produced was small.

The 4Ara33 and 1Cal13 peptides both produce vaterite at a 0.1mM concentration, which can be seen in Fig 4.17 (c) and (i). At the lower concentration of 0.05mM the 4Ara33 is still able to produce vaterite, but the 1Cal13 peptide is unable to do so as seen in Fig 4.17(d) and (j).

Quantification was done using an equation developed by Kontoyannis et al. In their paper they discuss that if one has a mixture of calcite, vaterite and aragonite it is possible to get the ratios of certain peaks and calculate the percentage of each compared to the whole.[166] They also discuss this principle if just two of the components are present. The following equation was used to calculate the percentage of the vaterite to calcite where I_C^{104} stands for intensity of the (104) reflection peak for calcite:

$$\frac{I_C^{104}}{I_V^{110}} = 7.691 \times \frac{X_C}{X_V} \quad [5]$$

This equation can be used for determining the percentage between the calcite and vaterite even if other components are present, unless those materials have similar peaks in the diffraction pattern which could offset the intensity ratio. For this reason the quartz peaks can be ignored since they are not close to the vaterite peak that is used for identification. Figure 4.18 displays the percentage of vaterite present for two different concentrations of the 4Ara33 peptide and the 1Cal13 peptide. From this graph it is clear that 4Ara33 is able to form more vaterite than 1Cal13, and can form this polymorph at a lower concentration then 1Cal13. The 1Cal13 also has a very large error bar which may be related to the fact that the vaterite morphology from the SEM

image appears to also rely on surface tension, which is very difficult to control.

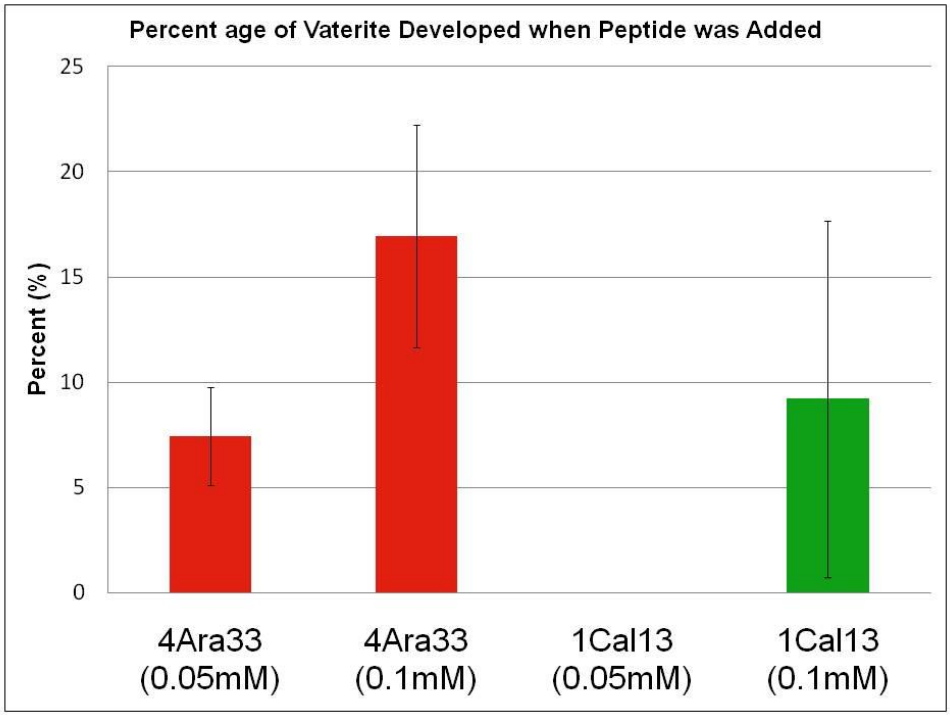

Figure 4.18: Percentage of vaterite developed for different concentrations of peptide added. Percentages calculated using equation 1.

Aragonite Formation with Peptides

The two peptides that altered the calcium carbonate polymorph, 4Ara33 and 1Cal13 were then used for mineralization in the aragonite forming solution described earlier in the materials and methods section where the . In the control, about 25% of the crystals formed were aragonite as seen from the XRD and SEM in fig 4.19. Aragonite has a needlelike morphology that all origninate from a single point while the calcite growth is inhibited so that they form flat ovals. When 0.1mM of 4Ara33 was added to the solution a film of unknown crystals were developed since the XRD did not show any peaks which indicates that this layer may be salt and so came off when the slide was rinsed. 1Cal13 also showed flat layering of crystals developing in the SEM and from the XRD they appeared to be calcium nitrate hydrate with a mixture of the three other $CaCO_3$ polymorphs. The calcite nitrate hydrate has a peak very close to the araognite peak that is used for calculations, so the percent aragonite was unable to be determined accurately for comparison with the control.

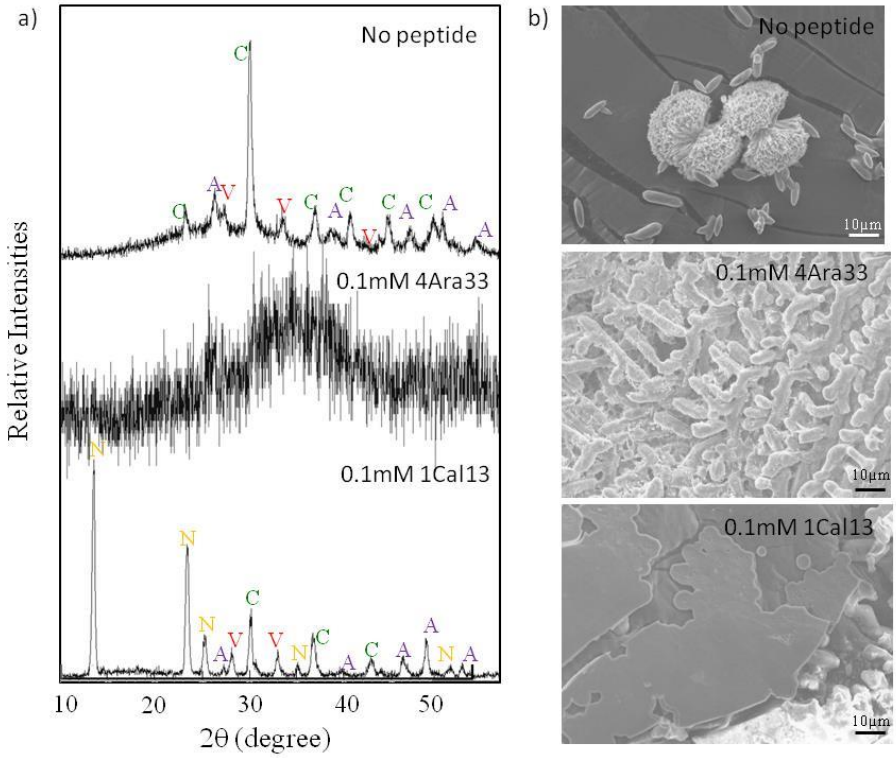

Figure 4.19: X-ray diffraction and scanning electron microscopy results of peptide addition to aragonite forming solution of 3:1 Mg:Cl ratio solution in a desiccator. (a) XRD and (b) SEM of with no peptide added, 0.1mM 4Ara33 and 0.1mM 1Cal13 added to the solution.

Mineralization was done on all peptides in a calcite forming environment and peptides that had the ability to control the polymorph were tried in an aragonite forming environment.

In the calcite forming environment several of the peptides had very unique morphologies compared to those found in the literature. 1Cal17, one of the peptides that were found to not bind to the surface also did not affect the morphology or polymorph of the $CaCO_3$. This indicates that binding affinity for calcite binding sequences may play a role in whether a peptide is able to affect the polymorph of $CaCO_3$. 4Ara17, was unable to be biotinylated so the binding affinity is unknown but it also forms calcite that it is similar to the control.

3Ara11, from the FM results also does not have an affinity to either polymorph, but does appear to form an unusual morphology of vaterite under the SEM while the calcite morphology is unchanged. The vaterite appears to have started forming normally with hexagonal platelets stacking on one another and then the platelets switch directions so that they are stack perpendicular to the original in random orientations with each other after that point. This morphology could be due to the peptide interrupting the growth of the vaterite at a certain point and then directing its organization onto a different pathway. The fact that the peptide does not affect the appearance of the calcite in any way is indicative that it does not bind or interact with this polymorph which is confirmed by the FM results. Perhaps 3Ara11 doesn't bind to either calcite or aragonite, but to vaterite. Unfortunately, since vaterite is not stable at standard condition the binding affinity of 3Ara11 to it could not be tested. Another explanation for this unusual platelet growth is perhaps the peptide nucleates vaterite at these odd orientations and then when the vaterite is no longer able to see the peptide it starts growing in the normal orientation of this crystal. Unfortunate, the formation of vaterite for this peptide was unable to be confirmed in the XRD, though from the SEM it appeared to be at least 10% of this polymorph formed most having this unique morphology.

For the aragonite binding peptide, 4Ara33, the vaterite that formed had the same morphology as those formed in the literature when stabilized by polymers. The polymers that are able to create this polymorph often have disordered structures that optimize the number of binding sites indicating that perhaps this peptide also prefers to be disordered. [170] This vaterite formation was confirmed and quantified by XRD. The calcite formed from this peptide appeared to form sheets normally with a few separate crystals being separate from these large agglomerations. A similar

morphology of layered calcite can be seen in Gower's work concerning poly(asp) chains, though our aragonite binding peptide only contains one aspartic acid residue it might have a similar mechanism of forming these films.[165] In that study the films were made of hexahydrate form of $CaCO_3$, a hydrated phase that forms a platy habit, which then changes into the more stable calcite while still retaining some aspects of the hydrated form.[165] The aragonite peptide may also utilize this mechanism, but it can't be confirmed since the final crystals are calcite and it is difficult to get a diffraction pattern from the hydrated $CaCO_3$.

For the calcite binding peptide, 1Cal13, the vaterite that was formed at 0.1mM concentrations had a flower like morphology similar to that found by Coelfen.[169] They determined that variations in water tension and hydrophobicity were affecting the vaterite superstructure.[169] The flower like vaterite morphologies were normally only found when there was very high surface tension under hydrophilic conditions which occur with phosphorylation.[169] The XRD confirmed that the crystals with these odd flower morphologies found in the SEM were indeed vaterite. In our case 1Cal13 most likely interacts with the vaterite at the surface of the solution stabilizing it and starting formation of the flat platelets next to each other. After the structure gains enough mass to break the surface tension the vaterite is then allowed to stack into a sphere. The vaterite extensions are flat because our peptide is hydrophilic so the superstructure drops from the surface sooner since nothing is keeping it from interacting with the water except surface tension. Calcite formed when 1Cal13 is added to the solution appears to have slightly etched surfaces. This morphology is most likely due to growth inhibition by the peptide binding to the growing edge.

Both of the de novo designed peptides showed vaterite spheres agglomerating into a larger structure though their organization appears to be slightly different as well as calcite crystals that looked similar to the control. Unfortunately, the XRD did not confirm that these spheres are vaterite, since the amount of peptide was too low to get accurate readings. For the high similarity aragonite binder, AP7-PDP1-AP7, the spheres appeared to be arranged in rings stacked on one another into a larger sphere. AP7-PDP2-AP7 on the other hand had a superstructure where all of spheres appeared to be originating at a single point and growing out into a sphere from there. Even though these peptides had different similarity to the aragonite binding peptides they both appeared to create vaterite and calcite in the mineralization solution. Comparing the sequences one can see why they both behave similar to the selected aragonite binding peptides. Both

sequences have a large number of charged groups both positive and negative spread evenly throughout the sequence. Even though AP7-PDP2-AP7 had a number of aromatic amino acids they did not seem to impede in the binding.

Aragonite mineralization was done with the two peptides, 4Ara33 and 1Cal13, that were able to affect the polymorph of calcium carbonate. The same concentration was used in this experiment as the one that created vaterite in the calcite mineralization. For the aragonite mineralization only 25% aragonite is formed in the original mineralization experiment with a mixture of vaterite and calcite present as well. When the aragonite binder is added to the solution a film is formed that could be made up of salt though this was not confirmed with XRD since either the amount of crystal was too low or it was rinsed off prior to analysis. The calcite binder also created a flat film under SEM though this was confirmed under XRD to be a mixture of calcite nitrate hydrate and the three polymorphs of calicum carbonate. Exact aragonite percentages were not able to be found because no formales have been created for mixtures of $CaCO_3$ polymorphs and calcite nitrate hydrate and since this chemical has peaks similar to aragonite it can not be ignored as with quartz.

4.4. Conclusion

In this study, peptides were selected that bound specifically to different polymorphs of calcium carbonate to observe their effect on the crystal structure and morphology. The selection was done using cell surface display with a unique counter selection at the end to ensure that the peptides only bound to one crystal structure. The cells were then sequenced and characterized on their particular polymorph into strong, medium and weak binders using FM. The strong binders were then tested for specificity by observing how many of the cells bound on the polymorph they were not selected for. Some of these peptides were then synthesized and characterized further.

A similarity analysis was performed on both sets of binders to see how the different binders compared to each other. The predicative power of the analysis was higher for the aragonite binders than for the calcite, 82% to 64%, indicating that aragonite strong binders are closer in similarity than the calcite ones. From these results we used the aragonite similarity analysis on several natural aragonite binding proteins to determine domains within them that may be responsible for their binding. The domains found in AP7 were chosen to be synthesized because AP7 has been shown to create aragonite in vitro and these domains were not folded inside the protein so could be involved with surface interaction.

The five peptides that were synthesized from the selection all bound strongly to their respective substrate on the cells, but varied in charge and pI. The binding affinity of the selected and the protein derived peptides for many were not consistent with what was seen with the cells. For instance, two of the peptides that showed very strong binding on the cells bound to neither of the substrates. Also the protein derived peptides bound to both polymorphs, but two of the selected peptides were found to preferentially bind to their selected substrate with little to no binding found on the other.

Calcite mineralization with the peptides produced vaterite for several of the peptides many having unique morphologies under SEM. 3Ara11 produced what appeared to be vaterite that has never been seen in the literature where platelets are stacked perpendicular at the end of the normal spherical superstructure. The XRD was unable to confirm vaterite formation expect for in two cases with the specific aragonite and calcite binders, which indicates that binding affinity

may play a role in polymorph control. The vaterite percentage in these mixtures was calculated and found to be related to peptide concentration for the aragonite binding peptide. The calcite binding peptide was only able to produce vaterite at a high enough concentration while at the lower concentrations tested it just formed calcite that showed signs of growth inhibition.

In the aragonite mineralization experiment 1Cal13 was able to produce calcium nitrate hydrate along with the other polymorphs of calcite carbonate in the solution, with the appearance of flat platelets. 4Ara33 was unable to produce enough crystals to be analyzed in the XRD, but under the SEM it also showed a film like substance forming.

Chapter 5: Peptide Mineral Surface Assembly

Taking the lessons previously learned concerning peptide assembly on surfaces and biomineralization the following chapter puts this knowledge together to understand a different biological system involving hydroxyapatite (HA). Where graphite is very important for technological device creation and calcium carbonate makes an excellent model system, hydroxyapatite has many biological and clinical uses. Hydroxyapatite is a major constituent of bone and teeth with many proteins being associated with its organization on the microscale level. These proteins are often found in organic extracellular matrices that are surrounding the newly forming mineral to allow more precise control over its growth. As discussed previously the organic matrix between the prismatic and nacre layer found within many shell species allows a greater toughness than each of these layers by themselves. One of the more well-known examples found in humans of this dynamic of mineral morphological switching is at the Dentin-enamel Junction (DEJ). These types of interfaces contain proteins and peptides that are able to not only bind a specific surface, but also mineralize from that surface a different morphology than it is on. Our group has successfully shown remineralization with a longer peptide (ADP5) selected from amelogenin using similarity analysis in a buffer solution.[171] ADP5 was shown to speed up the kinetics and create HA similar to that found from the full length peptide in buffer.[171] For this study we will be using a shorter length peptide (sADP5), which was rationally designed from the longer computationally designed peptide ADP5. We will be studying the change in kinetics and mineralization caused by the sADP5 using a novel double drop diffusion method mimicking the organic matrix and how this affects mineralization on a tooth surface.

5.1. Background

After calcium carbonates, calcium phosphates are the next most abundant mineral produced by organisms comprising about 25% of biogenic mineral.[172] This biogenic mineral is found predominately in the skeleton and teeth of vertebrates, though some amorphous forms may serve as calcium stores and can be found in diseased tissues.[173-175] Calcium apatites, which is just calcium phosphate that contains impurities of F^-, Cl^-, and OH^- is what is what most of these biogenic minerals are composed of since getting high purity calcium phosphate is unusual in nature. Hydroxyapatite, ($[Ca]_{10}[PO_4]_6[OH]_2$), is one of the most common of these apatites in

vertebrates making up 55-70% of the interconnected porosity found in bone, which is why is it is the main focus of our study.[176]

5.1.1. *Hydroxyapatite Mineral*

Hydroxyapatite is usually written as $Ca_{10}(PO_4)_6(OH)_2$ to denote that the crystal unit cell contains two molecules and comes in either monoclinic or hexagonal. Monoclinic HA forms only when the molecule has almost perfect stoichiometry and at low temperature so not particularly relevant in biomimicry.[177] The hexagonal structure is more common in HA's natural form since it allows for vacancies or impurity ions. These impurities or vacancies act as points that allow the OH^- ions to be reversed, stabilizing the HA hexagonal phase.[178,179] In the pure crystal temperatures above 483˚K still allow the OH^- groups to reorient and form the hexagonal structure. The primitive cell is rarely used to describe HA since it has the form of a triangular prism (Fig 5.1a), and lacks the clear symmetry that the rhombic prism has at two cells (Fig 5.1b). Many of the properties attributed to hydroxyapatite vary considerably on whether the sample is biological vs geological. One example is fracture toughness and hardness varies considerably depending on if the hydroxyapatite is geological or where it is incorporated into the body. For instance in geological HA the average fracture toughness is $0.37 MPam^{1/2}$ where in enamel the roughly 3 times that value.[180] The hardness on the other is a little less than half for the biological specimens when doing micro-indentation hardness measurements.[181] For many biological samples it matters which direction or orientation the experiment was in since the hierarchical structure can preferentially strengthen a direction. In the case of hardness on enamel for instance the xz direction (where the force is normally from

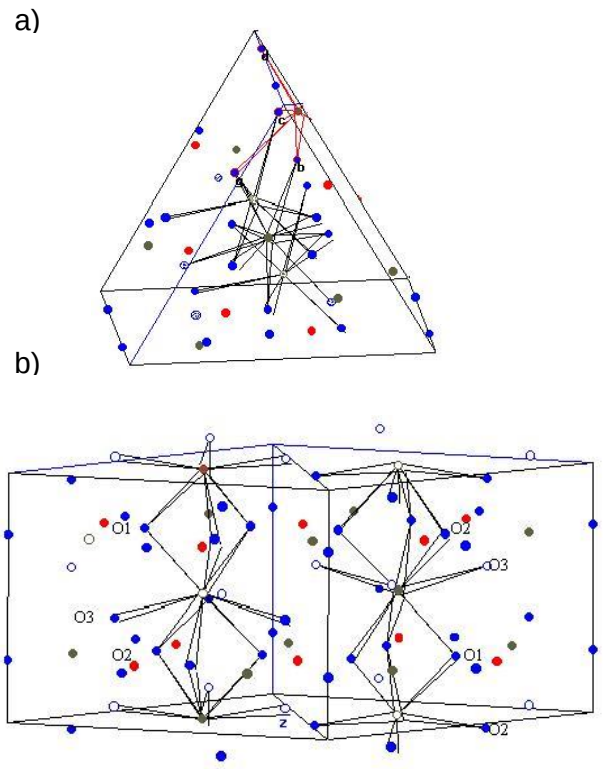

Figure 5.1: (a) primitive cell of hexagonal HA (b) unit cell of hexagonal HA. Blue circles oxygen, red circles phosphorous and grey circles calcium.[172]

mastication) is slightly harder than the xy direction which is on the side.[181] Vertebrate's ability to modify many aspects of this geological apatite is mostly likely why it is found in so many functions in the phyla Chordata.

5.1.2. *Hydroxyapatite's Biological Occurrences*

Biological hydroxyapatite is heavily linked with the organic matrix and proteins that make up many of the calcified structures in vertebrates. The ratio between the mineral and organic often leads to different mechanical properties of material and are quite versatile matching the demands of the tissue. Bone, for instance consists of about 70% mineral, 24% water, 6% collagen and a small amount of other proteins.[182] The collagen percentage in bone gives it overall higher toughness, but lowers its ultimate strength compared to higher mineral containing tissues.

In teeth there are three mineralized tissues, cementum, dentin and enamel, with different mineral to collagen ratios each based on the job that section preforms (Fig 5.2). Cementum is the layer bridging the gap between the dentin root and the gums. For this reason this layer has significantly more organic matter than dentin and even bone, with rough percentages of 61% mineral to 27% protein and rest being water.[183,184] Dentin on the other hand is comparable to bone in that it is about 70% mineral, but has only 20% proteinaceous material and surrounds the pulp providing fluid channels that act as nutrient supply routes.[183,184] In this layer most of the protein layer is composed of a collagen matrix that forms an intertwined network with HA mineralized around it providing strength.[181] Enamel the hard outer layer of the tooth and is the most mineralized biological tissue found in a healthy human body with around 96% HA mineral and only 1% protein material.[183,184] The increased HA content makes this layer ceramic-like, resulting in the highest hardness of any other tissues in the human body, but also being very brittle. Organization of the HA by the proteins within this layer gives enamel even better mechanical properties than it would on its own. Each enamel rod is a tightly packed mass of HA crystals all running in the same direction, that are "woven" together. This interwoven structure is created when these rods run obliquely to each other on alternating rows, leaving a

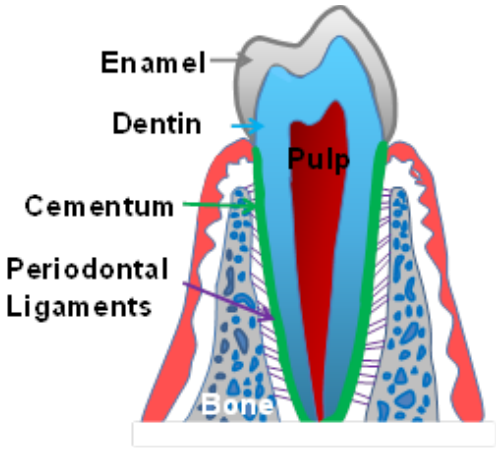

Figure 5.2: Schematic of anatomy of human tooth [Adapted from Hanson Fong's slides]

small space for interrod enamel that contains HA that is not as well oriented. The fact that all of these organizations are able to happen at body temperature (37°C) and atmospheric pressure is a true testament to the control that these proteins have over this mineral system. To date no synthetic technique has been able to duplicate the level of complex mineralization under biological or any other conditions that the body can achieve. One of the many locations that this biomineralization occurs and is well characterized is at the dentin-enamel junction (DEJ).

5.1.3. *Biomineralization at the Dentin-enamel Junction*

The dentin-enamel junction (DEJ) is the demarcation between enamel and dentin mineralization and exists due to the two sets of cells involved within the different processes. Before the start of mineralization, ameloblast cells along with odontoblast cells accumulate across from one another. Mineralization then begins extracellularly, with first the dentin layer being constructed and then the enamel rods being formed.[181,185] Ameloblast columns retreat away from the junction secreting proteins and ions, perpendicular to the long axis, creating one enamel rod. This receding during growth produces the triangulation front known as the Tome's process.[181,186] This front is considered to have three major steps: cell secretion of protein matrix, nucleation of HA and crystal growth in the [001] direction until the organic volume decreases.[181,184,186] Though this process sounds as if it would produce a perfectly straight line for the DEJ several studies have found this is not the case. Instead the DEJ appears to have a high concentration of sub-micrometer features as well as larger corrugation structures.[181,187-189] Variation in hardness and elastic modulus along this region also indicate that this is not as sharp of an interface as one might expect from its formation. [181,187,189] The matrix that allows for there to be a junction and growth is composed of amelogenins and non-amelogenin proteins. Amelogenin and its cleaved fragments make up 80-95% of the matrix and are expressed by the ameloblasts to form the enamel. [181,190] Our group has worked with this protein in order to discover possible functional sites that are important in the biomineralization process and it will be discussed in the next section.

5.1.4. *Peptide Modification of Calcium Phosphate*

Due to the importance of hydroxyapatite mineralization several groups have searched for ways of interacting with this mineral.[28,34,191-193] One group has taken the protein statherin which is associated with bone/tooth mineralization and found that the N-terminus seemed to be the

binding area for this protein.[191] They then synthesized a 15 amino acid peptide based on this N-term and attached multiple different functional groups that were known to have cell adhesion properties which were then able to bind to the hydroxyapatite surface to varying degrees.[191] Other groups have loosely found that poly(Aspartic acid) and poly(Glutamic acid) peptides have reasonable affinity to the hydroxyapatite surface.[192,193] These groups did no such binding assays, but rather would attempt to immobilize the functional group onto hydroxyapatite and compare the rate of adhesion with and without the peptide. In all of these cases the peptide conjugated bound better than just the functional group alone, be it RGD, pamidronate (a drug used against osteoporosis) and others.[191,192] Our group has also found peptides that preferentially bind to the hydroxyapatite surface, specifically synthetic HA powder, using phage display.[34] The 56 peptides found using the Ph.D. phage display peptide library kit were characterized for their binding strength by fluorescent imaging and designated as strong, medium or weak binders.[34] The strongest binder, HABP1 and one of the weakest binders, HABP2 were then synthesized and used to mineralize hydroxyapatite. HABP1 first off slowed down the mineralization considerably compared to the control without any peptide and created much larger needlelike HA spheres similar to naturally formed HA.[34] This indicated that perhaps these peptides might share a similarity to the naturally occurring proteins that are associated with HA's mineralization.

As covered briefly in the previous section, amelogenin and its cleaved parts makes up the vast majority of the proteins involved in enamel mineralization. Until recently, which segments of this large protein were instrumental in tooth creation was unknown. Our group was instrumental in determining amelogenin's possible binding regions and how they affect the kinetics of mineralization. Similarity analysis was done on the phage display discussed previously for the HABPs and this information concerning strong and weak binders were then compared with the full-length protein to see which regions were the most or least similar to the strong binders. From this computational analysis eight peptides were created with varying length from amelogenin and named and numbered accordingly, amelogenin derived peptide: ADP1-8. ADP1, 2, 4 and 7 all had high similarity to the strong binders where ADP3, 5, 6 and 8 had low similarity (Figure 5.3). These peptides were then synthesized and tested for how they affected the mineralization and kinetics and compared to the full length amelogenin protein. ADP7 was found to be the best binder and created mineral that morphologically was very similar to what the full-length protein made, but took a significant amount longer to do so.[33] This peptide would produce

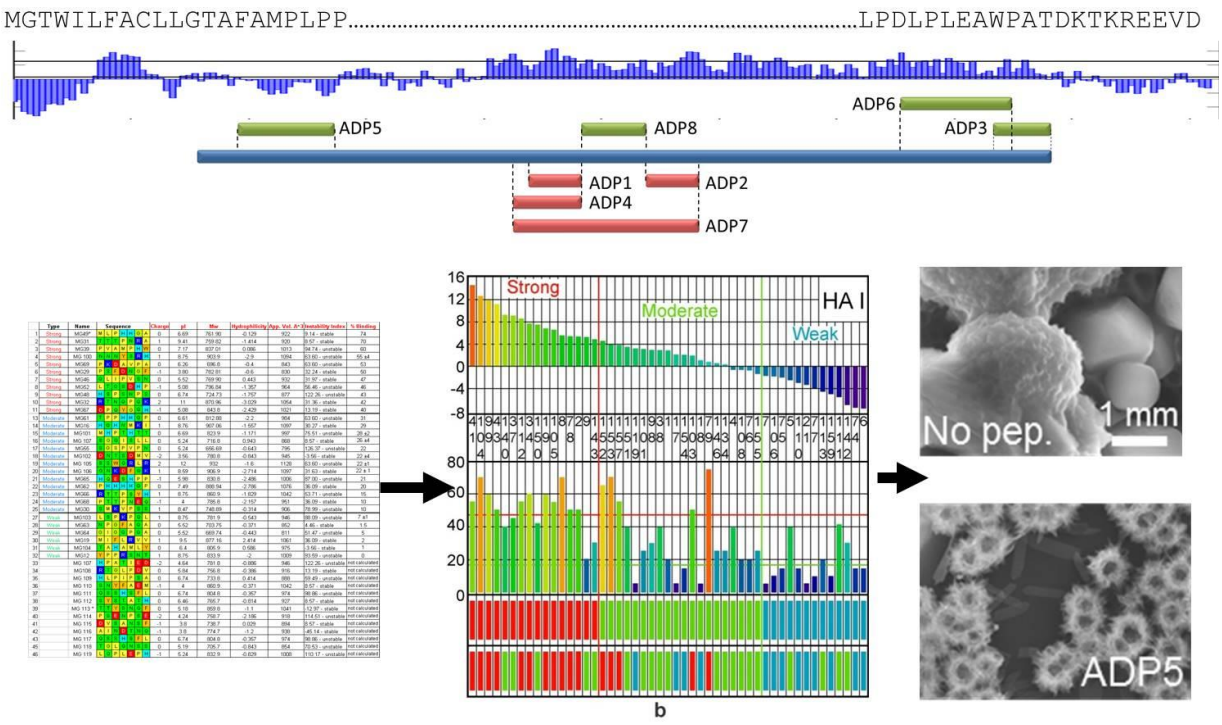

Figure 5.3: Summary of our groups work on amelogenins peptide creation and mineralization with ADP5.[33]

These studies are extremely valuable in understanding how we might be able to mimic the natural formation that happens within the DEJ or as a clinical application. There are certain things however that are very different between the natural forming peptide and these previous studies. First, at this point ADP5, has only been used to mineralize in a solution, and though this is a useful tool for understanding the process it is not as good for mimicking how nature is able to form this layer, which it does in a more viscous extracellular matrix. Secondly, for clinical purposes having ADP5 in a solution is not as advantageous as in a gel form where it can be localized to a certain area that it is needed instead of throughout the mouth. Thirdly, mineralization in a solution situation doesn't consider a lot of the complexities that this peptide would encounter within the mouth since saliva is not a true solution, being more viscous than just plain water and so getting the calcium and phosphate localized in a certain area would be difficult in this situation. Fourth, the root surfaces that were used by Mustafa Gungormous et al were tested on the cementum layer, but it is uncertain if they work as well with repairing enamel surfaces, which is where most caries develop in humans.[33] Along with this we found that ADP5 was often difficult to dissolve fully in just water and so when using a gel in our studies this presented an even larger difficulty and required us to rationally design a shorter version of it.

Finally, we created a double drop diffusion couple approach, which allowed use to determine mineralization kinetics in a non-solution environment such as this one and can be very useful for many other applications.

5.2. Methods

5.2.1. *Rationally Design of sADP5*

Creating the sADP5 was done by rationally modifying the original ADP5 peptide found previously by our group using similarity analysis on amelogenin. Due to ADP5s low water solubility, modifications were needed to get allow the peptide to dissolve in the gel formulation at the concentrations necessary for kinetic and surface modification work. From previous studies possible calcium binding sites had been identified and shown to be very important to the peptides function using knock out mutations.[33] After carefully going through the peptide sequence the first 6 amino acids on the N terminus and the last amino acid were removed due to their high hydrophobicity and distance from the known binding sites as seen in figure 5.4. The hydrophobicity was determined using a Protparam tool from expasy.org.[195]

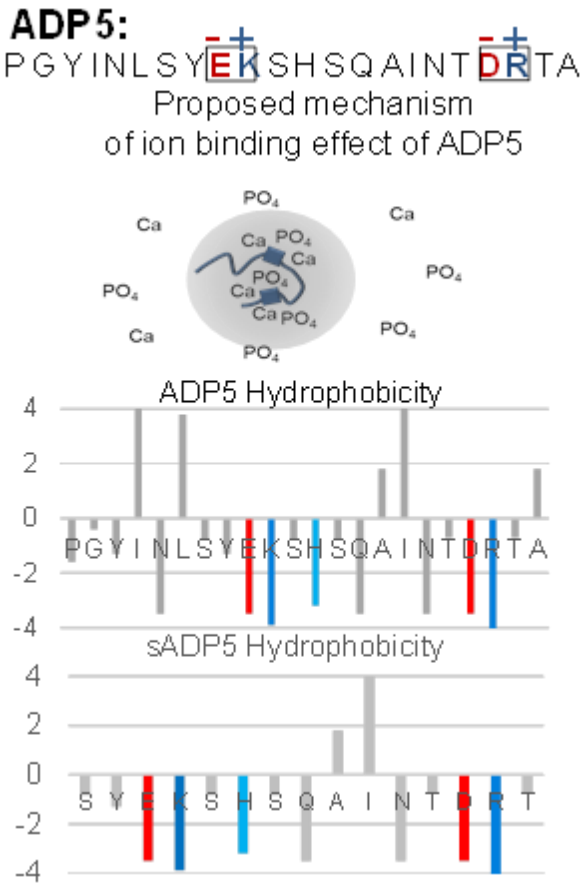

Figure 5.4: Rational Design of sADP5 peptide using hydrophobicity charts.[195]

5.2.2. *Gel Design*

Development of the gel formulation was based around the idea of toothpaste and the fact that this gel substance is able to adhere fairly well to the tooth surface while still allowing fluoride and other ions access to the surface. Children's toothpaste's viscosity and overall lack of many

additives made an ideal first attempt at a gel recipe to then be modified with added mineral, peptide or higher or lower percentage of thickener to dial in the viscosity. So after several attempts a recipe was created containing: 30% sweetener (sorbitol), 0.5% surfactant for its antifoaming properties, 0.5% preservatives to reduce microbial grow during experiments and increase storage life, 19% thickeners and 50% aqueous solution that contained the peptide, calcium chloride or potassium phosphate or some combination of them that was prepared in the solution preparation section. These ingredients (specifics will not be provided due to confidentiality agreement), were one and a time and mixed with an electric stirring machine while being heated slightly to 50°C-60°C to insure smoothness. When this formulation was viscous enough to stay put when placed on a glass slide and part of the tooth while it was lying flat without spreading significantly it was considered ready to be used for experiments.

5.2.3. *Kinetics*

In order to test the kinetics within the gel a new approach called the double drop diffusion couple (DDDC) method was developed to ensure that the sADP5 would still accelerate the mineralization within the formulated gel.

Solution Preparations

The Tris solutions was optimized by using either Tris HCl or Tris Base and an optimized concentration was found to be 24mM by checking the kinetics of several while keeping the $CaCl_2$ and KH_2PO_4 concentrations the same. The optimum pH was found to be pH 7.4 with no NaOH added for pH adjustment, since the Na^+ appeared to interfere with mineralization due to possible competition with the Ca^+ ion. Mineral concentration was also varied to be able to start mineralization after approximately 20mins in since if it was too early the peptide would not be able be able to interact with the mineral before precipitation. The best final concentration found for the solution that allowed for this rate of mineralization was 9.6mM $CaCl_2$ and 5.6mM KH_2PO_4 (USB Corp) (MW: 136.08). These concentrations were found to be too low to start mineralization in the gel DDDC experiments and so it was multiplied 5, 10 and 100 times and tested again. The 10 times amount appeared to work the best for getting the mineralization to start after 30 secs which was enough time to have the camera set up and ready to take images. Peptide solutions of sADP5 (MW: 1736.8) were prepared fresh every time in 24mM Tris buffer pH 7.4 and the concentrations were varied for different runs.

Precipitation Kinetics Approach

The TECAN absorbance reader was set for a wavelength of 820nm with a kinetic cycle selected to be approximately 2hrs or 200 cycles. A 96 well plate was used and 50 µl of the peptide solution was added to each well. Then 100µl of the $CaCl_2$ was added and then right before putting the plate into the reader 100µl of the KH_2PO_4 would be added and mixed with the pipet at least three times. For the absorbance readings the plate was heated to 37°C and shaken between each cycle for 3secs so that particles would not accumulate on the bottom of the well. These measurements were mainly used for optimizing what the buffer concentration and pH should be.

Double Drop Diffusion Couple

A novel procedure was created to determine the kinetics of the peptide in formulation and how the gel might affect the mineralization process. The method involved observing mineral formation at an interface between two gel droplets and recording the growth of the mineral layer once they came into contact with one another. Gels were created as described above with several different aqueous solutions added some of which incorporated peptide in the calcium chloride solution or the phosphate one or neither. The final ion concentrations were held the same between those solutions with and without peptide by diluting the stocks accordingly with the knowledge that a certain amount of the water would include the peptide. Once all of the different formulations were created, and

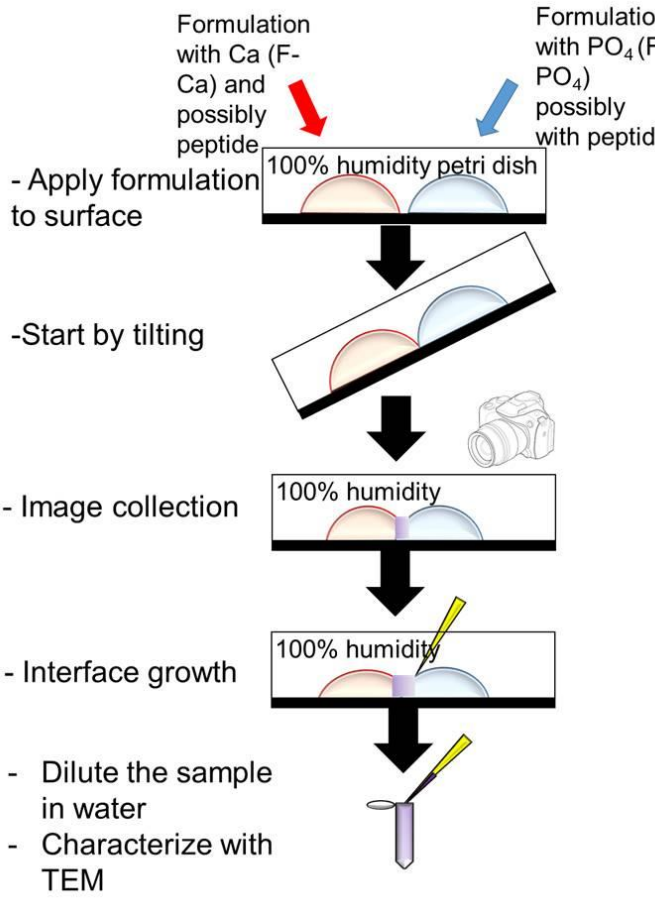

Figure 5.5: Schematic of double drop diffusion couple approach

thoroughly mixed they were then put into a syringe for storage as well as application purposes. A schematic of the set-up is depicted in Figure 5.5, where we would put equal amounts of gel onto the bottom a petri dish using the syringe and as close as possible without touching. Once the camera was set up we would then tilt the dish just enough so that the droplets came into contact with one another and start mineralizing. We would then put the dish into a container which had standing water within it, so that there would be closer to 100% humidity directly around the experiment reducing the effects of evaporation on our results. A ruler was also placed to the side of the droplets to be able to have some way to measure the mineralization front. Several different concentrations were tried so that the rate was such that we could accurately get the beginning of mineralization recorded. The 960mM $CaCl_2$ and 560mM KH_2PO_4 in 24mM Tris buffer at 7.4 gels appeared to work the best for creating a mineralization front after 30secs which allowed us time to set up the camera and get it in focus before then. Images were taken after 10sec, 30secs, 1min and then every 5 minutes once the rate slowed after tilting for computation analysis later by looking through every image and comparing it with the ruler to see its growth pattern. After allowing the diffusion coupling to precipitate several hours or overnight the middle interface was removed and diluted in water. This was then centrifuged to get the mineral deposit which was transferred to ethanol and then pipetted gently onto a TEM grid for further analysis (Transmission Electron Microscopy).

5.2.4. *Surface Mineralization*

Human teeth were used as the surface for remineralization. They were obtained with the help of dental students in the lab from their clinics. When collected they were stored in 100% alcohol, the soft tissues were removed with an explorer and 12-24hrs before experiment stored in 1% bleach and dried right before the experiment.

Tooth Surface Preparation

Enamel was prepared two different ways depending on the mineralization procedure.

For the solution mineralization the enamel surface was cut into 4 different sections using a microtome to maximize the amount of surface enamel available. Along with this a notch was done in the back of each to allow the layer to be exposed for imaging. For each segment, a high concentration etch was done on half of the sample by using Ultraetch™ for 10s. After etching the

samples were then rinsed with Tris buffer and soaked in buffer solution for at least 2hrs before the experiment. This clinical product is used to clean teeth for resin fillers and creates a deep etch unlike the gradual etching found from wear, but allowed remineralization to be observed in a reasonable amount of time. For our purpose of determining sADP's remineralization similarity to ADP5 this was an acceptable method.

Gel-formulation mineralization on the other had is meant a mimic for possible DEJ formation and as such using such strong etching procedures seemed unwise. Instead a more natural etching procedure was used. First a small window was created in the enamel by using nail polish to cover the rest of the tooth so that only a section would be demineralized. Then the tooth was incubated in a demineralization solution composed of 2.2mM KH_2PO_4 , 2.2mM $CaCl_2$, 50mM Acetic Acid and adjusted to make sure it was around 4.5 pH. Both were placed into a glass beaker and left on a rotator for many days for gentle break-up of the enamel to occur. Once demineralization was done the root was removed and the tooth was rinsed and soaked in Tris buffer for at least 2hrs before the experiment.

Remineralization on Enamel Surface in Solution

To insure that our sADP peptide was still able to mineralize on a tooth surface in the enamel region we used a similar approach created by Mustafa Gungormus and others in our group to confirm this affect. The prepared etched sample (tooth surface preparation) was fully submerge in peptide solution, at the concentrations ideal for solution mineralization (solution preparation), normally 100-300 µl, in a 48 or 12 well plate. This was then incubated for at 37°C for 10mins. After incubation the tooth sample was moved to a new well (48 or 12 well plate) and 300 µl of 9.6mM $CaCl_2$ and 300 µl of 5.6mM KH_2PO_4 was added and quickly mixed with a pipet tip. If the sample was very large, more mineralization solution was added making sure the ratios were the same. The sample was then incubated in the mineralization solution for 1hr to overnight, at 37°C. Sample was then rinsed for 20s and quickly dried in a vacuum for at least 30mins. The samples were then cracked at the notch to reveal the new layer to be imaged. SEM preparation was done by adding the sample to a SEM holder with carbon tape and with one side up so that the new layer could be seen as well as the surface and then coated with a small layer, 5nm, of gold or platinum (Scanning Electron Microscope). Figure 5.6a shows a schematic of this approach.

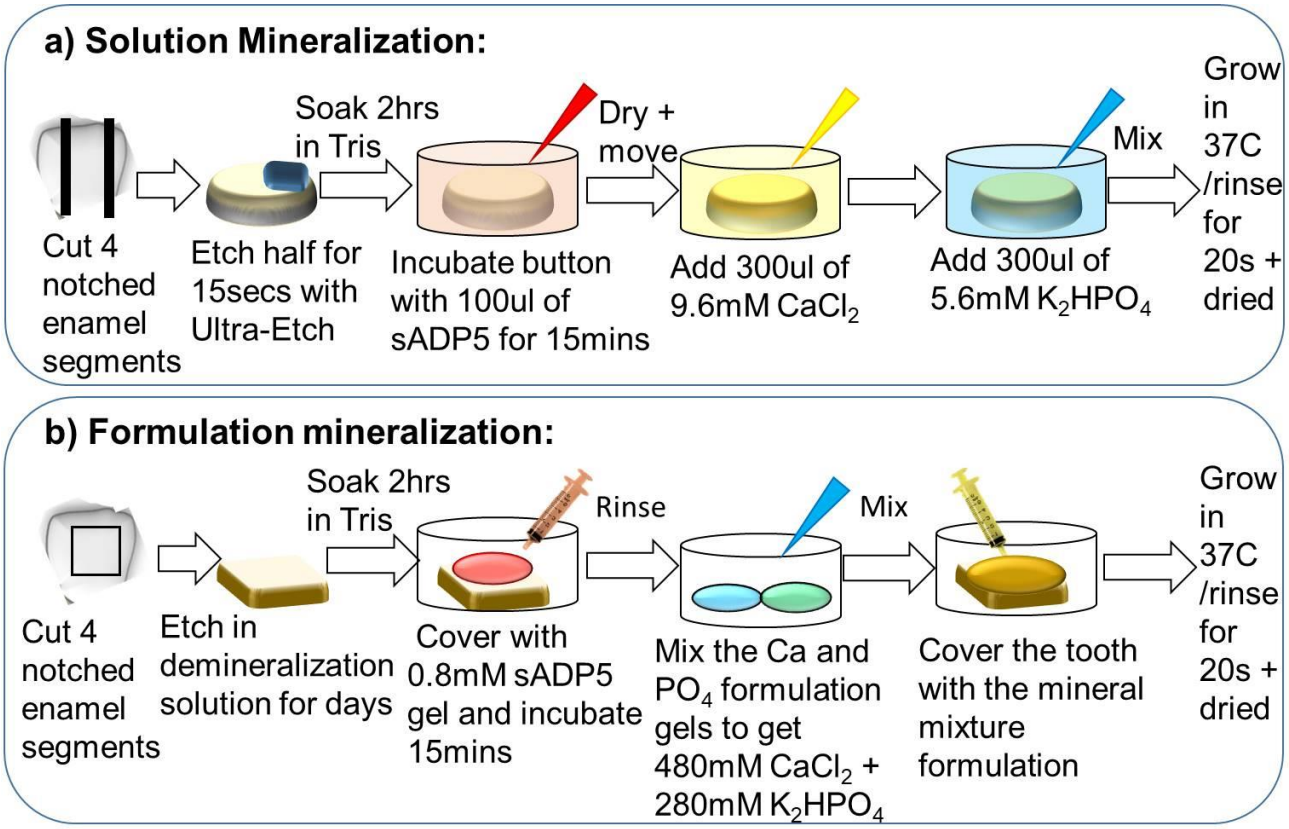

Figure 5.6: Schematic of peptide mineralization approach an enamel tooth surface a) in solution and b) with formulation gel

Remineralization on Enamel Surface with Formulation

The etched prepared sample (tooth surface preparation) was placed in a 12 well plate to reduce possible contamination and then enough gel was applied to fully cover the surface, normally 100µl out of the syringe is enough. This was incubated for at 37°C for 10mins. Near the end of this time approximately 100 µl of 960mM $CaCl_2$ and 100 µl of 560mM KH_2PO_4 gels were squeeze out of their syringe onto a petri dish and quickly mix with a pipet tip. After incubation rinse the tooth sample and move it to a new well and add mineral formulation mixture. The sample was then incubated with this gel for 1hr-overnight (overnight will result in a more uniform coverage) at 37°C. Sample was rinsed for 20s and dried in vacuum for at least 2 hrs to reduce moisture. The samples were then broken at the notch to reveal the new layer. Microscopy preparation was done by adding the sample to an SEM holder with carbon tape in the same

orientation as with the solution mineralized and coated with a small layer of gold or platinum to reduce charge. Figure 5.6b shows a schematic of this approach.

5.2.5. *Mineral Microscopy*

Scanning Electron Microscopy

After coating and applying the Characterization was done using an FEI Sirion microscope (Sirion, FEI, Hillboro, OR, USA) operated at 10 keV acceleration voltage. Chemical composition measurements were done by an onboard energy dispersive X-ray spectroscopy (EDXS) system (X-MaxN Si drift detector with AZtecEnergy software package, Oxford Instruments, Abingdon, Oxfordshire, UK). These measurements were done in at least 4 different locations on the different layers of the tooth and averaged. The averages and standard deviations were calculated and expressed as the mean ± standard error.

Transmission Electron Microscopy

After mineral and ethanol mixture was gently pipetted drop-wise onto the carbon coated TEM grid it was then vacuum dried for at last 30mins before being imaged on the FEI Tecnai (FEI, Hillboro, OR, USA) operating at 200 keV. The diffraction pattern found from certain crystals in the bright field images were then analyzed by comparing them to different calcium phosphate diffraction patterns by Deniz Yucesoy and found to be hydroxapatite.

5.3. Results and Discussion

5.3.1. *Kinetics*

The kinetics of our short sADP5 was found via our novel technique of double drop diffusion couple since solution mineralization would not be able to determine if our peptide would work within the confines of a gel framework. That being said we did some TECAN kinetic work to insure that our mineral solutions would still mineralize calcium phosphate in a reasonable amount of time with or without peptide. Certain things that were found was the addition of NaOH when adjusting the pH would slow down the mineralization considerably and if enough was added along with HCl, calcium phosphate refused to form even if the pH was at 7.4. One possible explanation for this was the Na^+ ion competing with the Ca^+ ion for PO stabilization, since if enough NaOH was added it could end up being in a higher concentration than the $CaCl_2$.

So all later solutions that were created for use in the gels only used HCl to adjust the pH down to 7.4 as well as a Tris buffer of 24mM since that was enough to stabilize this pH, but not so high that it would also affect mineralization time in solution.

Once these affects were taken into consideration the solutions were then created and mixed with the formulation to create the gel form. From many rounds of optimization it was found that gels containing 960mM $CaCl_2$ and 560mM KH_2PO_4 provided the rate we were interested in after 30secs. Once we were able to get a consistent rate without the peptide we then started adding peptide to the gels starting first by just putting the peptide gel in between the two to see if it would allow mineralization through it. This slowed the mineralization considerably and we were unable to see any precipitation until after 20mins. We would always start the control and peptide at the same time since they were both in the same petri dish, so when tilted they would both be connected. These droplet couples were places far enough apart that they were not touching, but close enough to get them in the same camera shot along with the ruler nearby and this was done for all the following experiments. After mineralization slowed with putting the gel between the mineral droplets a new peptide incorporated gel was created. The peptide was put into the mineral gels so that the final concentration would be 0.8mM sADP5 by first making a 1.6mM sADP5 solution in 24mM Tris buffer and diluting it with the $CaCl_2$ solutions and KH_2PO_4 doubled in concentration so that the final concentrations were correct and was called F-sADP5. When peptide was added to the gels and the droplets were tilted the control appeared to be the first to mineralize in all cases, but the mineralization rate appeared to be higher for peptides in less than a minute and was able to out –pace the control from then on (Figure 5.7 a, b) After a day or so of mineralization the interface layer was removed, rinsed and processed to be imaged under TEM. Figure 5.7c shows both the control and the sADP5 creating hydroxyapatite crystals highlighted with the red arrows and seen by the diffraction pattern, provided by Deniz Yucesoy.

The double drop diffusion couple approach is a novel method that provides a way to obverse differences in kinetics within a gel. This approached indicated that the sADP5 was able to increase the mineralization rate still within a gel type conditions and synthesize hydroxyapatite crystals both things that will be necessary for the next step in this study.

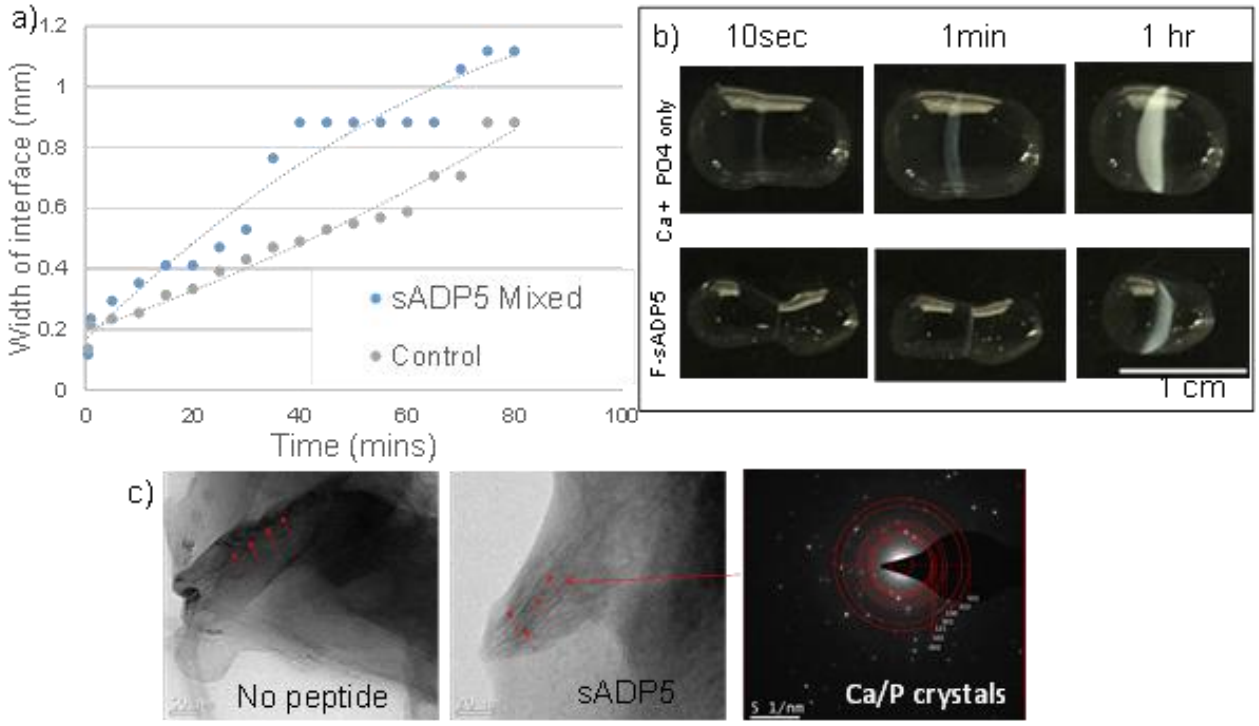

Figure 5.7: Double drop diffusion couple results.

5.3.2. *Surface Mineralization*

Mineralization was done via two methods: solution and formulation. The solution process was done to insure that the sADP5 peptide was still able to bind and mineralize similar to ADP5 even on an enamel surface. Gel was used to mimic the DEJ and observe possible morphological differences.

For the solution approach a similar peptide concentration was used in comparison to the DDDC work of 0.8mM sADP5 though several concentrations were tired, but this was the lowest that still allowed mineralization to be seen on the surface. The enamel was first soaked in this peptide solution then dried and added to a different well where mineralization solution was added so that the final concentrations of the minerals in solution were 9.6mM $CaCl_2$ and 5.6mM KH_2PO_4 once they were mixed. Figure 5.8 shows the SEM of the newly formed layer in comparison to the control enamel cross section. So first off the control samples' surface, on the side that wasn't etched, had waves on it which is indicative of perikymata, growth lines along the enamel formed during crown formation.[183] This indicates that there was no growth or deposition of calcium mineral onto the tooth surface for the control since they would have obscured this very biological

forming morphology. On the samples that were incubated with sADP5 in of them there is sometimes a clear demarcation between the new and old layer where the hydroxyapatite crystals are very prominently displayed. This clear line between is not always the case as seen in the 2hr image that is more difficult to determine where the new layer begins and ends though we have tried to mark it accordingly. Depending on incubation time and clear demarcating lines the layers varied between 2 to 5µm These new layers are a clear sign that the sADP5 is able to mineralize on the enamel surface similar to how the ADP5 did on a dentin tooth surface. The successful remineralization indicates this rationally designed peptide still has the similar functional groups that ADP5 has to interact with the surface of the mineralized tooth as well as sequester calcium and phosphate ions from the solution to aid its continued mineralization. sADP5 is not only easier to synthesize and dissolve, but due to this mineralization ability this shorter peptide may very well take the place of ADP5 in any potential future commercialized products.

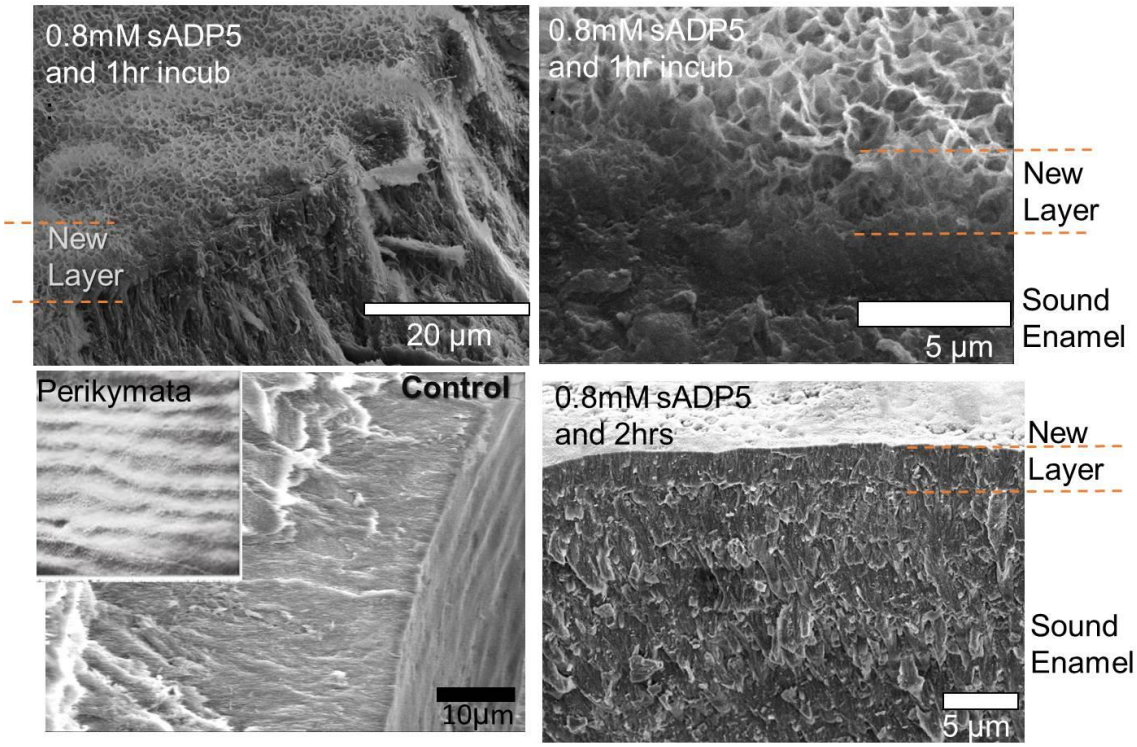

Figure 5.8: SEM images of the newly formed layer synthesized by sADP5 and it's the control under solution mineralization conditions and at different incubation times.

For the gel formulation approach the final peptide concentration within the gel was set so that it was at 0.8mM sADP5, same as in the DDDC and solution mineralization. The concentration of the calcium and phosphate gel was also kept consistent with the DDDC methodology at 960mM $CaCl_2$ and 560mM KH_2PO_4 and since it was able to show hydroxyapatite growth. After mixing equal amount of these two gels together the concentration halved in the final formulation added to the tooth after the peptide. Figure 5.9 shows the cross-sectional SEM images of these conditions, with and without any peptide after just 1 hr on the surface. In both the peptide and the control it is clear there was been serious etching of the enamel layer since what appear to be dentin tubules can be seen from the side with very little enamel on top of it. For the control there appears to be holes or a very rough surface on the enamel. Peptide exposed tooth on the other hand has what appears to be a layer formed which is slightly smoother in comparison. New layer thickness appears to be 1-2µm after 1hr.

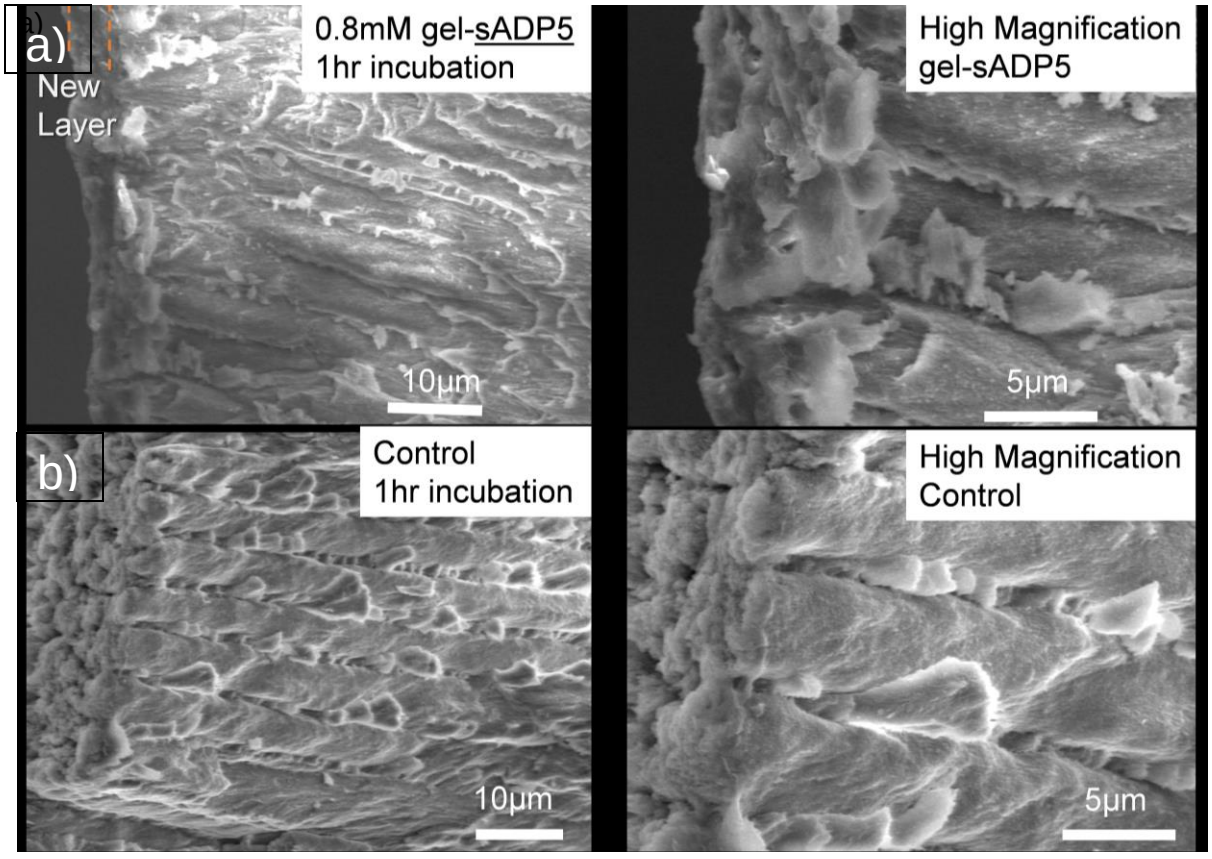

Figure 5.9: SEM images of the newly formed layer created by a) sADP in gel and b) tris buffer (control) on the surface of etched enamel under 1 hr incubation

The new layer formed from the 1hr incubation with 0.8mM sADP5 formulation was the analyzed with EDS to determine if it still contained the organic peptide within it. At least 4 different EDS points were taken for each of their respective locations, be it surface or inner part of the enamel. Figure 5.10b shows the EDS analysis of the newly formed layer vs the inner layer of the tooth sample (Figure 5.10a). The Ca/P ratio for both the new layer and the inner layers were within a standard deviation of one another. A calcium phosphate ratio of around 1.62 was found for the inner part of the tooth, but the surface was slightly higher at 1.68, but again the standard deviation of around 0.3 was such that they were comparable and most likely both hydroxyapatite. One of the major differences found the EDS was the amount of the carbon and oxygen elements found in the surface indicating that there is most likely organics incorporated within this layer. There was also trace amount of gold on the surface which was coated on the tooth to reduce charge.

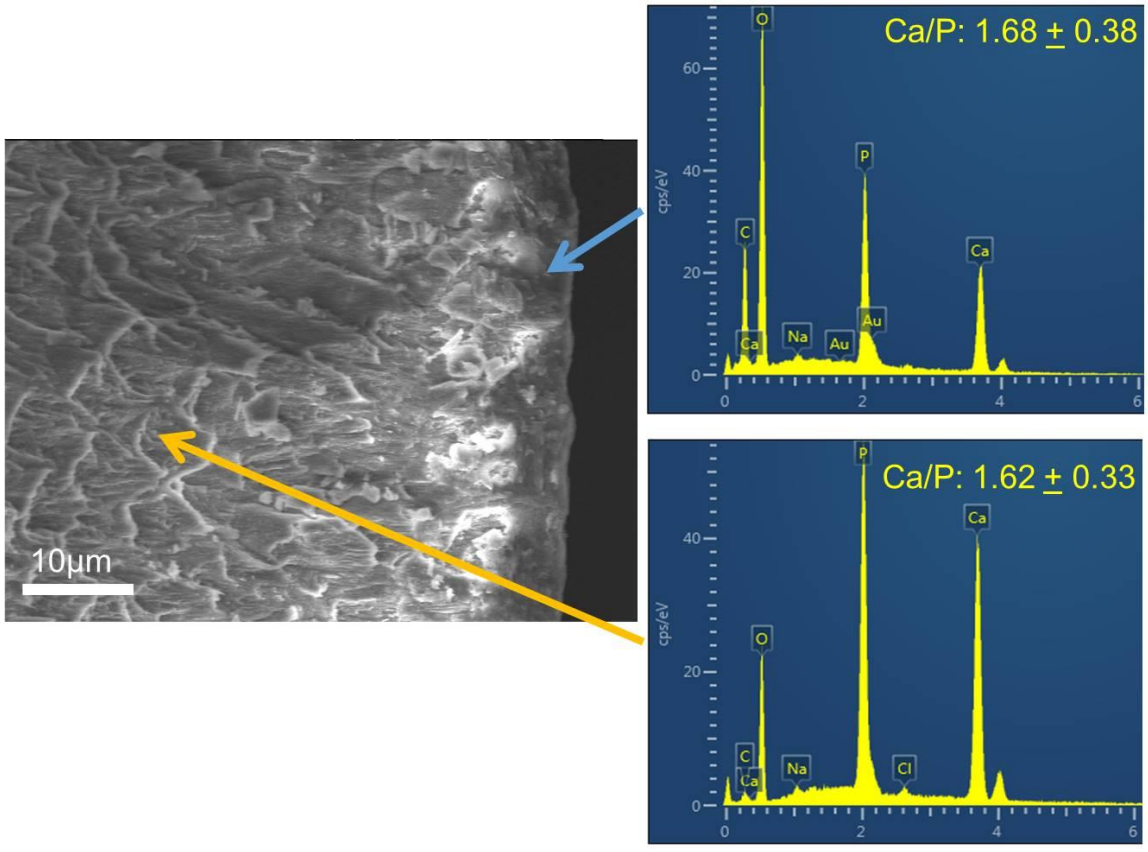

Figure 5.10: a) SEM images and b) EDS analysis of the newly formed layer created by sADP in gel on the

5.4. Conclusion

In the previous sections a shorter sADP5 peptide was rationally designed to having higher solubility and still mineralization hydroxyapatite on a tooth surface. This mineralization was done in both solution and a formulated gel to simulate the dentin enamel junction found in tooth development. The sADP5 mineralization in solution on enamel was able to create a new layer of hydroxyapatite that covered the surface of the tooth, unlike in the control. Mineralization with the longer peptide ADP5 had up this point only been used to mineralize on dentin button, but this confirmed that it would be acceptable to use on enamel as well.[33] Formulation was created to act similar to the extracellular matrix in terms of viscosity and to see how it would affect the mineralization of the peptide on the tooth surface after slight etching with a demineralization solution. We found that indeed a layer did appear to form onto the tooth surface and even appeared to have incorporated some of our peptide onto the surface during that step. In order to determine how this sADP5 was able to affect the kinetics in the gel we created a novel double-drop diffusion couple technique that allowed us to show that the peptide is in indeed increasing the mineralization rate slightly compared to the mineralization gel without it.

Chapter 6: **Highlights of Personal Contributions and Future Work**

The following are the highlights of the work I have accomplished during my graduate studies and what I have personally contributed to the field of molecular biomimetics, material science and peptide development.

6.1. Peptide Synthesis and Development

Many of the chimeric and solid binding peptides discussed in the first chapter from our lab's work I either had a hand in designing to have certain properties or synthesize over the years. The knowledge of synthesizing these peptides has helped me in my own work and all peptides used in this thesis were designed and synthesized by me with some help from undergraduates in training.

6.2. Rationally Designed Solid-Binding Amyloid Assembly Peptide

The shorter Aβ (12-24) was chosen after searching the literature for potential amyloid sequences that could recognize a graphite surface and retain its fibrillating abilities. This sequences length and location within the larger protein was determined by further research into the amyloid fibril creation and mechanisms and how they might be influenced by this segment of the full length protein. Once chosen I went about synthesizing the peptide and assembling it on the surface of graphite. Many different conditions were used including annealing at 37°C at one point to see if that would affect the formation. Assembly of the Aβ WT was found at 1μM after 3hrs of incubation consistently. After this was found I did molecular dynamics using Hyperchem 7.5 (taught to me by E.E. Oren) on this sequence and three other mutations as well to see how they might affect the conformation of the peptide on the surface. I then synthesized these mutations and tested each of them on graphite to see their morphology. Some of these peptides mainly the KOHH was able to bind even better to the surface than the wild type, but was unable to assemble due to not having the histadine present. None of them were able to assemble as well as the control, and only the knock-in mutation FF to YY showed any kind of fibril formation, but at a much higher concentration than the wild type, indicating possible assembly on its own monolayer rather than on the surface. Contact angle measurements were also done in order to determine the peptides effect on hydrophobicity and how much it is able to change the bare graphite. Only the knock-outs appeared to affect the angles at all making the surface more hydrophilic than either the WT or bare graphite. This study showed that a rationally designed

peptide from a fibril forming protein could be used to recognize and assemble onto a graphite surface.

Possible future paths that can be explored in this work are further analysis of the contact angle measurements and seeing how different concentrations might affect the surface coverage and the displayed motifs. Along with this more work concerning the KOFF inhibition could prove valuable as a possible anti-assembly approach for device regeneration or other more biologically relevant work.

6.3. Control of crystal polymorph by peptides

Having peptides recognize a surface and arrange themselves along certain planes indicated that they could also be used to recognize polymorphs and control their formation when used as a mineralization agent. In order to find these peptides I, with the help of Dr. Marketa Hnilova, selected peptides using cell surface display for the calcite and aragonite structures. I did everything related to the calcite binders in terms of selection and characterization, where Dr Marketa Hnilova did the aragonite binders and I learned from her in the process. These peptides were then characterized using fluorescent microscopy to determine binding strength. After characterization several of the strong binders were selected from each to synthesize and characterized again as peptides. AP7-derived peptides (DN-AraBP1 and DN-AraBP2) were found that had high and low similarities to the aragonite binders using similarity analysis. After characterization it was found that one of the strong binding aragonite binders was able to bind specifically to aragonite. Both of the AP7-derived peptides shows a high ability to bind to aragonite, but still had some slight binding to calcite as well. The calcite binder on the other hand bound very well to calcite, but also slightly to the aragonite. After binding characterization the peptides were then used to mineralize calcium carbonate using a modification of Colfen's procedure to better mimic natural calcium. Calcite mineralization with the peptides produced vaterite for several of the peptides many having unique morphologies under SEM. 3Ara11 produced what appeared to be vaterite that has never been seen in the literature where platelets are stacked perpendicular at the end of the normal spherical superstructure. The XRD was unable to confirm vaterite formation expect for in two cases with the specific aragonite and calcite binders, which indicates that binding affinity may play a role in polymorph control. The vaterite percentage in these mixtures was calculated and found to be related to peptide concentration for

the aragonite binding peptide. The calcite binding peptide was only able to produce vaterite at a high enough concentration while at the lower concentrations tested it just formed calcite that showed signs of growth inhibition.

Possible future paths for this research is doing this mineralization again in a gel formulation instead of under diffusion conditions since this might better mimic the extracellular matrix in the cell and as such produce aragonite. Another thing that could be done is DDDC on the different peptides to see if any significantly increases the kinetics of formation.

6.4. Peptide Mineral Surface Assembly

For the sADP5 peptide work I helped rationally design the peptide since the ADP5 was unable to solubilize at high enough concentrations to work within the formulation. The formulation recipe was created by Hanson Fong who was also instrumental in taking many of the SEM images. The sADP5 mineralization in solution on enamel was able to create a new layer of hydroxyapatite that covered the surface of the tooth, unlike in the control. Formulation was created to act similar to the extracellular matrix in terms of viscosity and to see how it would affect the mineralization of the peptide on the tooth surface after slight etching with a demineralization solution. A layer did appear to form onto the tooth surface and even to have incorporated some of our peptide onto the surface during that step. In order to determine how this sADP5 was able to affect the kinetics in the gel I created a novel double-drop diffusion couple technique that allowed us to show that the peptide is in indeed increasing the mineralization rate slightly compared to the mineralization gel without it.

Some ideas for future studies that have been done or are ongoing are to use this formulation clinically and by using in vivo studies. Due to patent related issues more information concerning this is confidential.

Author Publications

1 Gresswell, C.; So C.; Hayamizu Y.; Tamerler C.; and Sarikaya M. Self-Assembly of Mutant Amyloid Peptides on Graphite. (Being Submitted)

2 Gresswell, C.; Hnilova, M.; Oren, E. E. Sarikaya M.; and Tamerler C.; Calcium Carbonate Formation by Genetically Engineered Binding Peptides. (Being Submitted)

3 Hnilova, M.; Liu, X.; Yuca, E.; Jia, C.; Wilson, B.; Karatas, A. Y.; Gresswell, C.; Ohuchi, F.; Kitamura, K.; Tamerler, C. Multifunctional Protein-Enabled Patterning on Arrayed Ferroelectric Materials. *Acs Applied Materials & Interfaces* **2012**, *4*, 1865-1871.

4 Hnilova, M.; Khatayevich, D.; Carlson, A.; Oren, E. E.; Gresswell, C.; Zheng, S.; Ohuchi, F.; Sarikaya, M.; Tamerler, C. Single-step fabrication of patterned gold film array by an engineered multi-functional peptide. *Journal of Colloid and Interface Science* **2012**, *365*, 97-102.

5 Khatayevich, D.; So, C. R.; Hayamizu, Y.; Gresswell, C.; Sarikaya, M. Controlling the Surface Chemistry of Graphite by Engineered Self-Assembled Peptides. *Langmuir* **2012**, *28*, 8589-8593.

6 Khatayevich, D.; Page, T.; Gresswell, C.; Hayamizu, Y.; Grady, W.; Sarikaya, M. Selective Detection of Target Proteins by Peptide-Enabled Graphene Biosensor. *Small* **2014**, *10*, 1505-1513.

7 So, C. R.; Hayamizu, Y.; Yazici, H.; Gresswell, C.; Khatayevich, D.; Tamerler, C.; Sarikaya, M. Controlling Self-Assembly of Engineered Peptides on Graphite by Rational Mutation. *Acs Nano* **2012**, *6*, 1648-1656.

8 Dogan, S.; Fong, H. K.; Yucesoy, D. T.; Cousin, T.; Gresswell, C. G.; Dag, S.; Huang, G. J.; Sarikaya, M., Biomimetic Tooth Repair: Amelogenin-derived peptide enables in vitro remineralization of human enamel. *ACS Biomaterials Science & Engineering* **2018**.

Bibliography

1 Nelson, M. T. & Quayle, J. M. Physiological roles and properties of potassium channels in arterial smooth muscle. *The American journal of physiology* **268**, C799 (1995).

2 Patai, S. & Wiley, I. *The chemistry of the thiol group*. (London : Wiley-Interscience, 1974).

3 Allen, C. F. H., Fournier, J. O. & Humphlett, W. J. THE THERMAL REVERSIBILITY OF THE MICHAEL REACTION: IV. THIOL ADDUCTS. *Canadian Journal of Chemistry* **42**, 2616-2620, doi:10.1139/v64-383 (1964).

4 Nair, D. P. *et al.* The Thiol-Michael Addition Click Reaction: A Powerful and Widely Used Tool in Materials Chemistry. *Chemistry of Materials* **26**, 724-744, doi:10.1021/cm402180t (2014).

5 Zhang, W., Chen, K. & Chen, G. *Thiol-Based "Click" Chemistry for Macromolecular Architecture Design*. (2016).

6 Hoyle, C. E., Lowe, A. B. & Bowman, C. N. Thiol-click chemistry: a multifaceted toolbox for small molecule and polymer synthesis. *Chemical Society Reviews* **39**, 1355-1387, doi:10.1039/b901979k (2010).

7 Borzenkov, M. *et al.* Thermal and Chemical Stability of Thiol Bonding on Gold Nanostars. *Langmuir : the ACS journal of surfaces and colloids* **31**, 8081, doi:10.1021/acs.langmuir.5b01473 (2015).

8 Gilbert, H. F. [2] Thiol/disulfide exchange equilibria and disulfidebond stability. *Methods in Enzymology* **251**, 8-28, doi:10.1016/0076-6879(95)51107-5 (1995).

9 So, C. R. *et al.* Controlling Self-Assembly of Engineered Peptides on Graphite by Rational Mutation. *Acs Nano* **6**, 1648-1656, doi:10.1021/nn204631x (2012).

10 Khatayevich, D. *et al.* Selective Detection of Target Proteins by Peptide-Enabled Graphene Biosensor. *Small* **10**, 1505-1513, doi:10.1002/smll.201302188 (2014).

11 Khatayevich, D., So, C. R., Hayamizu, Y., Gresswell, C. & Sarikaya, M. Controlling the Surface Chemistry of Graphite by Engineered Self-Assembled Peptides. *Langmuir* **28**, 8589-8593, doi:10.1021/la300268d (2012).

12 Hnilova, M. *et al.* Fabrication of hierarchical hybrid structures using bio-enabled layer-by-layer self-assembly. *Biotechnology and Bioengineering* **109**, 1120-1130, doi:10.1002/bit.24405 (2012).

13 Tamerler, C. *et al.* Materials Specificity and Directed Assembly of a Gold-Binding Peptide. *Small* **2**, 1372-1378, doi:10.1002/smll.200600070 (2006).

14 Sterman, S. & Marsden, J. G. SILANE COUPLING AGENTS. *Industrial & Engineering Chemistry* **58**, 33-37, doi:10.1021/ie50675a010 (1966).

15 Atkinson, J. R. & Cicek, R. Z. Silane cross-linked polyethylene for prosthetic applications Part I. Certain physical and mechanical properties related to the nature of the material. *Biomaterials* **4**, 267-275, doi:10.1016/0142-9612(83)90026-1 (1983).

16 Witucki, G. L. Silane primer: chemistry and applications of alkoxy silanes. *Journal of Coatings Technology* **65**, 57-60 (1993).

17 Matinlinna, J. P., Lassila, L., Ozcan, M., Yli-Urpo, A. & Vallittu, P. K. in *Int. J. Prosthodont.* Vol. 17 155-164 (2004).

18 Chen, J. R. Characteristics of fire and explosion in semiconductor fabrication processes. *Process Safety Progress* **21**, 19-25, doi:10.1002/prs.680210106 (2002).

19 Chen, J.-R. *et al.* Analysis of a silane explosion in a photovoltaic fabrication plant. *Process Safety Progress* **25**, 237-244, doi:10.1002/prs.10136 (2006).
20 Seo, H. S. *et al.* A Three-Dimensional Nanostructured Array of Protein Nanoparticles. *Advanced Functional Materials* **20**, 4055-4061, doi:10.1002/adfm.201001144 (2010).
21 Knowles, T. P. J., Oppenheim, T. W., Buell, A. K., Chirgadze, D. Y. & Welland, M. E. Nanostructured films from hierarchical self-assembly of amyloidogenic proteins. *Nature Nanotechnology* **5**, 204-207, doi:10.1038/nnano.2010.26 (2010).
22 Sarikaya, M., Fong, H., Frech, D. W. & Humbert, R. Biomimetic assembly of nanostructured materials. *Bioceramics* **293**, 83-97 (1999).
23 Hnilova, M. *et al.* Multifunctional Protein-Enabled Patterning on Arrayed Ferroelectric Materials. *Acs Applied Materials & Interfaces* **4**, 1865-1871, doi:10.1021/am300177t (2012).
24 Tamerler, C. *et al.* Molecular Biomimetics: GEPI-Based Biological Routes to Technology. *Biopolymers* **94**, 78-94, doi:10.1002/bip.21368 (2010).
25 Hnilova, M. *et al.* Single-step fabrication of patterned gold film array by an engineered multi-functional peptide. *Journal of Colloid and Interface Science* **365**, 97-102, doi:10.1016/j.jcis.2011.09.006 (2012).
26 Honkanen, M. *et al.* Characterization of silane layers on modified stainless steel surfaces and related stainless steel–plastic hybrids. *Applied Surface Science* **257**, 9335-9346, doi:10.1016/j.apsusc.2011.05.058 (2011).
27 Aissaoui, N., Bergaoui, L., Landoulsi, J., Lambert, J.-F. & Boujday, S. Silane layers on silicon surfaces: mechanism of interaction, stability, and influence on protein adsorption. *Langmuir : the ACS journal of surfaces and colloids* **28**, 656, doi:10.1021/la2036778 (2012).
28 Yucesoy, D. *et al.* Chimeric Peptides as Implant Functionalization Agents for Titanium Alloy Implants with Antimicrobial Properties. *The Journal of The Minerals, Metals & Materials Society (TMS)* **67**, 754-766, doi:10.1007/s11837-015-1350-7 (2015).
29 Khatayevich, D. *et al.* Biofunctionalization of materials for implants using engineered peptides. *Acta Biomaterialia* **6**, 4634-4641, doi:10.1016/j.actbio.2010.06.004 (2010).
30 Yazici, H. *et al.* Engineered Chimeric Peptides as Antimicrobial Surface Coating Agents toward Infection-Free Implants. *ACS applied materials & interfaces* **8**, 5070, doi:10.1021/acsami.5b03697 (2016).
31 Matinlinna, J. P., Lung, C. Y. K. & Tsoi, J. K. H. Silane adhesion mechanism in dental applications and surface treatments: A review. *Dental Materials* **34**, 13-28, doi:10.1016/j.dental.2017.09.002 (2018).
32 Lung, C. & Matinlinna, J. P. in *Dent. Mater.* Vol. 28 467-477 (2012).
33 Gungormus, M. *et al.* Cementomimetics-constructing a cementum-like biomineralized microlayer via amelogenin-derived peptides. *International Journal of Oral Science* **4**, 69-77, doi:10.1038/ijos.2012.40 (2012).
34 Gungormus, M. *et al.* Regulation of in vitro Calcium Phosphate Mineralization by Combinatorially Selected Hydroxyapatite-Binding Peptides. *Biomacromolecules* **9**, 966-973, doi:10.1021/bm701037x (2008).
35 Smith, G. P. Filamentous fusion phage: novel expression vectors that display cloned antigens on the virion surface. *Science* **228**, 1315-1317 (1985).

36 Freudl, R., Macintyre, S., Degen, M. & Henning, U. Cell surface exposure of the outer membrane protein OmpA of Escherichia coli K-12. *Journal of Molecular Biology* **188**, 491-494, doi:10.1016/0022-2836(86)90171-3 (1986).
37 Stanley, B. Metal-recognition by repeating polypeptides. *Nature Biotechnology* **15**, 269, doi:10.1038/nbt0397-269 (1997).
38 Baneyx, F. & Schwartz, D. T. Selection and analysis of solid-binding peptides. *Current Opinion in Biotechnology* **18**, 312-317, doi:10.1016/j.copbio.2007.04.008 (2007).
39 Sidhu, S. S. Phage display in pharmaceutical biotechnology. *Current Opinion in Biotechnology* **11**, 610-616, doi:10.1016/S0958-1669(00)00152-X (2000).
40 Gao, C. *et al.* Making artificial antibodies: A format for phage display of combinatorial heterodimeric arrays. *Proceedings of the National Academy of Sciences of the United States of America* **96**, 6025-6030, doi:10.1073/pnas.96.11.6025 (1999).
41 Gray, B. P. & Brown, K. C. Combinatorial Peptide Libraries: Mining for Cell-Binding Peptides. *Chemical reviews* **114**, 1020-1081, doi:10.1021/cr400166n (2014).
42 Pinilla, C., Appel, J. R., Blanc, P. & Houghten, R. A. Rapid identification of high affinity peptide ligands using positional scanning synthetic peptide combinatorial libraries. *BioTechniques* **13**, 901 (1992).
43 Dooley, C. T. & Houghten, R. A. Synthesis and screening of positional scanning combinatorial libraries. *Methods in molecular biology (Clifton, N.J.)* **87**, 13-24 (1998).
44 Gaskin, D. J. H., Starck, K. & Vulfson, E. N. Identification of inorganic crystal-specific sequences using phage display combinatorial library of short peptides: A feasibility study. *Biotechnology Letters* **22**, 1211-1216 (2000).
45 Iannolo, G., Minenkova, O., Gonfloni, S., Castagnoli, L. & Cesareni, G. Construction, exploitation and evolution of a new peptide library displayed at high density by fusion to the major coat protein of filamentous phage. *Biological chemistry* **378**, 517, doi:10.1515/bchm.1997.378.6.517 (1997).
46 Sarikaya, M., Tamerler, C., Schwartz, D. T. & Baneyx, F. MATERIALS ASSEMBLY AND FORMATION USING ENGINEERED POLYPEPTIDES. *Annual review of materials research* **34**, 373-408, doi:10.1146/annurev.matsci.34.040203.121025 (2004).
47 Freudl, R., Schwarz, H., Degen, M. & Henning, U. The signal sequence suffices to direct export of outer membrane protein OmpA of Escherichia coli K-12. *The Journal of Bacteriology* **169**, 66, doi:10.1128/jb.169.1.66-71.1987 (1987).
48 Yoshida, H., Baik, S.-H. & Harayama, S. An effective peptide screening system using recombinant fluorescent bacterial surface display. *Biotechnology Letters* **24**, 1715-1722, doi:10.1023/A:1020688427952 (2002).
49 Eric, T. B. & Wittrup, K. D. Yeast surface display for screening combinatorial polypeptide libraries. *Nature Biotechnology* **15**, 553, doi:10.1038/nbt0697-553 (1997).
50 Gai, S. A. & Wittrup, K. D. Yeast surface display for protein engineering and characterization. *Current Opinion in Structural Biology* **17**, 467-473, doi:10.1016/j.sbi.2007.08.012 (2007).
51 Sidhu, S. S., Lowman, H. B., Cunningham, B. C. & Wells, J. A. Phage display for selection of novel binding peptides. *Methods in Enzymology* **328**, 333-363 (2000).
52 Li, C. M., Botsaris, G. D. & Kaplan, D. L. Selective in vitro effect of peptides on calcium carbonate crystallization. *Crystal Growth & Design* **2**, 387-393, doi:10.1021/cg0255467 (2002).

53 Gebauer, D., Verch, A., Borner, H. G. & Colfen, H. Influence of Selected Artificial Peptides on Calcium Carbonate Precipitation - A Quantitative Study. *Crystal Growth & Design* **9**, 2398-2403, doi:10.1021/cg801292p (2009).
54 Hnilova, M. *et al.* Effect of Molecular Conformations on the Adsorption Behavior of Gold-Binding Peptides. *Langmuir* **24**, 12440-12445, doi:10.1021/la801468c (2008).
55 Kacar, T. *et al.* Quartz Binding Peptides as Molecular Linkers towards Fabricating Multifunctional Micropatterned Substrates. *Advanced Materials* **21**, 295-299, doi:10.1002/adma.200801877 (2009).
56 Vol. 8 42-42 (1992).
57 Dooley, C. T. & Houghten, R. A. Synthesis and screening of positional scanning combinatorial libraries. *Methods in molecular biology (Clifton, N.J.)* **87**, 13 (1998).
58 Vanhee, P. *et al.* Computational design of peptide ligands. *Trends in biotechnology*. **29**, 231-239, doi:10.1016/j.tibtech.2011.01.004 (2011).
59 Attwood, T. K. Genomics. The Babel of bioinformatics. *Science (New York, N.Y.)* **290**, 471, doi:10.1126/science.290.5491.471 (2000).
60 Oren, E. E. *et al.* A novel knowledge-based approach to design inorganic-binding peptides. *Bioinformatics* **23**, 2816-2822, doi:10.1093/bioinformatics/btm436 (2007).
61 Oren, E. E. *et al.* Probing the Molecular Mechanisms of Quartz-Binding Peptides. *Langmuir* **26**, 11003-11009, doi:10.1021/la100049s (2010).
62 Suárez-Díaz, E. Making room for new faces: evolution, genomics and the growth of bioinformatics. *History and philosophy of the life sciences* **32**, 65 (2010).
63 Henikoff, S. & Henikoff, J. G. Amino Acid Substitution Matrices from Protein Blocks. *Proceedings of the National Academy of Sciences of the United States of America* **89**, 10915-10919, doi:10.1073/pnas.89.22.10915 (1992).
64 Henikoff, S. & Henikoff, J. G. Position-based sequence weights. *Journal of Molecular Biology* **243**, 574-578, doi:10.1016/0022-2836(94)90032-9 (1994).
65 Jones, D. T., Taylor, W. R. & Thornton, J. M. The rapid generation of mutation data matrices from protein sequences. *Bioinformatics* **8**, 275-282, doi:10.1093/bioinformatics/8.3.275 (1992).
66 DeOliveira, D. B. & Laursen, R. A. Control of calcite crystal morphology by a peptide designed to bind to a specific surface. *Journal of the American Chemical Society* **119**, 10627-10631 (1997).
67 Masica, D. L., Schrier, S. B., Specht, E. A. & Gray, J. J. De Novo Design of Peptide-Calcite Biomineralization Systems. *Journal of the American Chemical Society* **132**, 12252-12262, doi:10.1021/ja1001086 (2010).
68 Vanhee, P. *et al.* PepX: a structural database of non-redundant protein-peptide complexes. *Nucleic acids research* **38**, D545, doi:10.1093/nar/gkp893 (2010).
69 Wang, S.-H. & Yu, J. Structure-based design for binding peptides in anti-cancer therapy. *Biomaterials* **156**, 1-15, doi:10.1016/j.biomaterials.2017.11.024 (2018).
70 Juretić, D., Vukičević, D., Ilić, N., Antcheva, N. & Tossi, A. Computational design of highly selective antimicrobial peptides. *Journal of Chemical Information and Modeling* **49**, 2873-2882, doi:10.1021/ci900327a (2009).
71 Pacella, M. S. & Gray, J. J. A Benchmarking Study of Peptide-Biomineral Interactions. *Crystal Growth and Design* **18**, 607-616, doi:10.1021/acs.cgd.7b00109 (2017).

72 Lévy, R. *et al.* Rational and Combinatorial Design of Peptide Capping Ligands for Gold Nanoparticles. *Journal of the American Chemical Society* **126**, 10076-10084, doi:10.1021/ja0487269 (2004).
73 Korendovych, I. V. Rational and Semirational Protein Design. *Methods in molecular biology (Clifton, N.J.)* **1685**, 15, doi:10.1007/978-1-4939-7366-8_2 (2018).
74 Michenfelder, M. *et al.* Characterization of two molluscan crystal-modulating biomineralization proteins and identification of putative mineral binding domains. *Biopolymers* **70**, 522-533, doi:10.1002/bip.10536 (2003).
75 Fu, G., Valiyaveettil, S., Wopenka, B. & Morse, D. E. CaCO3 biomineralization: Acidic 8-kDa proteins isolated from aragonitic abalone shell nacre can specifically modify calcite crystal morphology. *Biomacromolecules* **6**, 1289-1298, doi:10.1021/bm049314v (2005).
76 Shen, X. Y., Belcher, A. M., Hansma, P. K., Stucky, G. D. & Morse, D. E. Molecular cloning and characterization of lustrin A, a matrix protein from shell and pearl nacre of Haliotis rufescens. *Journal of Biological Chemistry* **272**, 32472-32481 (1997).
77 Collino, S., Kim, I. W. & Evans, J. S. Identification of an "acidic" C-terminal mineral modification sequence from the mollusk shell protein Asprich. *Crystal Growth & Design* **6**, 839-842, doi:10.1021/cg060016m (2006).
78 Samata, T. *et al.* A new matrix protein family related to the nacreous layer formation of Pinctada fucata. *Febs Letters* **462**, 225-229 (1999).
79 Amos, F. F., Ndao, M. & Evans, J. S. Evidence of Mineralization Activity and Supramolecular Assembly by the N-Terminal Sequence of ACCBP, a Biomineralization Protein That Is Homologous to the Acetylcholine Binding Protein Family. *Biomacromolecules* **10**, 3298-3305, doi:10.1021/bm900893f (2009).
80 Miyamoto, H. *et al.* A carbonic anhydrase from the nacreous layer in oyster pearls. *Proceedings of the National Academy of Sciences of the United States of America* **93**, 9657-9660 (1996).
81 Amos, F. F., Destine, E., Ponce, C. B. & Evans, J. S. The N- and C-Terminal Regions of the Pearl-Associated EF Hand Protein, PFMG1, Promote the Formation of the Aragonite Polymorph in Vitro. *Crystal Growth & Design* **10**, 4211-4216, doi:10.1021/cg100363m (2010).
82 Evans, J. S. "Tuning in" to Mollusk Shell Nacre- and Prismatic-Associated Protein Terminal Sequences. Implications for Biomineralization and the Construction of High Performance Inorganic-Organic Composites. *Chemical Reviews* **108**, 4455-4462, doi:10.1021/cr078251e (2008).
83 Tsukamoto, D., Sarashina, I. & Endo, K. Structure and expression of an unusually acidic matrix protein of pearl oyster shells. *Biochemical and Biophysical Research Communications* **320**, 1175-1180, doi:10.1016/j.bbrc.2004.06.072 (2004).
84 Kim, I. W., DiMasi, E. & Evans, J. S. Identification of mineral modulation sequences within the nacre-associated oyster shell protein, n16. *Crystal Growth & Design* **4**, 1113-1118, doi:10.1021/cg049919a (2004).
85 Keene, E. C., Evans, J. S. & Estroff, L. A. Matrix Interactions in Biomineralization: Aragonite Nucleation by an Intrinsically Disordered Nacre Polypeptide, n16N, Associated with a beta-Chitin Substrate. *Crystal Growth & Design* **10**, 1383-1389, doi:10.1021/cg901389v (2010).

86 Metzler, R. A. *et al.* Probing the organic-mineral interface at the molecular level in model biominerals. *Langmuir* **24**, 2680-2687, doi:10.1021/la7031237 (2008).
87 Wustman, B. A., Weaver, J. C., Morse, D. E. & Evans, J. S. Characterization of a Ca(II)-, mineral-interactive polyelectrolyte sequence from the adhesive elastomeric biomineralization protein lustrin A. *Langmuir* **19**, 9373-9381, doi:10.1021/la034857w (2003).
88 Zimenkov, Y. *et al.* Rational Design of a Reversible pH-Responsive Switch for Peptide Self-Assembly. *Journal of the American Chemical Society* **128**, 6770-6771, doi:10.1021/ja0605974 (2006).
89 Sipe, J. D. & Cohen, A. S. Review: History of the amyloid fibril. *Journal of Structural Biology* **130**, 88-98 (2000).
90 Kisilevsky, R., Raimondi, S. & Bellotti, V. Historical and Current Concepts of Fibrillogenesis and In vivo Amyloidogenesis: Implications of Amyloid Tissue Targeting.(Report)(Brief article). *Frontiers in Molecular Biosciences* **3**, doi:10.3389/fmolb.2016.00017 (2016).
91 Alan, S. C. & Evan, C. Electron Microscopic Observations on a Fibrous Component in Amyloid of Diverse Origins. *Nature* **183**, 1202, doi:10.1038/1831202a0 (1959).
92 Fändrich, M. On the structural definition of amyloid fibrils and other polypeptide aggregates. *Cellular and Molecular Life Sciences* **64**, 2066-2078, doi:10.1007/s00018-007-7110-2 (2007).
93 Nilsson, M. R. Techniques to study amyloid fibril formation in vitro. *Methods* **34**, 151-160, doi:10.1016/j.ymeth.2004.03.012 (2004).
94 Harper, J. D., Wong, S. S., Lieber, C. M. & Lansbury, P. T. Assembly of A beta amyloid protofibrils: An in vitro model for a possible early event in Alzheimer's disease. *Biochemistry* **38**, 8972-8980 (1999).
95 Kumar, S. & Udgaonkar, J. B. Mechanisms of amyloid fibril formation by proteins. *Current Science* **98**, 639-656 (2010).
96 Koo, E. H., Lansbury, P. T. & Kelly, J. W. Amyloid diseases: Abnormal protein aggregation in neurodegeneration. *Proceedings of the National Academy of Sciences of the United States of America* **96**, 9989-9990, doi:10.1073/pnas.96.18.9989 (1999).
97 Harper, J. D., Wong, S. S., Lieber, C. M. & Lansbury, P. T. Observation of metastable A beta amyloid protofibrils by atomic force microscopy. *Chemistry & Biology* **4**, 119-125, doi:10.1016/s1074-5521(97)90255-6 (1997).
98 Chiti, F. & Dobson, C. M. Protein misfolding, functional amyloid, and human disease. *Annual Review of Biochemistry* **75**, 333-366, doi:10.1146/annurev.biochem.75.101304.123901 (2006).
99 Blackley, H. K. L. *et al.* In-situ atomic force microscopy study of beta-amyloid fibrillization. *Journal of Molecular Biology* **298**, 833-840, doi:10.1006/jmbi.2000.3711 (2000).
100 Gallo, G. R. *et al.* Characterization of tissue amyloid by immunofluorescence microscopy. *Clinical Immunology and Immunopathology* **39**, 479-490, doi:10.1016/0090-1229(86)90175-3 (1986).
101 Khurana, R., Uversky, V. N., Nielsen, L. & Fink, A. L. Is Congo red an amyloid-specific dye? *The Journal of biological chemistry* **276**, 22715, doi:10.1074/jbc.M011499200 (2001).

102 Ashburn, T. T., Han, H., McGuinness, B. F. & Lansbury, P. T. Amyloid probes based on Congo Red distinguish between fibrils comprising different peptides. *Chemistry & Biology* **3**, 351-358 (1996).
103 Stopa, B. *et al.* The structure and protein binding of amyloid-specific dye reagents. *Acta biochimica Polonica* **50**, 1213 (2003).
104 Skowronek, M. *et al.* Self-assembly of Congo Red - A theoretical and experimental approach to identify its supramolecular organization in water and salt solutions. *Biopolymers* **46**, 267-281, doi:10.1002/(SICI)1097-0282(19981015)46:5<267::AID-BIP1>3.0.CO;2-N (1998).
105 Fox, N. C. *et al.* Presymptomatic hippocampal atrophy in Alzheimer's disease - A longitudinal MRI study. *Brain* **119**, 2001-2007 (1996).
106 Jack, C. R. *et al.* Serial PIB and MRI in normal, mild cognitive impairment and Alzheimer's disease: implications for sequence of pathological events in Alzheimer's disease. *Brain* **132**, 1355-1365, doi:10.1093/brain/awp062 (2009).
107 Magnin, B. *et al.* Support vector machine-based classification of Alzheimer's disease from whole-brain anatomical MRI. *A Journal Devoted to Neuroimaging and Interventional Neuroradiology* **51**, 73-83, doi:10.1007/s00234-008-0463-x (2009).
108 Falk, R. H. & Dubrey, S. W. Amyloid Heart Disease. *Progress in Cardiovascular Diseases* **52**, 347-361, doi:10.1016/j.pcad.2009.11.007 (2010).
109 Monzawa, S. *et al.* A case with primary amyloidosis of the liver and spleen: radiologic findings. *European Journal of Radiology* **41**, 237-241, doi:10.1016/S0720-048X(01)00407-7 (2002).
110 Harper, J. D. & Lansbury, P. T. Models of amyloid seeding in Alzheimier's disease and scrapie: Mechanistic truths and physiological consequences of the time-dependent solubility of amyloid proteins. *Annual Review of Biochemistry* **66**, 385-407, doi:10.1146/annurev.biochem.66.1.385 (1997).
111 Alzheimer, s Disease, E., amp & Referral, C. *Alzheimer's disease*. (Bethesda, Md. : U.S. Dept. of Health and Human Services, National Institutes of Health, Alzheimer's Disease Education & Referral Center, 2011).
112 Carlos, G. D. & Bart De, S. Alzheimer's dementia by circulation disorders: when trees hide the forest. *Nature Cell Biology* **11**, 114, doi:10.1038/ncb0209-114 (2009).
113 Sveinbjornsdottir, S. Vol. 139 318-324 (2016).
114 Crosiers, D., Theuns, J., Cras, P. & Van Broeckhoven, C. Parkinson disease: Insights in clinical, genetic and pathological features of monogenic disease subtypes. *Journal of Chemical Neuroanatomy* **42**, 131-141, doi:10.1016/j.jchemneu.2011.07.003 (2011).
115 Irvine, G. B., El-Agnaf, O. M., Shankar, G. & Walsh, D. M. in *Mol. Med.* Vol. 14 451-464 (2008).
116 Haataja, L., Gurlo, T., Huang, C. J. & Butler, P. C. in *Endocr. Rev.* Vol. 29 303-316 (2008).
117 Husby, G. Amyloidosis and rheumatoid arthritis. *Clinical and experimental rheumatology* **3**, 173 (1985).
118 Itzhaki, R. *et al.* Microbes and Alzheimer's disease. *Journal of Alzheimer's Disease* **51**, doi:10.3233/JAD-160152 (2016).
119 Little, C. S., Hammond, C. J., Macintyre, A., Balin, B. J. & Appelt, D. M. Chlamydia pneumoniae induces Alzheimer-like amyloid plaques in brains of BALB/c mice. *Neurobiology of Aging* **25**, 419-429, doi:10.1016/S0197-4580(03)00127-1 (2004).

120 Kumar, D. K. V. *et al.* Amyloid-β peptide protects against microbial infection in mouse and worm models of Alzheimer's disease. *Science translational medicine* **8**, 340ra372, doi:10.1126/scitranslmed.aaf1059 (2016).
121 Wozniak, M. A., Itzhaki, R. F., Shipley, S. J. & Dobson, C. B. Herpes simplex virus infection causes cellular β-amyloid accumulation and secretase upregulation. *Neuroscience Letters* **429**, 95-100, doi:10.1016/j.neulet.2007.09.077 (2007).
122 Wozniak, M. A. & Itzhaki, R. F. Intravenous immunoglobulin reduces beta amyloid and abnormal tau formation caused by herpes simplex virus type 1. *Journal of Neuroimmunology* **257**, 7-12, doi:10.1016/j.jneuroim.2013.01.005 (2013).
123 Gottlieb, S. Head injury doubles the risk of Alzheimer's disease. *BMJ* **321**, 1100, doi:10.1136/bmj.321.7269.1100/d (2000).
124 Petkova, A. T. *et al.* A structural model for Alzheimer's beta-amyloid fibrils based on experimental constraints from solid state NMR. *Proceedings of the National Academy of Sciences of the United States of America* **99**, 16742-16747, doi:10.1073/pnas.262663499 (2002).
125 Malavolta, L. & Nakaie, C. R. Comparative fibril formation of analogs corresponding to the (12-24) segment of the beta-amyloid peptide. *Neurological Sciences* **32**, 1123-1127, doi:10.1007/s10072-011-0749-3 (2011).
126 Abe, H., Kawasaki, K. & Nakanishi, H. pH-dependent aggregate forms and conformation of Alzheimer amyloid beta-peptide (12-24). *Journal of Biochemistry* **132**, 863-874 (2002).
127 Tjernberg, L. O. *et al.* A molecular model of Alzheimer amyloid beta-peptide fibril formation. *Journal of Biological Chemistry* **274**, 12619-12625, doi:10.1074/jbc.274.18.12619 (1999).
128 Balbach, J. J. *et al.* Amyloid fibril formation by A beta(16-22), a seven-residue fragment of the Alzheimer's beta-amyloid peptide, and structural characterization by solid state NMR. *Biochemistry* **39**, 13748-13759, doi:10.1021/bi0011330 (2000).
129 Hilbich, C., Kisterswoike, B., Reed, J., Masters, C. L. & Beyreuther, K. SUBSTITUTIONS OF HYDROPHOBIC AMINO-ACIDS REDUCE THE AMYLOIDOGENICITY OF ALZHEIMERS-DISEASE BETA-A4 PEPTIDES. *Journal of Molecular Biology* **228**, 460-473, doi:10.1016/0022-2836(92)90835-8 (1992).
130 Esler, W. P. *et al.* Point substitution in the central hydrophobic cluster of a human beta-amyloid congener disrupts peptide folding and abolishes plaque competence. *Biochemistry* **35**, 13914-13921, doi:10.1021/bi961302+ (1996).
131 Kowalewski, T. & Holtzman, D. M. In situ atomic force microscopy study of Alzheimer's beta-amyloid peptide on different substrates: New insights into mechanism of beta-sheet formation. *Proceedings of the National Academy of Sciences of the United States of America* **96**, 3688-3693 (1999).
132 Yates, E. A., Cucco, E. M. & Legleiter, J. Point Mutations in A beta Induce Polymorphic Aggregates at Liquid/Solid Interfaces. *Acs Chemical Neuroscience* **2**, 294-307, doi:10.1021/cn200001k (2011).
133 Yip, C. M. & McLaurin, J. Amyloid-beta peptide assembly: A critical step in fibrillogenesis and membrane disruption. *Biophysical Journal* **80**, 1359-1371 (2001).
134 Novoselov, K. S. *et al.* Electric field effect in atomically thin carbon films. *Science* **306**, 666-669, doi:10.1126/science.1102896 (2004).

135 Cherny, I. & Gazit, E. Amyloids: Not only pathological agents but also ordered nanomaterials. *Angewandte Chemie-International Edition* **47**, 4062-4069, doi:10.1002/anie.200703133 (2008).
136 Zhang, S. G. Fabrication of novel biomaterials through molecular self-assembly. *Nature Biotechnology* **21**, 1171-1178, doi:10.1038/nbt874 (2003).
137 Wetzel, R. Kinetics and thermodynamics of amyloid fibril assembly. *Accounts of Chemical Research* **39**, 671-679, doi:10.1021/ar050069h (2006).
138 Arimon, M. *et al.* Fine structure study of A beta(1-42) fibrillogenesis with atomic force microscopy. *Faseb Journal* **19**, 1344-+, doi:10.1096/fj.04-3137fje (2005).
139 Xu, Z. P., Paparcone, R. & Buehler, M. J. Alzheimer's A beta(1-40) Amyloid Fibrils Feature Size-Dependent Mechanical Properties. *Biophysical Journal* **98**, 2053-2062, doi:10.1016/j.bpj.2009.12.4317 (2010).
140 Delhaes, P. *Graphite and precursors*. (Australia ; Great Britain : Gordon & Breach, 2001).
141 group, U. o. I. B. *Visual Molecular Dynamic Website*.
142 Yang, G., Wong, M. K., Lin, L. E. & Yip, C. M. Nucleation and growth of elastin-like peptide fibril multilayers: an in situ atomic force microscopy study. *Nanotechnology* **22**, doi:494018

10.1088/0957-4484/22/49/494018 (2011).
143 Roman, T., Dino, W. A., Nakanishi, H. & Kasai, H. Amino acid adsorption on single-walled carbon nanotubes. *European Physical Journal D* **38**, 117-120, doi:10.1140/epjd/e2006-00043-1 (2006).
144 Tsang, S. C. *et al.* IMMOBILIZATION OF SMALL PROTEINS IN CARBON NANOTUBES - HIGH-RESOLUTION TRANSMISSION ELECTRON-MICROSCOPY STUDY AND CATALYTIC ACTIVITY. *Journal of the Chemical Society-Chemical Communications*, 1803-1804, doi:10.1039/c39950001803 (1995).
145 Meldrum, F. C. Calcium carbonate in biomineralisation and biomimetic chemistry. *International Materials Reviews* **48**, 187-224, doi:10.1179/095066003225005836 (2003).
146 Mann, S. *Biomimetic Materials Chemistry*. (John Wiley & Sons, 1995).
147 Sarikaya, M. & Aksay, I. A. *Biomimetics: design and processing of materials*. (AIP Press, 1995).
148 Sarikaya, M. Biomimetics: Materials fabrication through biology. *Proceedings of the National Academy of Sciences of the United States of America* **96**, 14183-14185, doi:10.1073/pnas.96.25.14183 (1999).
149 Lippmann, F. *Sedimentary carbonate minerals*. (Springer-Verlag, 1973).
150 Reeder, R. J. & Mineralogical Society of America. *Carbonates : mineralogy and chemistry*. (Mineralogical Society of America, 1983).
151 Kulik, D. A., Vinograd, V. L., Paulsen, N. & Winkler, B. (Ca,Sr)CO3 aqueous-solid solution systems: From atomistic simulations to thermodynamic modelling. *Physics and Chemistry of the Earth* **35**, 217-232, doi:10.1016/j.pce.2010.04.011 (2010).
152 Ji, B. H. & Gao, H. J. Mechanical properties of nanostructure of biological materials. *Journal of the Mechanics and Physics of Solids* **52**, 1963-1990, doi:10.1016/j.jmps.2004.03.006 (2004).
153 Mayer, G. & Sarikaya, M. Rigid biological composite materials: Structural examples for biomimetic design. *Experimental Mechanics* **42**, 395-403 (2002).

154 Mayer, G. Rigid biological systems as models for synthetic composites. *Science* **310**, 1144-1147, doi:10.1126/science.1116994 (2005).
155 Wilbur, K. M. & Bernhardt, A. M. EFFECTS OF AMINO-ACIDS, MAGNESIUM, AND MOLLUSCAN EXTRAPALLIAL FLUID ON CRYSTALLIZATION OF CALCIUM-CARBONATE - INVITRO EXPERIMENTS. *Biological Bulletin* **166**, 251-259 (1984).
156 Morse, J. W., Wang, Q. W. & Tsio, M. Y. Influences of temperature and Mg:Ca ratio on CaCO3 precipitates from seawater. *Geology* **25**, 85-87 (1997).
157 Ries, J. B. Aragonite production in calcite seas: effect of seawater Mg/Ca ratio on the calcification and growth of the calcareous alga Penicillus capitatus. *Paleobiology* **31**, 445-458, doi:10.1666/0094-8373(2005)031[0445:apicse]2.0.co;2 (2005).
158 Cheng, X. G., Varona, P. L., Olszta, M. J. & Gower, L. B. Biomimetic synthesis of calcite films by a polymer-induced liquid-precursor (PILP) process 1. Influence and incorporation of magnesium. *Journal of Crystal Growth* **307**, 395-404, doi:10.1016/j.jcrysgro.2007.07.006 (2007).
159 Jacob, D. E. *et al.* Nanostructure, composition and mechanisms of bivalve shell growth. *Geochimica Et Cosmochimica Acta* **72**, 5401-5415, doi:10.1016/j.gca.2008.08.019 (2008).
160 Trubitt, M. B. D. The production and exchange of marine shell prestige goods. *Journal of Archaeological Research* **11**, 243-277 (2003).
161 Cats, A. *et al.* RANDOMIZED, DOUBLE-BLINDED, PLACEBO-CONTROLLED INTERVENTION STUDY WITH SUPPLEMENTAL CALCIUM IN FAMILIES WITH HEREDITARY NONPOLYPOSIS COLORECTAL-CANCER. *Journal of the National Cancer Institute* **87**, 598-603 (1995).
162 Mortensen, L. & Charles, P. Bioavailability of calcium supplements and the effect of vitamin D: Comparisons between milk, calcium carbonate, and calcium carbonate plus vitamin D. *American Journal of Clinical Nutrition* **63**, 354-357 (1996).
163 Gigac, J., Kuna, V. & Schwartz, J. EFFECTS OF FIBERS AND FILLERS ON THE OPTICAL AND MECHANICAL CHARACTERISTICS OF PAPER. *Tappi Journal* **78**, 162-167 (1995).
164 Page, M. G. & Colfen, H. Improved control of CaCO3 precipitation by direct carbon dioxide diffusion: Application in mesocrystal assembly. *Crystal Growth & Design* **6**, 1915-1920, doi:10.1021/cg060152r (2006).
165 Gower, L. A. & Tirrell, D. A. Calcium carbonate films and helices grown in solutions of poly(aspartate). *Journal of Crystal Growth* **191**, 153-160 (1998).
166 Kontoyannis, C. G. & Vagenas, N. V. Calcium carbonate phase analysis using XRD and FT-Raman spectroscopy. *Analyst* **125**, 251-255 (2000).
167 Kitano, Y., Hood, D. W. & Park, K. PURE ARAGONITE SYNTHESIS. *Journal of Geophysical Research* **67**, 4873-&, doi:10.1029/JZ067i012p04873 (1962).
168 Ahn, J. W., Choi, K. S., Yoon, S. H. & Kim, H. Synthesis of aragonite by the carbonation process. *Journal of the American Ceramic Society* **87**, 286-288 (2004).
169 Rudloff, J. & Colfen, H. Superstructures of temporarily stabilized nanocrystalline CaCO3 particles: Morphological control via water surface tension variation. *Langmuir* **20**, 991-996, doi:10.1021/la0358217 (2004).
170 Kasparova, P., Antonietti, M. & Colfen, H. Double hydrophilic block copolymers with switchable secondary structure as additives for crystallization control. *Colloids and*

Surfaces a-Physicochemical and Engineering Aspects **250**, 153-162, doi:10.1016/j.colsurfa.2004.03.033 (2004).
171 Mustafa, G. *et al.* Cementomimetics— constructing a cementum- like biomineralized microlayer via amelogenin- derived peptides. *International Journal of Oral Science* **4**, 69, doi:10.1038/ijos.2012.40 (2012).
172 Mukherjee, S. *Applied mineralogy : applications in industry and environment*. (Dordrecht ; New York : Springer ; New Delhi, India : Capital Publishing Co., 2011).
173 Pasteris, J. D., Wopenka, B. & Valsami-Jones, E. Bone and tooth mineralization; why apatite? *Elements*, 97-104, doi:10.2113/GSELEMENTS.4.2.97 (2008).
174 Young, R. A. Biological apatite vs hydroxyapatite at the atomic level. *Clinical orthopaedics and related research* **113**, 249 (1975).
175 Cheung, H. S. Role of calcium-containing crystals in osteoarthritis. *Frontiers in bioscience : a journal and virtual library* **10**, 1336-1340 (2005).
176 Ozgür Engin, N. & Tas, A. Manufacture of macroporous calcium hydroxyapatite bioceramics. *Journal of the European Ceramic Society* **19**, 2569-2572, doi:10.1016/S0955-2219(99)00131-4 (1999).
177 Ikoma, T., Yamazaki, A., Nakamura, S. & Akao, M. Preparation and Structure Refinement of Monoclinic Hydroxyapatite. *Journal of solid state chemistry* **144**, 272-276, doi:10.1006/jssc.1998.8120 (1999).
178 Suda, H., Yashima, M., Kakihana, M. & Yoshimura, M. Monoclinic .tautm. Hexagonal Phase Transition in Hydroxyapatite Studied by X-ray Powder Diffraction and Differential Scanning Calorimeter Techniques. *The journal of physical chemistry* **99**, 6752-6754, doi:10.1021/j100017a068 (1995).
179 Hanson, B. *<p class="MsoNormal" style="mso-margin-top-alt:auto;margin-bottom:0in;margin-left:.5in;margin-bottom:.0001pt;text-align:justify;text-justify:inter-ideograph;text-indent:-.5in;line-height:normal"> Hydroxyapatitecrystal structure*, 2001).
180 White, S. N. *et al.* Vol. 80 321-326 (2001).
181 Fong, H. K. *Towards enamel biomimetics : structure, mechanical properties & biomineralization of dental enamel*. (Thesis (Ph. D.)--University of Washington,2003, 2003).
182 Skinner, H. C. W. Biominerals. *Mineralogical Magazine* **69**, 621-641, doi:10.1180/0026461056950275 (2005).
183 Schroeder, H. E. *Oral structure biology : embryology, structure, and function of normal hard and soft tissues of the oral cavity and temporomandibular joints*. (Stuttgart ; New York : G. Thieme Verlag ; New York : Thieme Medical Publishers, 1991).
184 Nanci, A. *Ten Cate's oral histology : development, structure, and function*. Eighth edition / Antonio Nanci. edn, (St. Louis, Missouri : Elsevier Mosby, 2013).
185 White, S. N. *et al.* The Dentino-enamel Junction is a Broad Transitional Zone Uniting Dissimilar Bioceramic Composites. *Journal of the American Ceramic Society* **83**, 238-240, doi:10.1111/j.1151-2916.2000.tb01181.x (2000).
186 Ross, M. H. *Histology : a text and atlas*. 3rd ed. edn, (Baltimore : Williams & Wilkins, 1995).
187 Marshall, S. J. *et al.* The dentin–enamel junction—a natural, multilevel interface. *Journal of the European Ceramic Society* **23**, 2897-2904, doi:10.1016/S0955-2219(03)00301-7 (2003).

188 Imbeni, V., Kruzic, J. J., Marshall, G. W., Marshall, S. J. & Ritchie, R. O. The dentin–enamel junction and the fracture of human teeth. *Nature materials* **4**, 229-232, doi:10.1038/nmat1323 (2005).
189 White, S. N. *et al.* The Dentino-enamel Junction is a Broad Transitional Zone Uniting Dissimilar Bioceramic Composites. *Journal of the American Ceramic Society* **83**, 238-240, doi:10.1111/j.1151-2916.2000.tb01181.x (2000).
190 Smith, C. E. Cellular and chemical events during enamel maturation. *Critical reviews in oral biology and medicine : an official publication of the American Association of Oral Biologists* **9**, 128 (1998).
191 Stayton, P. S., Drobny, G. P., Shaw, W. J., Long, J. R. & Gilbert, M. Molecular recognition at the protein-hydroxyapatite interface. *Critical reviews in oral biology and medicine : an official publication of the American Association of Oral Biologists* **14**, 370 (2003).
192 Murphy, M. B., Hartgerink, J. D., Goepferich, A. & Mikos, A. G. Synthesis and in vitro hydroxyapatite binding of peptides conjugated to calcium-binding moieties. *Biomacromolecules* **8**, 2237, doi:10.1021/bm070121s (2007).
193 Hirabayashi, H. & Fujisaki, J. Bone-specific drug delivery systems approaches via chemical modification of bone-seeking agents.(Leading Article). *Clinical Pharmacokinetics* **42**, 1319, doi:10.2165/00003088-200342150-00002 (2003).
194 Dogan, S. *et al.* Biomimetic Tooth Repair: Amelogenin-derived peptide enables in vitro remineralization of human enamel. *ACS Biomaterials Science & Engineering*, doi:10.1021/acsbiomaterials.7b00959 (2018).
195 Bioinformatics, S. S. I. o. *Protparam tool*.
196 Keene, E. C., Evans, J. S. & Estroff, L. A. Silk Fibroin Hydrogels Coupled with the n16N-beta-Chitin Complex An in Vitro Organic Matrix for Controlling Calcium Carbonate Mineralization. *Crystal Growth & Design* **10**, 5169-5175, doi:10.1021/cg1009303 (2010).